IAEA TECDOC SERIES

IAEA-TECDOC-2023

IAEA-TECDOC-2023

Energy Neutral Mineral Processing with High Temperature Reactors: Resource Identification, Uranium Recovery and Thermal Processes

Final Report of a Coordinated Research Project

IAEA
International Atomic Energy Agency

ENERGY NEUTRAL MINERAL PROCESSING WITH HIGH TEMPERATURE REACTORS: RESOURCE IDENTIFICATION, URANIUM RECOVERY AND THERMAL PROCESSES

The following States are Members of the International Atomic Energy Agency:

AFGHANISTAN
ALBANIA
ALGERIA
ANGOLA
ANTIGUA AND BARBUDA
ARGENTINA
ARMENIA
AUSTRALIA
AUSTRIA
AZERBAIJAN
BAHAMAS
BAHRAIN
BANGLADESH
BARBADOS
BELARUS
BELGIUM
BELIZE
BENIN
BOLIVIA, PLURINATIONAL STATE OF
BOSNIA AND HERZEGOVINA
BOTSWANA
BRAZIL
BRUNEI DARUSSALAM
BULGARIA
BURKINA FASO
BURUNDI
CAMBODIA
CAMEROON
CANADA
CENTRAL AFRICAN REPUBLIC
CHAD
CHILE
CHINA
COLOMBIA
COMOROS
CONGO
COSTA RICA
CÔTE D'IVOIRE
CROATIA
CUBA
CYPRUS
CZECH REPUBLIC
DEMOCRATIC REPUBLIC OF THE CONGO
DENMARK
DJIBOUTI
DOMINICA
DOMINICAN REPUBLIC
ECUADOR
EGYPT
EL SALVADOR
ERITREA
ESTONIA
ESWATINI
ETHIOPIA
FIJI
FINLAND
FRANCE
GABON
GEORGIA
GERMANY
GHANA
GREECE
GRENADA
GUATEMALA
GUYANA
HAITI
HOLY SEE
HONDURAS
HUNGARY
ICELAND
INDIA
INDONESIA
IRAN, ISLAMIC REPUBLIC OF
IRAQ
IRELAND
ISRAEL
ITALY
JAMAICA
JAPAN
JORDAN
KAZAKHSTAN
KENYA
KOREA, REPUBLIC OF
KUWAIT
KYRGYZSTAN
LAO PEOPLE'S DEMOCRATIC REPUBLIC
LATVIA
LEBANON
LESOTHO
LIBERIA
LIBYA
LIECHTENSTEIN
LITHUANIA
LUXEMBOURG
MADAGASCAR
MALAWI
MALAYSIA
MALI
MALTA
MARSHALL ISLANDS
MAURITANIA
MAURITIUS
MEXICO
MONACO
MONGOLIA
MONTENEGRO
MOROCCO
MOZAMBIQUE
MYANMAR
NAMIBIA
NEPAL
NETHERLANDS
NEW ZEALAND
NICARAGUA
NIGER
NIGERIA
NORTH MACEDONIA
NORWAY
OMAN
PAKISTAN
PALAU
PANAMA
PAPUA NEW GUINEA
PARAGUAY
PERU
PHILIPPINES
POLAND
PORTUGAL
QATAR
REPUBLIC OF MOLDOVA
ROMANIA
RUSSIAN FEDERATION
RWANDA
SAINT KITTS AND NEVIS
SAINT LUCIA
SAINT VINCENT AND THE GRENADINES
SAMOA
SAN MARINO
SAUDI ARABIA
SENEGAL
SERBIA
SEYCHELLES
SIERRA LEONE
SINGAPORE
SLOVAKIA
SLOVENIA
SOUTH AFRICA
SPAIN
SRI LANKA
SUDAN
SWEDEN
SWITZERLAND
SYRIAN ARAB REPUBLIC
TAJIKISTAN
THAILAND
TOGO
TONGA
TRINIDAD AND TOBAGO
TUNISIA
TÜRKİYE
TURKMENISTAN
UGANDA
UKRAINE
UNITED ARAB EMIRATES
UNITED KINGDOM OF GREAT BRITAIN AND NORTHERN IRELAND
UNITED REPUBLIC OF TANZANIA
UNITED STATES OF AMERICA
URUGUAY
UZBEKISTAN
VANUATU
VENEZUELA, BOLIVARIAN REPUBLIC OF
VIET NAM
YEMEN
ZAMBIA
ZIMBABWE

The Agency's Statute was approved on 23 October 1956 by the Conference on the Statute of the IAEA held at United Nations Headquarters, New York; it entered into force on 29 July 1957. The Headquarters of the Agency are situated in Vienna. Its principal objective is "to accelerate and enlarge the contribution of atomic energy to peace, health and prosperity throughout the world''.

IAEA-TECDOC-2023

ENERGY NEUTRAL MINERAL PROCESSING WITH HIGH TEMPERATURE REACTORS: RESOURCE IDENTIFICATION, URANIUM RECOVERY AND THERMAL PROCESSES

FINAL REPORT OF A COORDINATED RESEARCH PROJECT

INTERNATIONAL ATOMIC ENERGY AGENCY
VIENNA, 2023

COPYRIGHT NOTICE

For further information on this publication, please contact:

Nuclear Fuel Cycle and Materials Section
International Atomic Energy Agency
Vienna International Centre
PO Box 100
1400 Vienna, Austria
Email: Official.Mail@iaea.org

Printed by the IAEA in Austria
April 2023

IAEA Library Cataloguing in Publication Data

Names: International Atomic Energy Agency.
Title: Energy neutral mineral processing with high temperature reactors : resource identification, uranium recovery and thermal processes / International Atomic Energy Agency.
Description: Vienna : International Atomic Energy Agency, 2023. | Series: IAEA TECDOC series, ISSN 1011–4289 ; no. 2023 | Includes bibliographical references.
Identifiers: IAEAL 23-01589 | ISBN 978–92–0–118823–6 (paperback : alk. paper) | ISBN 978–92–0–118723–9 (pdf)
Subjects: LCSH: Uranium — Metallurgy. | Thorium — Metallurgy. | Nuclear reactors. | Nuclear energy.

FOREWORD

Around the world, the demand for mineral commodities continues to grow; at the same time, linear economy models are being transformed into circular ones. To ensure a steady supply of inexpensive raw materials required for development, thermal processes capable of processing resources that currently cannot be developed using traditional chemical processing might have to be employed to process lower grade ores or yesterday's mine wastes. These thermal mineral extraction processes can be cleaner and can generate smaller quantities of waste than current wet chemical processes, but they depend on the availability of large amounts of energy. Currently, the unavailability of affordable and low carbon energy limits the sustainable application of such thermal processes in extractive industries.

Thermal processes using high temperature nuclear heat or high temperature concentrated solar heat could be a more sustainable and environmentally benign alternative to wet chemical processing or fossil fuel fired thermal processes. Affordable, low carbon energy could enable the production of higher quality end products from lower grade ores or mine tailings, which could also improve the overall economics of the operation.

In this context, many mineral deposits contain low concentrations of accompanying uranium and/or thorium that could be recovered and, after processing, used as nuclear reactor fuel. If the amount of accompanying uranium/thorium is sufficient to provide energy for primary ore and mine tailings processing and uranium/thorium recovery, as well as for other energy requirements along the way, the process can be called an energy neutral mineral process. The idea of energy neutral mineral processing was first developed at the IAEA and led to the coordinated research project entitled 'Uranium/Thorium Fuelled High Temperature Gas Cooled Reactor Applications for Energy Neutral and Sustainable Comprehensive Extraction and Mineral Product Development Processes'. Project participants generated basic data on the availability and characteristics of various potentially suitable mineral resources and process residues; determined and developed suitable technologies for the recovery of natural uranium and thorium from some of these resources; and conducted conceptual and pre-feasibility studies on appropriate thermal processes in which uranium/thorium fuelled high temperature gas cooled reactors and concentrated solar power plants could provide the required energy for mineral processing in the form of process heat.

The IAEA officers responsible for this publication were H. Tulsidas, P. Woods and N. Haneklaus of the Division of Nuclear Fuel Cycle and Waste Technology and F. Reitsma of the Division of Nuclear Power.

EDITORIAL NOTE

This publication has been prepared from the original material as submitted by the contributors and has not been edited by the editorial staff of the IAEA. The views expressed remain the responsibility of the contributors and do not necessarily represent the views of the IAEA or its Member States.

Neither the IAEA nor its Member States assume any responsibility for consequences which may arise from the use of this publication. This publication does not address questions of responsibility, legal or otherwise, for acts or omissions on the part of any person.

The use of particular designations of countries or territories does not imply any judgement by the publisher, the IAEA, as to the legal status of such countries or territories, of their authorities and institutions or of the delimitation of their boundaries.

The mention of names of specific companies or products (whether or not indicated as registered) does not imply any intention to infringe proprietary rights, nor should it be construed as an endorsement or recommendation on the part of the IAEA.

The authors are responsible for having obtained the necessary permission for the IAEA to reproduce, translate or use material from sources already protected by copyrights.

The IAEA has no responsibility for the persistence or accuracy of URLs for external or third party Internet web sites referred to in this publication and does not guarantee that any content on such web sites is, or will remain, accurate or appropriate.

CONTENTS

1. INTRODUCTION

1.1 BACKGROUND

In contrast to the linear economy the circular economy aims to create closed-loop systems that minimize resource input and waste creation. Realizing circular economy principles in mining is challenging and presently limited to mine tailings utilization and reducing inputs of primary materials as much as possible. Energy neutral mineral processing supports this approach to mining by promoting processing of presently considered unconventional ores and mine tailings that contain relevant concentrations of uranium and/or thorium. The basic idea behind energy neutral mineral processing is that unconventional uranium (and/or thorium) is recovered during primary ore/mine tailings processing for use as raw material to produce nuclear reactor fuel. Energy neutrality is then reached if the extracted unconventional uranium (and/or thorium) is used to generate energy equivalent to, or larger than, the amount of energy required for mineral processing of the primary ore/mine tailings and uranium/thorium extraction, -conversion, -enrichment and -fuel production. Figure 1 illustrates the very basic idea of energy neutral mineral processing for uranium.

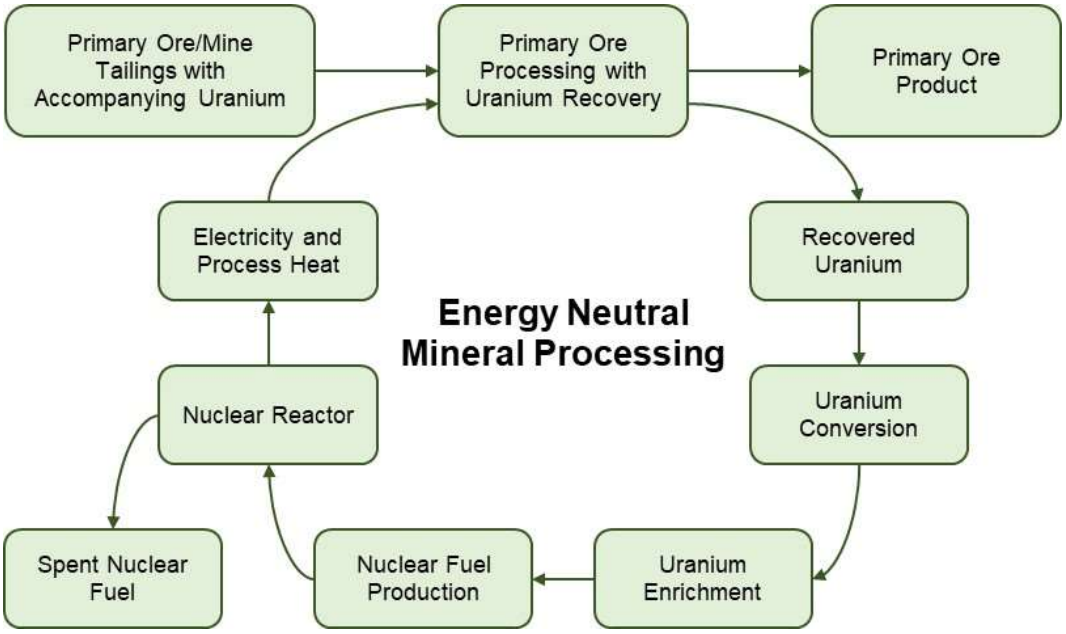

FIG. 1. Brief overview of energy neutral mineral processing.

Extracted uranium, usually shipped as uranium ore concentrate (UOC), can be sent for uranium conversion/enrichment and later for nuclear fuel production to a nuclear fuel manufacturer in the same way that traditional uranium mines handle their product. Poly-metallic mines such as the Olympic Dam mine in Australia (copper, uranium, silver, and gold) are already in operation today. The efficiency of energy neutral mineral processing may further be enhanced if the energy source is deployed in the vicinity of the processing plant and even more so, if it is used to directly supply process heat for energy intensive mineral ore development and/or supporting energy intensive operations such as water desalination. Spent nuclear fuel from the energy source can be safely stored or reprocessed. The idea has the potential to decarbonize a relevant share of the energy intensive mineral processing industry that accounts for a considerable amount of anthroprogenic carbon emissions. Besides, mine tailings with elevated uranium and/or thorium concentrations can pose a considerable risk to local communities and the environment as well as an economic burden to the entities

responsible for their management. In the longterm, processing such mine tailings is probably the best solution to mitigating the mobilization of radiotoxic uranium and/or thorium.

1.2 OBJECTIVE

This publication summarizes the activities that were carried out under the IAEA coordinated research project (CRP) (T11006) on “uranium/thorium fuelled high temperature gas-cooled reactor applications for energy neutral and sustainable comprehensive extraction and mineral product development” (UTHAM).

1.3 SCOPE

The scope of the CRP was to generate basic data on resource identification, unconventional uranium/thorium recovery and non-fossil fuel powered thermal processing that is relevant to Member States. These achievements are found in the case studies published here as well as the other publications that resulted from the CRP that are listed in Annex I. Besides, the CRP provided an indepth and often interdisciplinary analysis of energy neutral mineral processing, or the feasibility of using nuclear reactors to provide process heat applications for the mineral industry.

1.4 STRUCTURE

The CRP generated basic data on the availability and characteristics of various mineral resources potentially suitable for energy neutral mineral processing that have been summarized in Chapter 1: Resource Identification. Case studies were provided for Argentina and the United Republic of Tanzania. Argentina is a particularly interesting case since although the country has a very active nuclear program, conventional uranium mining is only allowed in few provinces. Unconventional recovery of uranium could be particularly interesting for Argentina since the recovery of radiotoxic uranium from intermediate products such as fertilizers could be environmentally desirable while providing a domestic source of uranium for the nuclear power program. The United Republic of Tanzania is an equally interesting case in a way that the (unconventional) uranium concentrations in Minjingu phosphate rock in the northern part of the country are among the highest in the world, higher than for instance uranium concentrations in conventional uranium ore from Namibia.

Participants further determined and developed suitable technologies for the recovery of unconventional uranium and thorium from some of these resources. These efforts were summarized in Chapter 2: Unconventional Uranium/Thorium Recovery. Here Egypt and Morocco provided case studies for unconventional uranium recovery from phosphoric acid, an intermediate product during mineral fertilizer production. Both countries are among the largest phosphate fertilizer producers in the world and also have considerable shares of the world’s phosphate ore resources. The case studies provide meaningful introduction on how unconventional uranium recovery can with little effort be already incorporated in existing fertilizer production.

Lastly, participating experts conducted conceptual and pre-feasibility studies on appropriate thermal processes in which low carbon energy sources such as thorium/uranium fuelled high temperature gas-cooled reactors (HTGRs) or concentrated solar power (CSP) plants could provide the required energy in the form of process heat for mineral processing. These efforts have been summarized in Chapter 3: Thermal Mineral Ore Processing. India, Indonesia,

Malaysia, and Venezuela that operate or plan to operate energy intensive thermal mineral ore processing operations provided meaningful case studies.

Figure 2 provides a graphic overview of the structure of this document.

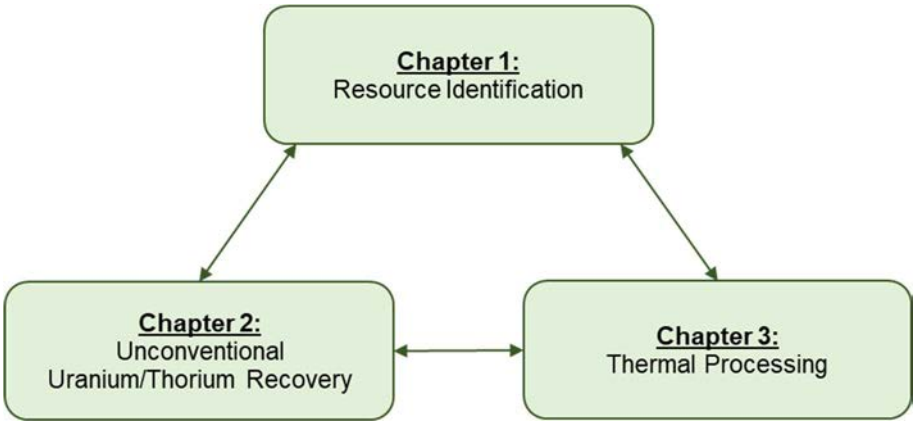

FIG. 2. Structure of the document.

CHAPTER 1 CASE STUDIES ON RESOURCE IDENTIFICATION

1.1 ARGENTINA: PROSPECTING STUDIES OF UNCONVENTIONAL URANIUM IN PHOSPHATE BASINS

Since the 1970s, the Argentinean Geological Mining Survey undertook systematic prospecting studies to identify phosphate deposits in sedimentary basins. As part of these studies, eighteen areas were delineated in various marine basins with phosphate potential, comprising a total area of about 640 000 km^2 [1.1]. While these studies were still taking place, a group of researchers of the Department of Geology of the University of Buenos Aires entered a new phase of phosphates prospecting (mid-80s) with the study of new areas predominantly focused on the genesis and paleo-depositional environments of phosphate-bearing deposits in Argentinean basins. All the published information about these works, along with new data, was compiled in a database which made it possible to define the main phosphate occurrences and correlate them with the global phosphogenic events (Cambrian, Ordovician, Jurassic-Cretaceous, Cretaceous-Paleocene, Miocene and Modern). [1.2].

In the framework of the IAEA Coordinated Research Project on "Uranium-thorium fuelled HTGR applications for energy neutral sustainable comprehensive extraction and mineral product development", the National Atomic Energy Commission of Argentina (CNEA) and the University of Buenos Aires, in co-operation with the National University of Salta, have carried out the project denominated "Assessment of the uranium potential of phosphate rock and testing low-grade phosphate ores extraction". The project, whose main results are summarized in this chapter, pursues the aim of accounting for a potential assessment of unconventional uranium, thorium and rare earth element (REE) resources related to phosphate rock. Moreover, it also strives toward a better understanding of how HTGRs can be used to beneficiate and process these lower grade phosphate ores from Argentinean sedimentary basins. [1.3].

General tasks carried out during the project, include both geological field work and specific petrographic, mineralogical and chemical determinations at specialized laboratory facilities of different institutions. Four field trips were carried out at different sites of phosphate-uranium interest in order to perform geological characterization, sampling and ground gamma-ray radiometric surveys.

Specific determinations can be summed up as following:

- Thin sections petrographic and mineralogical studies of phosphates;
- Ground gamma-ray total count data taken with a SRAT SPP2 NaI detector;
- Ground gamma-ray spectrometry data taken with a Radiation Solutions-230 BGO detector and a Radiation Solutions-125 NaI detector;
- Chemical analyses by X ray fluorescence, carried out at CNEA laboratories and with the NITON 3LX-THERMO portable device;
- Chemical determinations performed by Neutron Activation Analysis at the RA-3 CNEA Research Reactor facility.

The research project involved studies in three sedimentary basins, where lower grade phosphate mineralization and uranium anomalies (up to approximately 200 ppm uranium) have been detected. After completion of the evaluation of available information specific study areas of the Ordovician North-Western Basin, Upper Jurassic - Lower Cretaceous Neuquén

Basin, and Paleocene - Miocene Patagonia Basin were defined. Figure 1.1 shows the location of the basins in question at country scale.

FIG. 1.1. Location map: Ordovician North-Western Basin, Upper Jurassic - Lower Cretaceous Neuquén Basin, Paleocene - Miocene Patagonia Basin.

At the beginning of the project, the study has focused on the phosphate rock of the Ordovician North-Western basin. On the basis of prior information two sites were selected within the basin: Mojotoro Range (Salta Province) and Tilcara Range (Jujuy Province) which are located approximately 1500 km and 1600 km away from Buenos Aires city (see Fig. 1.2).

Within the study area, six phosphogenic intervals were recognized in the Ordovician succession; its Tremadocian to Floian part is composed of predominantly shales, sandstones and coquinas characterized by higher content of P_2O_5; its Dapingian to Sandbian part is composed of mainly sandstones with some fossil-rich shales and eventual phosphatics coquinas with lower content of P_2O_5. The distribution of Ordovician phosphate deposits can be linked to the paleogeographic basin evolution and to the temporal and spatial arrangement of its phosphate-bioclastic accumulations [1.3].

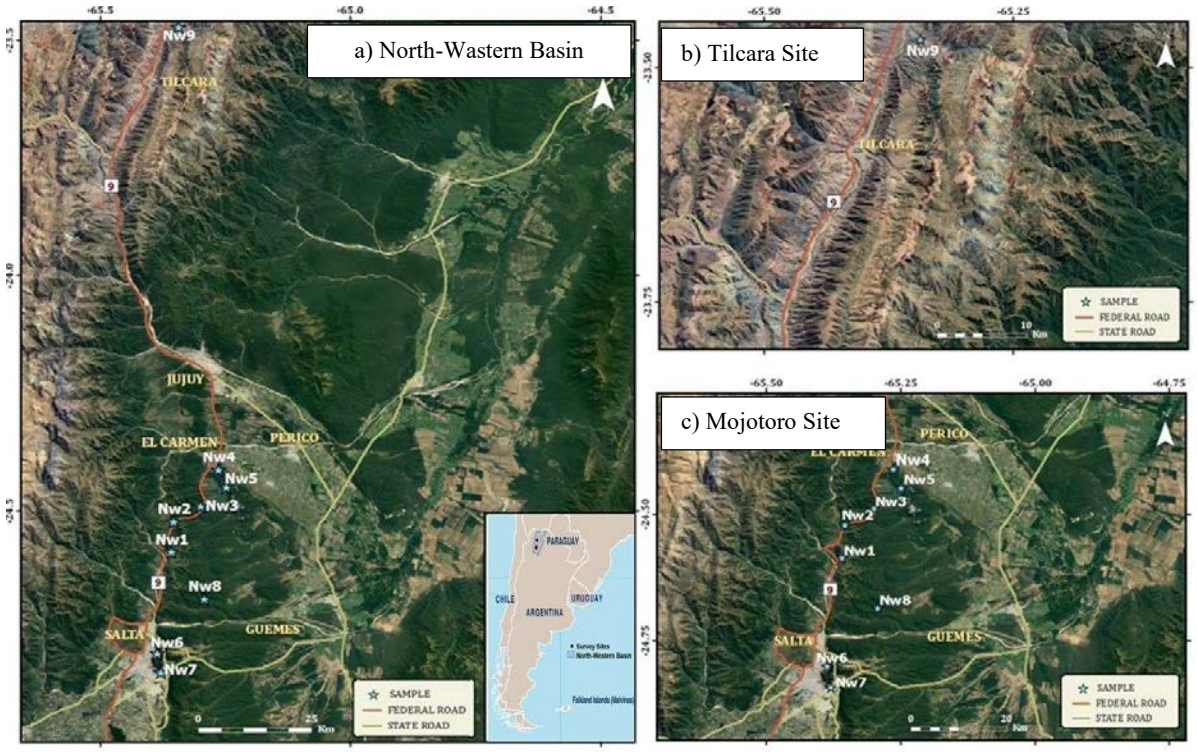

FIG. 1.2. Studied North-Western Basin (a) with highlighted Tilcara- (b) and Mojotoro (c) site.

Two surveys were conducted in the selected sites that covered a total of nine stations. Geological characterization, sampling and ground gamma-ray radiometric were implemented on each station. Approximately 10 kg samples of phosphatic rocks, including all the mineralized levels as well as the barren material as a background were placed into plastic bags, labelled and sealed and were sent to the laboratories for specific analysis such as: mineralogical determination, chemical characterization and an experimental study of integral recovery of uranium and phosphorus.

Data of major, trace elements and some REEs for the studied phosphate samples were obtained. The phosphorus grade ranges from 2.1% to 12.6% with an average of 5.8%. There is a roughly positive correlation between phosphorus and uranium content (see Fig. 1.3). All samples exhibit significant enrichment in Y, Sr, La, Yb, U, Th, Pb, Zr and REEs, if compared to background/earth crust concentrations, which encourage further comprehensive extraction tests (see Fig. 1.4).

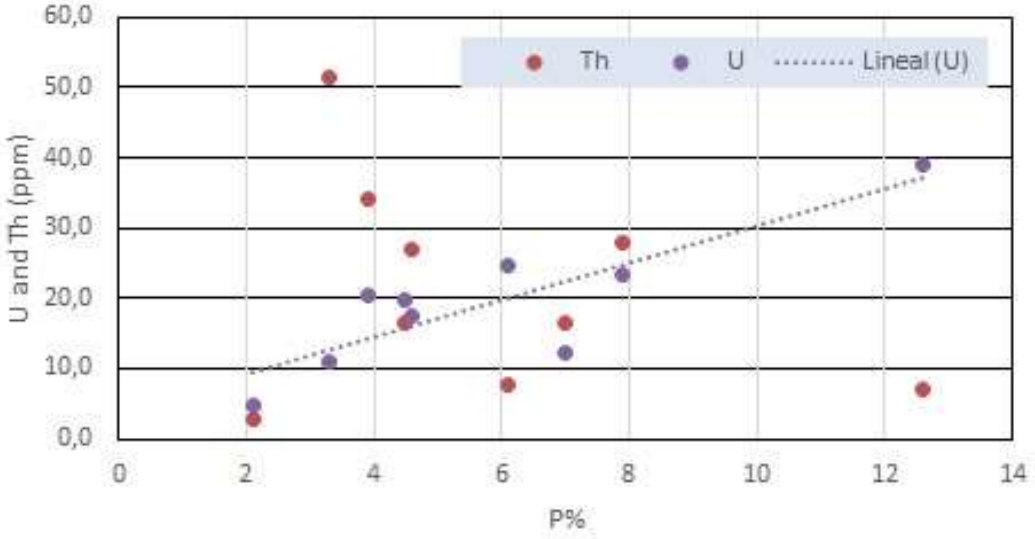

Fig. 1.3. Correlation between the concentration of phosphorus with uranium and thorium (by neutron activation analysis).

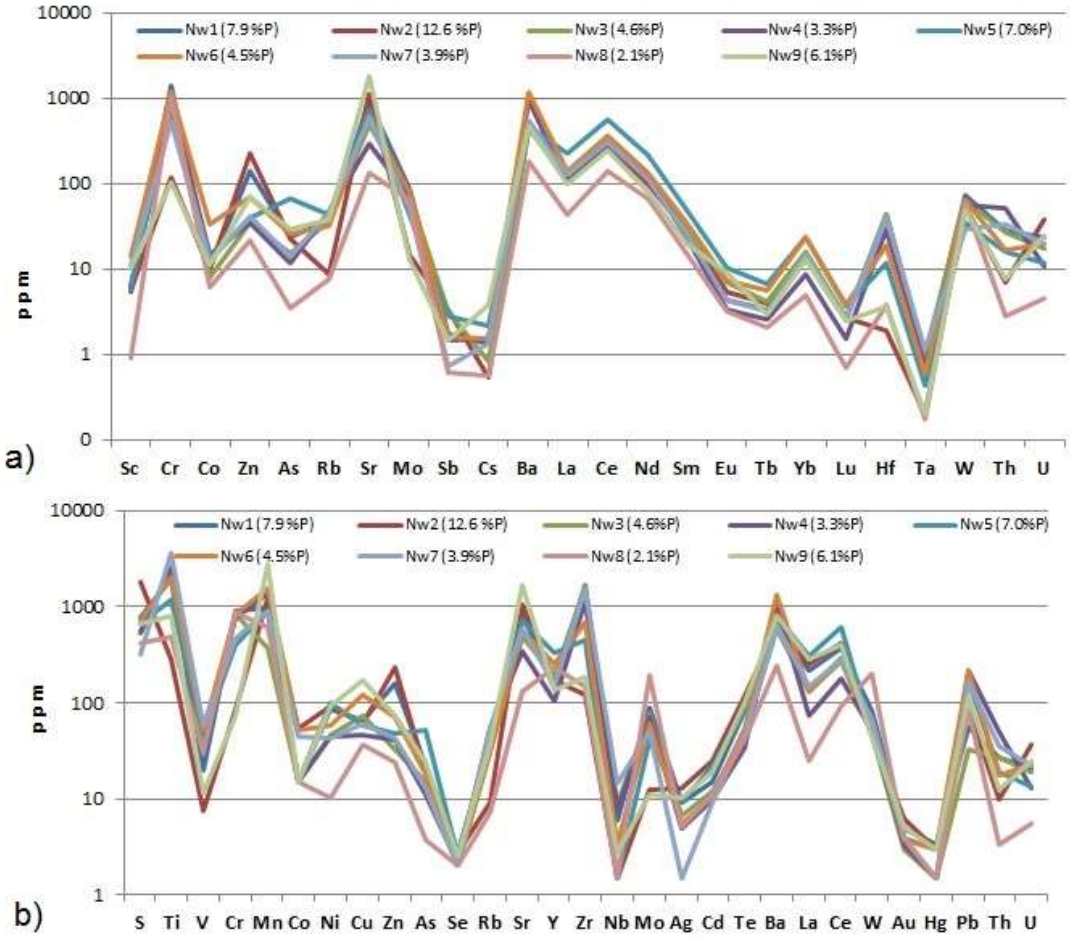

FIG. 1.4. Geochemical characterization of samples from the North-Western Basin by: a) Neutron Activation Analysis and b) X-Ray Fluorescence.

At a second stage of the project, the focus has been on the Upper Jurassic - Lower Cretaceous Neuquén basin. In the southern part of this basin. Two sites were selected for investigation: the Cerro Salado site and the Vaca Muerta site, which are located in the Neuquén province, approximately 1300 km away from Buenos Aires city (see Fig. 1.5)

The sedimentary phosphate occurrences are assigned to the Quintuco and the Vaca Muerta Formations. The Vaca Muerta Formation consists of black shales with 20 m thickness and bears early mid Berriasian ammonites. The Quintuco Formation consists of wackestones, bioclastic rudstones and hybrid sandstones, is 218 m thick and bears middle Berriasian to early Valanginian ammonites. The phosphate is present mainly in the form of nodules and to a lesser extent in partially or totally phosphatized shells. This episode of phosphogenesis does correspond with rising sea level and highstands in combination with low rates of clastic sedimentation. In addition, such concentrations of phosphate particles are typical for periods of reworking by waves due to the rise and fall of the sea level [1.1].

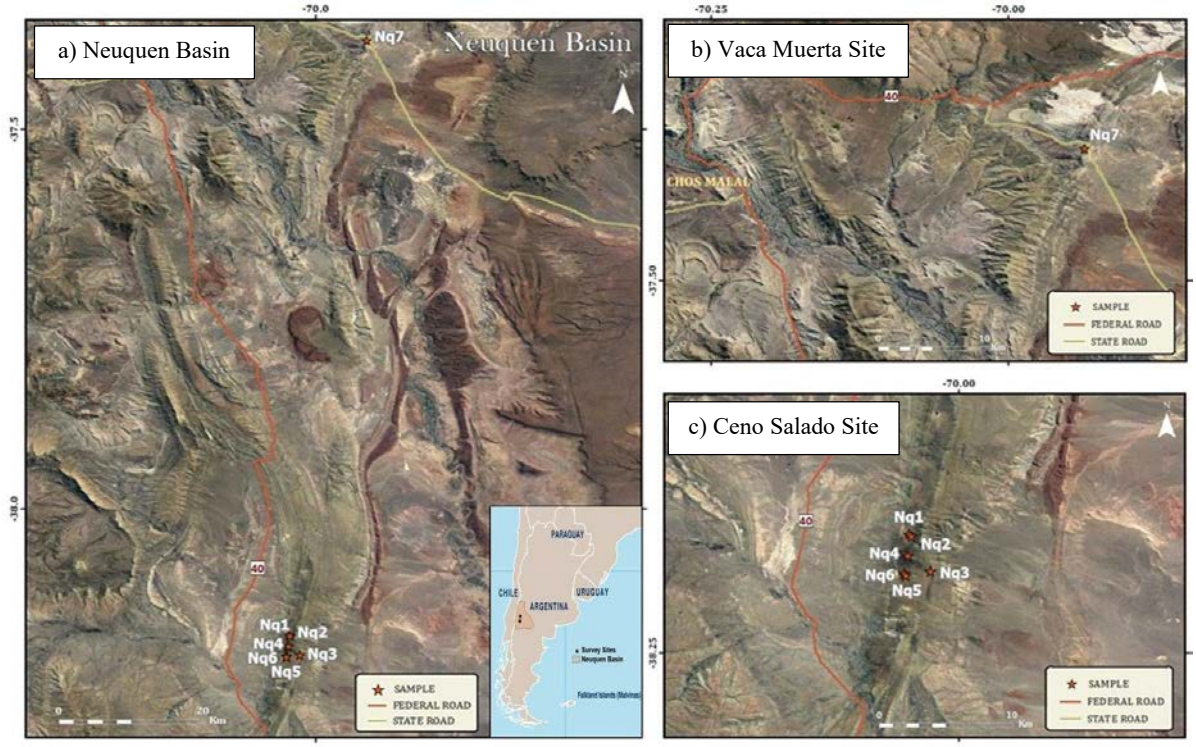

FIG. 1.5. Studied Neuquen Basin (a) with highlighted Vaca Muerta- (b) and Ceno Salado (c) site.

A survey was conducted in the above-mentioned sites totaling seven locations where geological characterization, sampling and ground gamma-ray spectrometry were implemented. The methodology to study the samples was the same applied to those belonging to the Ordovician North-Western Basin. The phosphorus grade ranges from 0,03% to 3.5% with an average of 1.5%. The values are lower than average phosphate concentrations of the Ordovician North-Western Basin. There is a strong positive correlation between phosphorus and uranium content. The concentrations of major elements, trace elements and some REEs of the studied phosphate samples is depicted in Fig. 1.6.

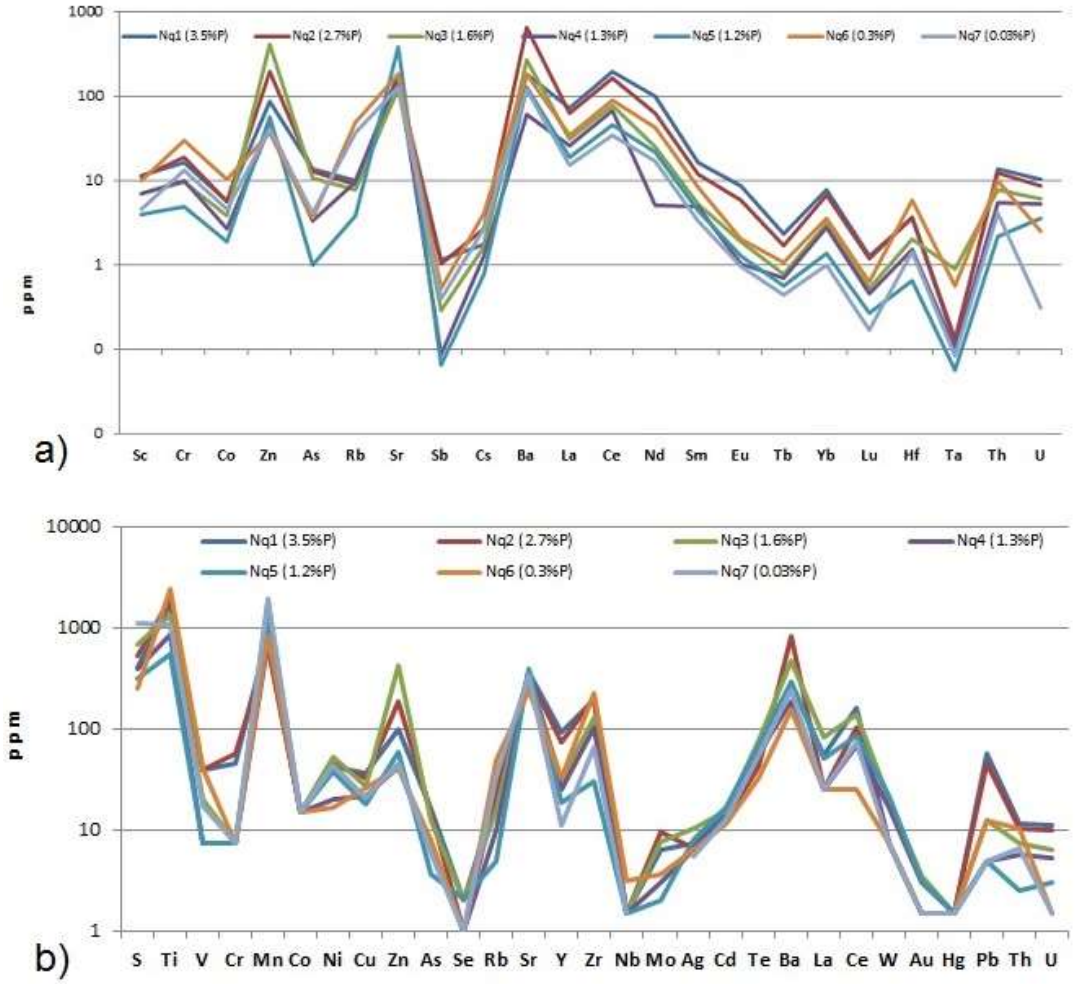

FIG. 1.6. Geochemical characterization by: a) Neutron Activation Analysis and b) X-Ray Fluorescence of the Upper Jurassic - Lower Cretaceous Neuquén Basin.

The final part of the project has been devoted to the characterization of phosphate rock of Paleocene - Miocene Patagonia basin. The study area is located in Chubut province, close to the towns of Trelew, Rawson and Puerto Madryn, approximately 1400 km away from Buenos Aires city. In Fig. 1.7 location maps at different scales are shown.

The Patagonian phosphates are found in Early Miocene sediments of the Gaiman Formation and equivalent strata. The Gaiman Formation is composed of a coarsening upward sequence of mudstones, fine tuffs, tuffs, sandstones, tuffaceous sandstones and coquinas. These sediments represent a storm-dominated shallow marine environment. Two types of phosphatic levels were identified based on lithology and sedimentary environment: one consists of "in situ" concretions which have developed within early transgressive highstand system tracts, and the other is related to reworking and mechanical concentration of resistant particles such as concretions, ooids, teeth, bones, etc., associated with transgressive surfaces. Phosphogenesis of this period is related to the flooding of shelf environments with cold and corrosive water mixed with warmer surficial water, probably because of the combined effects of a global climatic transition and the increased oceanic circulation during the Late Oligocene - Early Miocene [1.2].

Within the study area, a survey was conducted covering a total of six locations where geological studies, collecting 5 kg samples of phosphatic rock and ground gamma ray radiometry were implemented. The phosphorus grade ranges from 4.6% to 8.2% with an average of 6.6%. The value is similar to the average of the phosphate ore of the Ordovician North-Western basin. Meanwhile, the concentration of uranium ranges from 50 to 192 ppm averaging 130 ppm. This is within the common range of uranium concentrations (50–300 ppm) in marine phosphate rock deposits. The concentrations of major elements, trace elements and some REEs for the studied phosphate samples are shown in Fig. 1.8.

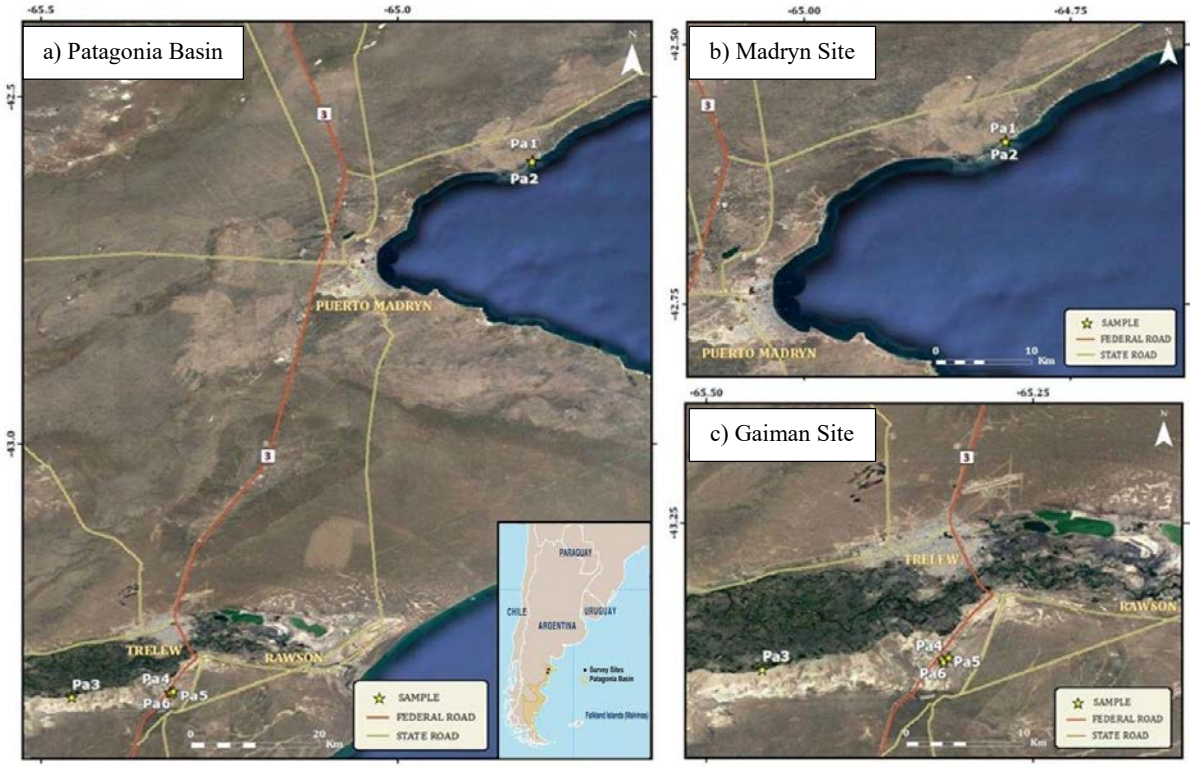

FIG. 1.7. Patagonia Basin (a) with highlighted Madryn- (b) and Gaiman (c) site.

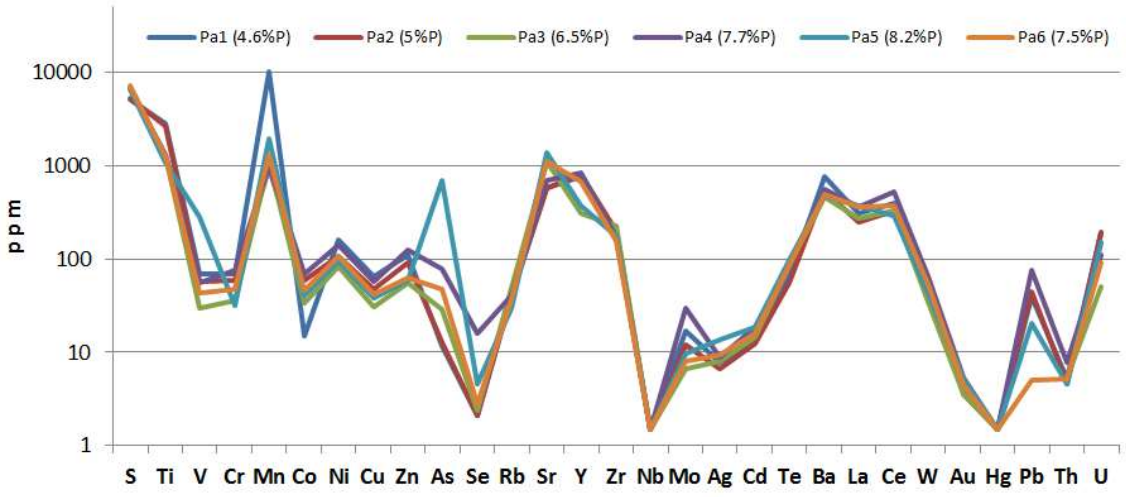

FIG. 1.8. Geochemical characterization by X-Ray Fluorescence of the Paleocene - Miocene Patagonia Basin.

Since 1997, no uranium has been produced in the country, neither privately nor by the state, while the uranium needs from operating nuclear power plants have been met with raw material imports from abroad (i.e. Uzbekistan, Czech Republic, Kazakhstan and Canada). The agricultural industry demands some 1 200 000 t phosphate fertilizer per year, of which approximately 75% is directly imported as mineral fertilizers and the remaining 25% is produced domestically from imported phosphate rock at a plant near Buenos Aires city. For example, in 2017 this plant processed approximately 300 000 t phosphate rock containing between 68 and 122 ppm uranium. A recent study estimated the amount of uranium that could theoretically be recovered from all phosphate fertilizers used in Argentina [3]. It is important to note that to date no economically exploitable deposit of phosphate rock has been found in Argentina and therefore commercial production of this material has not been carried out yet either. Likewise, it can be mentioned that in the Neuquén and North-Western basins, 1 000 000 t P_2O_5 have been evaluated as inferred resources, with grades between 2.5% and 6.3% P_2O_5. Regarding the unconventional uranium resources contained in phosphates, they have a low degree both of geological knowledge and confidence level of estimates. Besides, P+U comprehensive recovery tests have only been carried out on a laboratory scale yet, and therefore the respective technical feasibility and economic viability have not been established. However, the existence of favorable basins and different mineralization models suggest promising conditions to set up new projects to develop the phosphate potential in the country, taking into consideration the perspective of uranium co-recovery from these sources.

The project carried out and described here is essentially prospective and provides basic characterization studies that can guide future exploration activities in the basins under study or in other areas of the country that have mining interest in uranium linked to phosphate sediments. Likewise, other investigations at the level of characterization and comprehensive recovery tests could focus on other unconventional sources of uranium such as porphyry copper and carbonaceous shales.

Finally, it is noted that the IAEA project CRP on neutral uses of HTGRs would allow accounting for a better understanding of heat processing of low-grade phosphates. It is thought that this would aid to increase the socio-economic viability and technical feasibility to set up productive projects in the long term This process would aid to increase the socio-economic viability and technical feasibility to set up productive projects in the long term by providing positive implications regarding food and energy security.

1.2 UNITED REPUBLIC OF TANZANIA: URANIUM AND RARE EARTH ELEMENT RESOURCES IN MINJINGU PHOSPHATE ROCKS, TAILINGS AND FERTILIZER PRODUCTS

The United Republic of Tanzania is endowed with sedimentary-, igneous- and guano type phosphate rock resources [1.4]. The country's two principal phosphate rock deposits are the igneous Panda Hill deposit in the southern part of the United Republic of Tanzania and the lucastrine sedimentary Minjingu deposit in northern part of the United Republic of Tanzania [1.5]. Agriculture contributes to more than 25% of the gross domestic product (GDP) and employs around 75% of the labour force in the United Republic of Tanzania [1.6]. A large ammonia and urea fertilizer plant is currently constructed at Mtwara in the southern part of the United Republic of Tanzania with the goal to provide affordable fertilizer to farmers in the United Republic of Tanzania and also to the East- and Southeast African countries starting in 2022 [1.7]. At present, the Minjingu fertilizer plant is the only domestic source of mineral phosphate fertilizer, producing some 100 000 t beneficiated phosphate rock per year for direct use. 30 000 t fertilizer per year can be produced with a granulation plant [1.8]. This output does not cover the 400 000 t fertilizer needed annually in the United Republic of Tanzania [1.9].

According to the Minjingu Mines & Fertiliser Ltd. the Minjingu phosphate rock deposit consists of a proven 10 000 000 t hard and soft phosphate rock with 29–30 wt% P_2O_5 [1.8]. The soft phosphate rock consists of interbedded layers of soft and semi hard siliceous rock which is mined and beneficiated into different types of fertilizers. Phosphate rock can show elevated concentrations of trace elements [1.10, 1.11]. Minjingu phosphate rock show particularly high uranium levels. Bianconi first reported a maximum uranium content of 680 ppm [1.12]. While there is presently no legal limit for uranium in fertilizers, the German Commission for the Protection of Soils, proposed setting it to 50 mg U/kg P_2O_5 [1.11] or 167 mg/kg uranium for fertilizer with 30 wt% P_2O_5. Besides Bianconi's assessment, a similarly high value of 9550 Bq kg^{-1}. ^{238}U or 767 ppm eU (uranium equivalent) was reported by Mustonen and Annanmaki [1.13] for the uppermost phosphate rock layer, while reduced radiation levels of 2850 Bq kg^{-1} ^{226}Ra or 232 mg/kg eU was reported for the lower phosphate rock layer. Makweba and Holm [1.14] who analysed ground phosphate rock, two fertilizers (triple superphosphate and single superphosphate) and phosphogypsum from the Minjingu mine reported concentrations of 337 and 377 mg/kg eU using alpha-spectrometry and 408 and 481 mg/kg eU using gamma ray spectrometry for ground phosphate rock. Banzi et al. [1.15] complemented these works with activity measurements of phosphate rock, mine tailings, leaf vegetation, cattle flesh, chicken feed and surface water as well as ambient radiation background measurements around the Minjingu mine. Phosphate rock was assessed with 5760 Bq kg^{-1} ^{226}Ra or 468 mg/kg eU and mine tailings with 4250 Bq kg^{-1} ^{226}Ra or 346 mg/kg eU. Renewed interest in the unique composition at the Minjingu deposit motivated this work to systematically assess major elements (MgO, P_2O_5, CaO), heavy metals (Al, V, Cr, Fe, Mn, Co, Ni, Cu, Zn, Ba, Pb), uranium and thorium as well as selected REEs (Y, La, Ce, Pr, Nd, Sm, Eu, Gd, Dy, Ho, Er, Tm, Yb) in 10 Minjingu phosphate rock layers, four Minjingu mine tailings and the five presently produced Minjingu fertilizer products.

After mining, Minjingu phosphate rock is concentrated in a way that unwanted material is removed by handpicking. The remaining material is spread on the ground for sun drying. After two to three weeks, the dried ore is inserted into an impact crusher, preliminary sieved and passed into a hot air furnace in which the material is heated at 800–1000ºC. The dried ore is once more sieved before it is sent to gravity classification. Fertilizer powder that already has a high P_2O_5 content, is extracted after final sieving and applied directly on acidic soils in the

United Republic of Tanzania, South Africa, Zambia, Kenya, Uganda and Rwanda [1.8]. After gravity classification, fertilizer granules are produced in a granulation step. Lastly these granules can be blended to obtain the final fertilizer products Mazao, Nafaka and Top Dressing. Figure 1.9 provides a brief overview of the Minjingu phosphate rock process flow with the red boxes indicating at which point samples were drawn. Samples were collected from the phosphate rock (before hand-picking), the mine tailings, the fertilizer powder, the fertilizer granules, and the final fertilizer products.

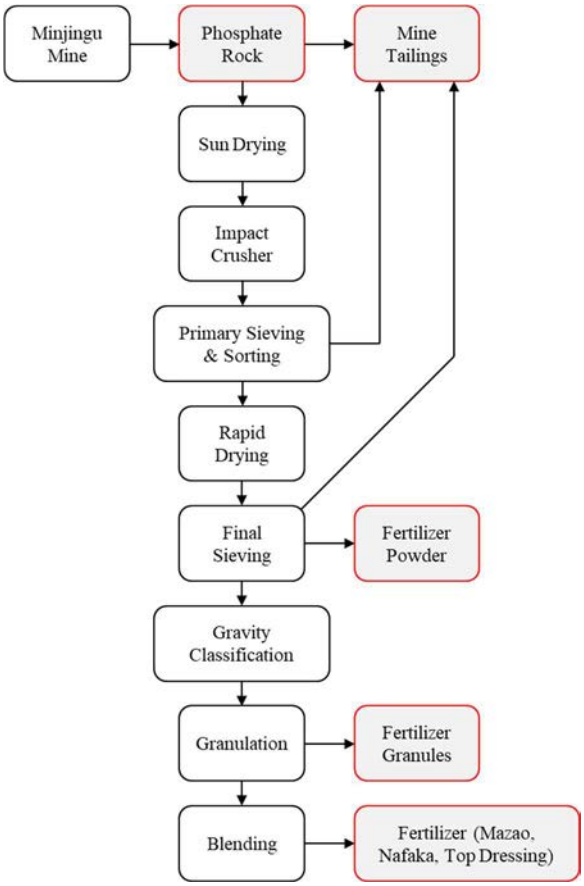

FIG. 1.9. Minjingu phosphate rock process flow chart.

In total, samples from ten different phosphate rock layers (L0–9) were analysed for this study. For each layer, ten 100 g dry samples were drawn, crushed, ground and oven dried at 100 ºC for 24 hours until a constant weight was reached, sieved in 150 µm standard sieves and poured into a bowl together with four spherical balls each of 3 mm radius, and inserted into a pulverizer for homogenization. The pulverizer was operated at a speed of 150 rpm for 30 minutes for each sample. After homogenization, 50 g from each representative sample were drawn and sent to Centre National de l'Energie, des Sciences et des Techniques Nucléaires in Morocco for Inductively Coupled Plasma-Mass spectrometry (ICP-MS) analysis. In the same way, three samples of each of the four different types of tailings (T1–2) were analysed. Samples from fertilizer powder, fertilizer granules and final fertilizer products (Mazao, Nafaka, granules, powder and top dressing) (F1–5) were digested directly. Table 1.1 describes the location of the 10 different phosphate rock layers (L0–9), 4 different tailings (T1–4) and 5 different fertilizer samples (F1–5) that were analysed in this study.

TABLE 1.1. OVERVIEW OF THE ANALYSED SAMPLES

Sample	Location
L0	0.0 m surface
L1	2.0 m phosphate layer (hard rock)
L2	2.5 m phosphate layer (soft rock)
L3	3.5 m phosphate layer (semi hard rock)
L4	4.5 m phosphate layer (soft rock)
L5	5.0 m phosphate layer (semi hard rock)
L6	6.0 m phosphate layer (semi hard rock)
L7	7.0 m phosphate layer (soft rock)
L8	8.0 m phosphate layer (semi hard rock)
L9	9.0 m phosphate layer (semi hard rock)
T1	Contaminated soil (surface)
T2	Overburden (surface)
T3	Tailing hip 1 (surface)
T4	Tailing hip 2 (surface)
F1	Fertilizer powder
F2	Fertilizer granules
F3	Mazao fertilizer
F4	Nafaka fertilizer
F5	Top dressing fertilizer

50 mg of each sample were digested in an acid mixture (3 mL HNO_3 ultrapure 60% + 5 mL HF 40%) at high pressure and temperature by microwave SPEEDWAVE4 (BERGHOF). After cooling, the liquid was transferred quantitatively in 50 mL flasks and filled to the desired volume with high purity water. Nitric acid and ultra-pure hydrofluoric acid were purchased from Merck. The measurements were conducted using the XSERIES 2 ICP-MS Thermo Fischer Scientific. The spectrometer has been optimized to provide the minimum values of CeO^+/Ce^+ and $Ba2^+/Ba^+$ and optimal density of analyses. External calibration was performed using single-component CertiPrep SPEX solutions and lanthanoids of the ASTASOL mixture (AN 9088 (MN)). The correlation coefficient for all the calibration curves was 0.99. SRM 694 Western Rock Phosphate (National Institute of Standards and Techniques, Gaithersburg, MD, USA) was used as standard reference material to verify the accuracy of the method. Rh 0.01 mg/L and Ir 0.01 mg/L were used for internal procedures. The results of this study are

presented in Fig. 1.10 (phosphate rock), Fig. 1.11 (mine tailings) and Fig. 1.12 (final fertilizer products). The major elements measured in phosphate rock were MgO, CaO and P_2O_5 as shown in Fig. 1.10.

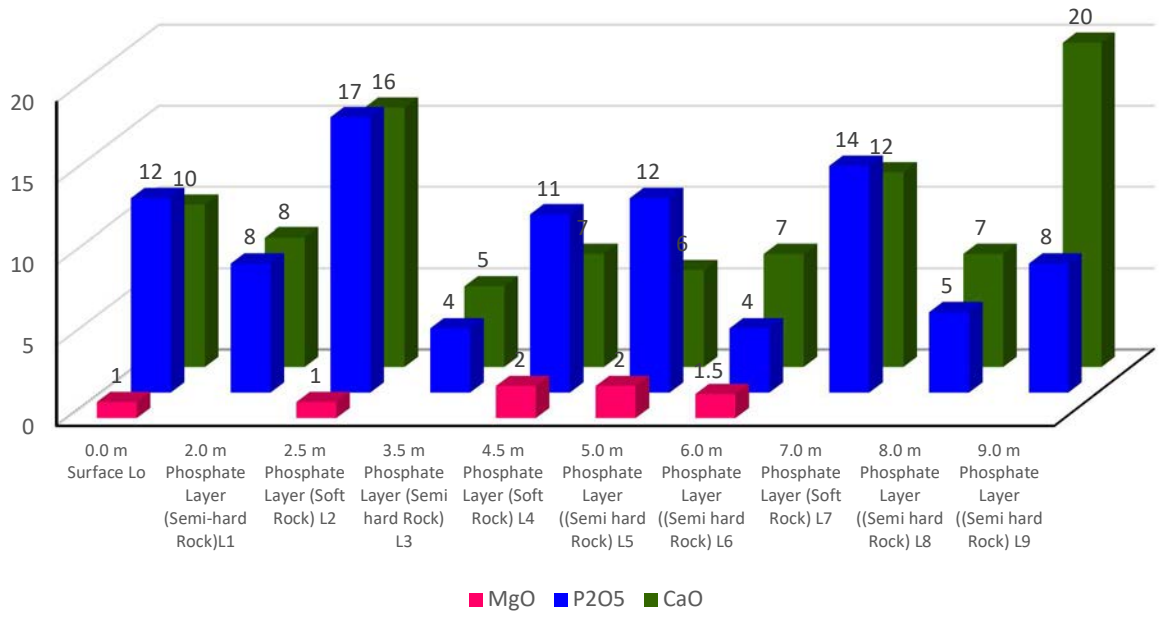

FIG. 1.10. Major elements in Minjingu phosphate rock process.

The average concentration of major elements of concern in the phosphate rock include MgO, CaO and P_2O_5. The concentrations of major elements in Minjingu phosphate rock, tailings and fertilizers were assessed, based on criteria of saleable phosphate rock conditions, high P_2O_5 content (>30%), low CaO/P_2O_5 ratio (<1.6) and low MgO content (<1%) [16]. The average concentration of P_2O_5 in the phosphate rock layers is about 10%. The concentration of MgO ranges between 1% and 4% which is slightly higher than the recommended value of 1%. The ratio of CaO/P_2O_5 ranges between 0.5 and 1.5, while the average at 1.16 is comparable to the required values for other commercial phosphate rock. Moreover, the concentration of P_2O_5 is less than 30%. This requires ore upgrade either through the wet or the thermal process. The concentrations of MgO, CaO and P_2O_5 were determined from mine tailings and overburden stockpiled around the mine area as shown in Fig. 1.11.

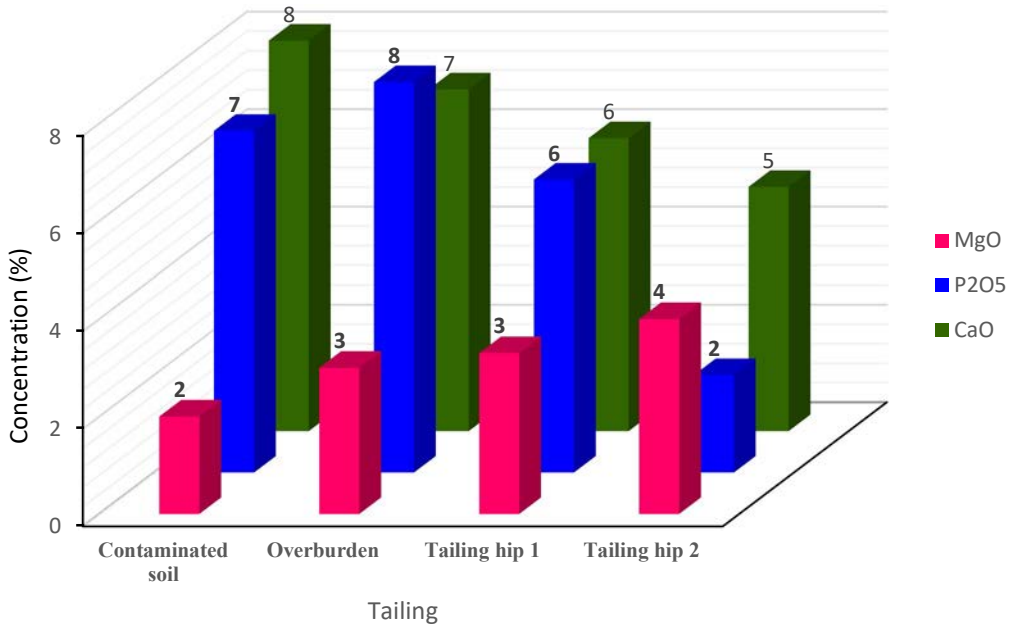

FIG. 1.11. Major elements in Minjingu tailings.

The average concentration of P_2O_5 in mine tailings is 6%, which is comparable to that of semi hard phosphatic layers.

The Minjingu phosphate mine and fertilizer company produce five types of fertilizers from Minjingu phosphate rock. The phosphate fertilizers produced are Mazao, Nafaka, powder, granules, and top dressing. The concentrations of MgO, CaO and P_2O_5 were determined as indicated in Fig. 1.12.

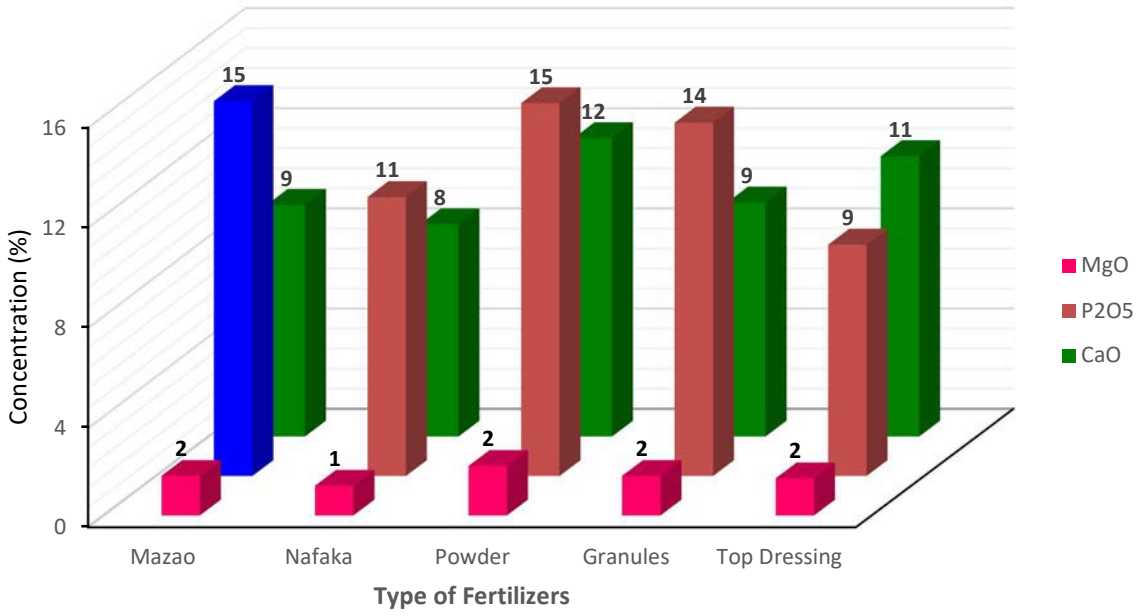

FIG. 1.12. Major elements in Minjingu phosphate fertilizers.

The average concentration of P_2O_5 is 13%, which is less than the minimum recommendable concentration of >30% for commercial phosphate fertilizers. However, it has been reported that Minjingu phosphate fertilizer is agronomically effective for direct application in acid soils, similar to superphosphate fertilizer [1.17]. The concentrations of uranium and REEs in Minjingu phosphate rock, mine tailings and final fertilizer products were determined as shown in Figs 1.13, 1.14 and 1.15 below.

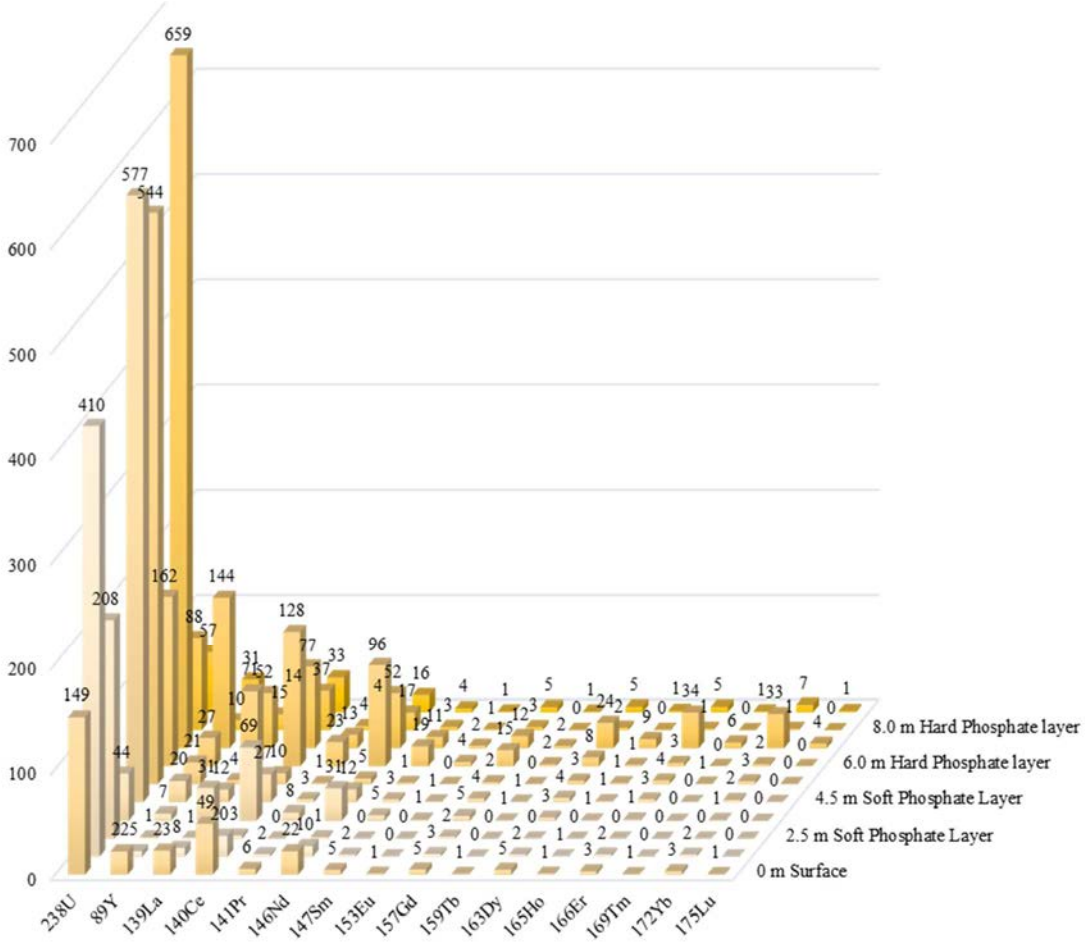

FIG. 1.13. Rare earth elements (REEs) and uranium concentrations in Minjingu phosphate rock.

The concentrations of uranium and REEs in mine tailings were determined and are presented in Fig. 1.14.

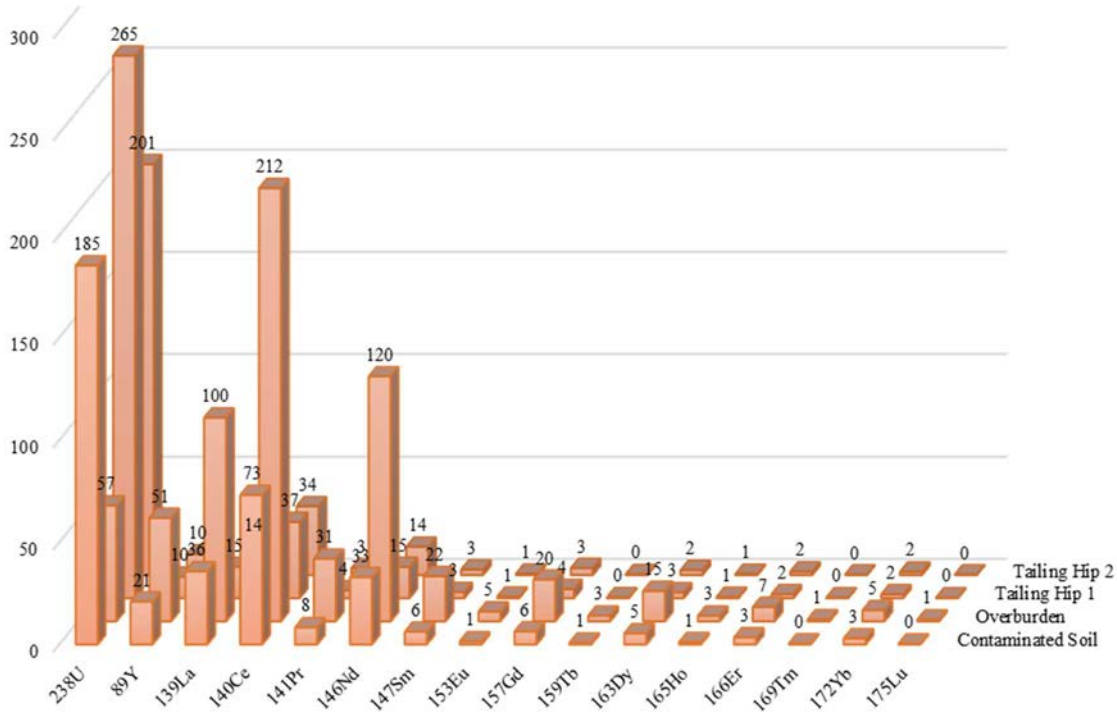

FIG. 1.14. Rare earth elements (REEs) and uranium concentrations in Minjingu mine tailings.

The mine produce five types of fertilizers from Minjingu phosphate rock. The phosphate fertilizers produced are Mazao, Nafaka, powder, granules and top dressing. The concentrations of MgO, CaO and P_2O_5 were determined as indicated in Fig. 1.15.

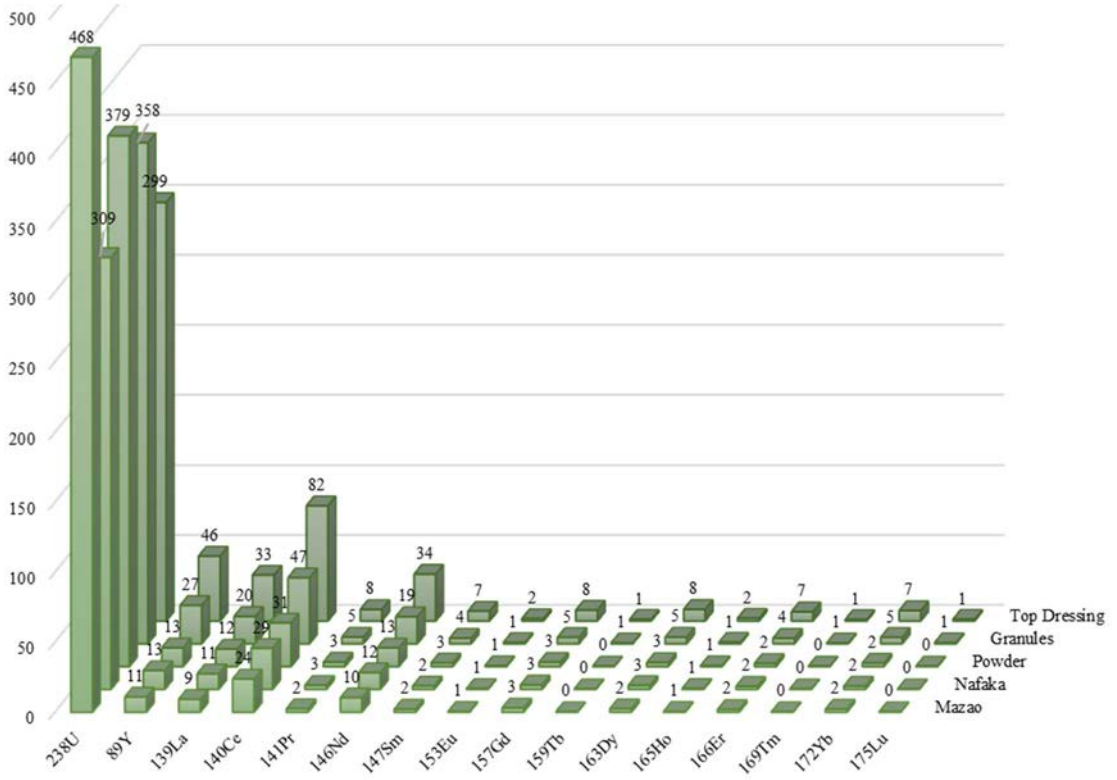

FIG. 1.15. Rare earth elements (REEs) and uranium concentrations in Minjingu final fertilizer products.

The uranium concentrations in Minjingu phosphate rock and fertilizers range from 149 to 659 ppm with an average of 387 ppm. Previous estimates on an average uranium concentration of 390 ppm in Minjingu phosphate rock agree well with the results of this study. The Minjingu Mines & Fertilizers Ltd. reports that the annual phosphate production is about 100 000 t. This means that some 39 t uranium are mined as an accompanying element at the Minjingu mine each year. The available and recoverable amount of uranium that can be recovered from the 10 Mt of Minjingu phosphate using state of the art techniques, were estimated and are presented in Table 1.2.

TABLE 1.2. UNCONVENTIONAL URANIUM (U) RESOURCES AT THE MINJINGU PHOSPHATE ROCK DEPOSIT IN THE UNITED REPUBLIC OF TANZANIA.

Phosphate rock resources	Estimated U concentration	Estimated U content	Estimated recoverable U
10 000 000 t	390 ppm	3900 t	2359 t

The observed difference between the available and recoverable uranium from Minjingu phosphate rocks are based on the assumption that 72% of the phosphate production, is devoted to phosphoric acid with an overall recovery rate of 84%.

Minjingu phosphate rock is mostly used for direct application, so that extracting radiotoxic uranium may not only be relevant from a resource conserving point of view, but also be beneficial for the environment and in particular for human health. The renewed interest in the unique composition of Minjingu phosphate rock motivated this work to systematically assess uranium and REEs in 10 Minjingu phosphate rock layers, 4 Minjingu mine tailings and the 5 presently produced Minjingu final fertilizer products.

In addition to uranium, Minjingu phosphate rock contains significant concentrations of REEs. As part of this work, average REE concentrations of above 500 ppm were measured in several Minjingu phosphate rock layers and mine tailings. This means that the Minjingu plant could, in addition to phosphoric acid, produce significant amounts of unconventional uranium and REEs which could enhance the economy and the GDP of the United Republic of Tanzania.

REFERENCES TO CHAPTER 1

[1.1] LEANZA, H., SPIEGELMAN, A., HUGO, C., MASTANDREA, O., OBLITAS, C., "Phanerozoic sedimentary phosphatic rocks of Argentina", in Phosphate Rocks Resources, Cambridge 2(24) (1989).

[1.2] CASTRO, L.N., SCASSO, R.A., "Phosphate deposits in Argentina: State of the art", Conf. III, The 3rd Int. Conf. Valorization of Phosphates and Phosphorus Compounds: Phosphate Fundamentals, Processes and Technologies in a Changing World, Marrakesh (2009).

[1.3] LÓPEZ, L., CASTRO, L.N., SCASSO, R.A., GRANCEA, L., TULSIDAS, H., HANEKLAUS, N., Uranium supply potential from phosphate rocks for Argentina's nuclear power fleet, Resour. Policy **62** (2019) 397–404.

[1.4] VAN KAUWENBERGH, S.J., Overview of phosphate deposits in East and Southeast Africa, Fertil. Res. **30** (1991) 127–150.

[1.5] MCHIHIYO, E.P., Phosphate potential in Tanzania, Fertil. Res. **30** (1991) 177–180.

[1.6] BIRYABAREMA, E., Tanzania to Build $3-B Fertilizer Plant, http://www.hydrocarbonprocessing.com/news/2016/05/tanzania-to-build-3-b-fertilizer-plant (Accessed on 11 March 2018).

[1.7] Ng'wanakilala Tanzania to begin Building $3 bln Fertiliser Plant this Year, https://www.reuters.com/article/tanzania-investment/tanzania-to-begin-building-3-bln-fertiliser-plant-this-year-idUSL5N18H192 (Accessed on 18 March 2018).

[1.8] Minjingu Mines & Fertilizer Ltd. Minjingu Mines http://minjingumines.com/ (Accessed on 11 March 2018).

[1.9] TAIRO, A., Tanzania Spells Out Pricing Guidelines for Fertiliser, http://www.theeastafrican.co.ke/business/Tanzania-spells-out-pricing-guidelines--for-fertilisers-/2560-4075954-gt2bka/index.html (Accessed on 11 March 2018).

[1.10] CHEN, M., GRAEDEL, T.E., The potential for mining trace elements from phosphate rock, J. Clean. Prod. **91** (2015) 337–346.

[1.11] KRATZ, S., SCHICK, J., SCHNUG, E., Trace elements in rock phosphates and P containing mineral and organo-mineral fertilizers sold in Germany, Sci. Total Environ. 542 (2016) 1013–1019.

[1.12] BIANCONI, F., "Uranium geology of Tanzania", Proc. Uranium Symposium on the Occasion of the DMG-GDMB-SGA Joint Meeting: Aachen, Germany, Monograph Series on Mineral Deposits: No. 27, Friedrich G., Gatzweiler R., Vogt, J., Eds, Bornträger: Berlin, Germany (1985) 11–25.

[1.13] MUSTONEN, R., ANNANMAKI, M., Studies on the Radiation Exposure of Workers in Connection with Processing of the Minjingu Phosphate in Tanzania, Supplementary Report to the Finnish Center for Radiation and Nuclear Safety, 666/622/87 (1988).

[1.14] MAKWEBA, M.M., HOLM, E., The natural radioactivity of the rock phosphates, phosphatic products and their environmental implications, Sci. Total Environ. **133** (1993) 99–110.

[1.15] BANZI, F.P., KIFANGA, L.D., BUNDALA, F.M., Natural radioactivity and radiation exposure at the Minjingu phosphate mine in Tanzania, J. Radiol. Prot. **20** (2000) 41–51.

[1.16] PTÁČEK, P., Mining and Beneficiation of Phosphate Ore. In open access peer-reviewed Chapter DOI:10.5772/62215 (2016).

[1.17] SZILAS, C., KOCH, C.B., MSOLLA, M.M., BORGGAARD, O.K., The reactivity of Tanzanian Minjingu phosphate rock can be assessed from the chemical and mineralogical composition, Geoderma **147** (2008) 172–177.

CHAPTER 2 CASE STUDIES ON UNCONVENTIONAL URANIUM AND THORIUM RECOVERY

2.1 EGYPT: URANIUM RECOVERY WITH LOW-COST AL_2O_3-GRAFTED KAOLINITE

Uranium is a radiotoxic element that is present in our environment. It can enter water bodies as a result of leaching from natural deposits, release from mine- and mill tailings, emissions from the nuclear industry, the combustion of coal [2.1] and other fuels as well as in the use of mineral fertilizers that can contain considerable amounts of accompanying natural uranium [2.2]. Chemical precipitation, ion exchange, liquid membrane extraction, solvent extraction (SX) and adsorption are the methods commonly used to remove uranium from wastewaters. Adsorption is one of the most effective methods for the removal of uranium (VI) from liquid waste, frequently reaching recovery efficiencies well above 90%. Three types of adsorbents can be differentiated: natural and modified clay minerals, synthetic adsorbents and bio-sorbents. Natural and modified clay minerals may have an advantage over the other mentioned adsorbents, in a way that they can be easily obtained at low prices, while showing high chemical stability during the adsorption process.

Three or four main groups of clays: kaolinites, montmorillonite-smectites, illites, and chlorites are usually differentiated. Chlorites are sometimes classified as a separate group within the phyllosilicates. Roughly 30 different types of pure clays exist in the aforementioned categories. Uranium (VI) adsorption was investigated by numerous researchers, using pure clays as well as naturally occurring clays, that contain mixtures of different clay types, along with other weathered minerals.

This work investigates uranium (VI) adsorption, using Al_2O_3 grafted kaolinite. Kaolinite and kaolin (natural rocks rich in kaolinite) have been used before for uranium (IV) adsorption from aqueous solutions. Payne et al. [2.3], Krepelova et al. [2.4] as well as Sachs and Bernhard [2.5] investigated uranium (IV) adsorption with treated Georgia kaolinite. Guerra et al. [2.6, 2.7] treated Amazon kaolinite and Campos et al. [2.8] natural kaolinite from Portugal. Chemically pure kaolinite was further treated in numerous ways and used for uranium (VI) adsorption from aqueous solution [2.9–2.15]. Ohnuki et al. [2.16] further accumulated uranium (IV) by a bacteria in a slurry of kaolinite clay. Additionally, Gao et al. [2.17] and Taha et al. [2.18] investigated uranium recovery from intermediate products of the phosphate fertilizer industry, using treated kaolinite materials.

In this work low-cost adsorbents, fabricated from aluminium oxide (Al_2O_3) grafted kaolinite that can remove uranium (IV) from an aqueous solution, are presented. The influence of contact time, solution pH, initial uranium concentration, adsorption temperature and adsorbent amount on the adsorption of uranium (VI) ions from a uranium standard solution was examined. The aforementioned experiments were used to determine optimized process conditions that can be used for the treatment of an exemplary liquid waste sample with 100 mg/L uranium.

A uranium standard solution assaying 1000 mg/L was prepared by dissolving 0.1782 g uranyl acetate [UO_2 $(CH_3COO)_2.2H_2O$] (purchased from BDH Chemicals Ltd. Poole, UK) in 100 mL distilled water. An actual liquid waste sample (raffinate solution) that was provided by the Uranium Purification Unit of the Nuclear Materials Authority of Egypt was further used for the experiments. The chemical composition of the waste sample is provided in Table 2.1.

TABLE 2.1. CHEMICAL COMPOSITION OF THE PROVIDED LIQUID WASTE SAMPLE (RAFFINATE SOLUTION).

Constituent	**Content**
Fe_2O_3	0.60 g/L
HNO_3	1 M
U	100 mg/L
Ca^{2+}	1.9 g/L

Uranium was analysed, using the Arsenazo-III spectrophotometric method described by Marczenko [2.19]. The absorbance of the formed uranium Arsenazo-III complex was measured at 650 nm against proper standard solutions using a Perkin-Elmer, USA UV/VIS spectrophotometer. SO_4^{2-} and Fe^{3+} were determined spectro-photometrically. The initial pH of the working solution was adjusted using a buffer solution.

Commercial kaolinite clay samples were obtained from the Al-Amier Ceramic Company, Egypt. The chemical composition of the kaolinite samples is provided in Table 2.2.

TABLE 2.2. CHEMICAL COMPOSITIONS OF THE PROVIDED KAOLINITE SAMPLES.

Constituent	**wt%**
SiO_2	52.65
Al_2O_3	28.31
Fe_2O_3	4.71
TiO_2	1.54
CaO	0.31
MgO	0.18
Na_2O	0.19
Loss of ignition	11.27

Obtained kaolinite samples were crushed, ground and sieved to grain sizes of 90 μm, using the American Standard Test Sieve Series. Samples were subsequently analysed using X-ray powder diffraction (XRD). Figure 2.1 shows the XRD pattern of the kaolinite samples.

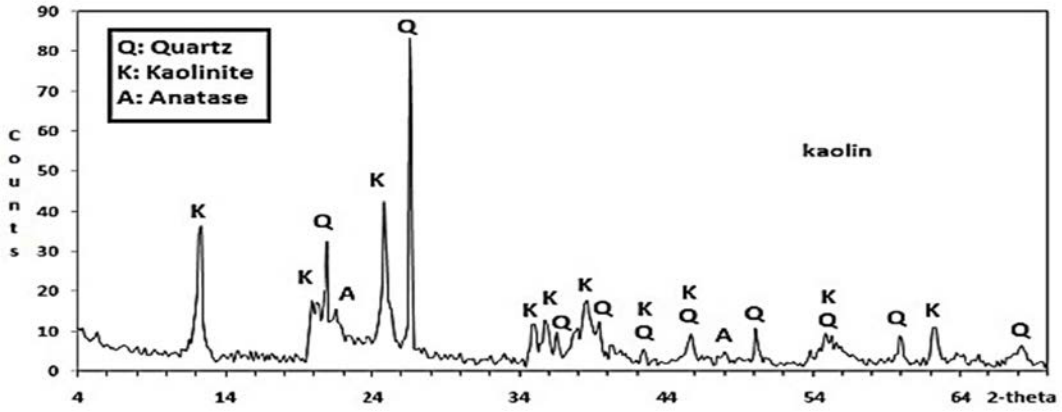

FIG. 2.1. XRD pattern of the natural kaolinite samples.

Kaolinite samples were grafted using Al_2O_3, following the description provided by Ding et al. [2.20] who grafted natural clay with NiO. The grafting process involved the following steps: 10 g of the dried clay was added to 100 mL of a 0.5 M $AlCl_3$ solution and mixed carefully for about 10 min. Then, 100 mL of 1 M NaOH solution was gradually added to the mixture. The resulting mixture was left to react for 1 hour under energetic stirring at 70°C. Subsequently the kaolinite clay was repeatedly washed (to be nearly neutral), centrifuged and dried at 105°C. Finally, the dried clay was ground into powder form and heated in air at 600°C for 1 hour in a muffle furnace.

A series of batch experiments were conducted with the standard uranium synthetic solution, to understand the effect of the contact time, ph, initial uranium concentration, temperature, and adsorbent amount on the adsorption performance. The attained results were used to determine Langmuir- and Freundlich isotherms. All adsorption experiments were performed by mixing 0.01 g of the grafted kaolinite with 15 mL of the uranium synthetic solution (of 100 mg/L initial uranium concentration) using a magnetic stirrer. The adsorbed amounts of uranium were determined by comparing differences between the equilibrium concentrations and the initial concentrations. The amount of uranium retained in the solid phase, q_e [mg/g] was calculated using the following equation:

$$q_e = (C_0 - C_e)\frac{V}{m} \quad (2.1)$$

where

C_o and C_e are the initial concentrations [mg/L] and the equilibrium concentrations [mg/L] of the uranium;

V [L] is the volume of the aqueous phase;

m [g] is the weight of the grafted clay material.

The per cent of ions that were successfully removed from the aqueous phase can be calculated using the following equation:

$$Uranium\ adsorption\ \% = \frac{C_0 - C_e}{C_0} 100 \quad (2.2)$$

The distribution coefficient (K_d) of uranium between the aqueous bulk phase and the solid phase was calculated using the following equation:

$$K_d = \frac{C_0 - C_e}{C_0} \frac{V}{m} \quad (2.3)$$

To elute (desorption process) the loaded uranium from the grafted kaolinite, the kaolinite was first washed with a diluted nitric acid solution that had a molarity equal to that of the working liquor. Afterwards, several eluents (ascorbic acid, citric acid, H_2O, HCl, HCl and NaCl acidified by H_2SO_4) were tested. Uranium distribution in this study was done using the hydra-medusa chemical equilibrium software.

The effect of the contact time was examined by contacting a fixed mass (0.01 g) of the grafted kaolinite with the uranium solution (15 mL) having a concentration of 100 mg/L. Experiments were conducted at room temperature with a pH = 4 and a volume phase ratio of 0.66 g grafted kaolinite per litre solution. The studied time intervals ranged from 1 to 180 min. Results are depicted in Fig. 2.2.

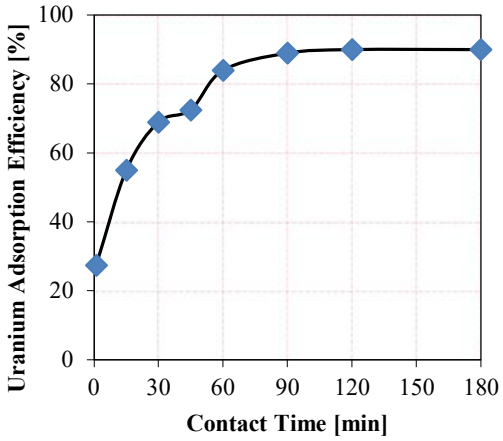

FIG. 2.2. Effect of the contact time on the uranium adsorption efficiency.

After 15 minutes contact time the uranium adsorption efficiency is approximately 55%. Further increasing the contact time to 60 minutes, increases the uranium adsorption efficiency to approximately 84%. This efficiency could further be increased to 89% after 90 min contact time. After 90 min contact time, the absorption efficiency could not be further increased.

The influence of the pH of the solution on the uranium adsorption of the grafted kaolinite was examined, using a fixed mass of grafted kaolinite (0.01g) and a fixed volume (15 mL) of the prepared standard uranium solution (100 mg/L) again at 25°C for 90 min. A volume phase ratio of 0.66 g grafted kaolinite per litre solution was chosen. The examined pH values ranged from 0.6 to 8.2. The determined uranium adsorption efficiency, dependent on the pH of the solution and is shown in Fig. 2.3.

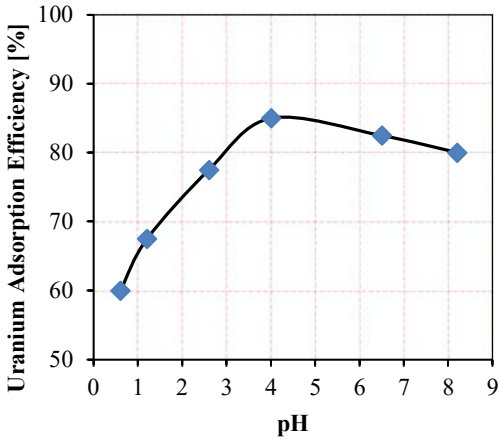

Fig. 2.3. Effect of the pH of the solution on the uranium adsorption efficiency.

Results depicted in Fig. 2.3 shows that the uranium adsorption efficiency increases gradually with increasing pH values until pH = 4 is reached, at which point the uranium adsorption efficiency reaches a maximum of approximately 85%. At pH = 6 the uranium adsorption efficiency slightly deceases to about 82%. The last experiment was conducted with pH = 8.2 and a uranium adsorption efficiency of approximately 80%. These results show that a relatively wide pH range from ph = 4 to pH = 8 results in good uranium adsorption efficiencies.

Uranium adsorption is strongly dependent on the pH of the solution. At low (≤4) pH values, the number of H_3O^+ ions exceed the numbers of UO_2^{2+} ions several times and the surface is most likely covered with H_3O^+ ions that reduce the number of binding sites available for the adsorption of UO_2^{2+} ions. At high (≥4) pH values on the other hand, more H_3O^+ ions leave the clay mineral surface, making the sites available for a cation exchange with the UO_2^{2+} ions, so that hydrolysis precipitation can start, due to the formation of complexes such as $UO_2(OH)^+$, $(UO_2)_2(OH)_2^{2+}$, $(UO_2)_3(OH)_5^{3+}$ and $(UO_2)(OH)_2$, in the aqueous solution that increases uranium (VI) adsorption [2.21–2.25].

The aqueous speciation distribution of uranium was calculated, using hydra-medusa and results are shown in Fig. 2.4. The results indicate that the complexes of $UO_2(NO_3)^+$ and UO_2^{2+} were the predominant species at the pH range of 0–4 with a mean total per cent of 34% and 66% respectively. U-hydroxide complexes start to dominate the aqueous phase at pH near 3 of $(UO_2)_2(OH)_2^{2+}$ and $(UO_2)_2OH^{3+}$. At pH 4.5, the $UO_2(OH)_2.H_2O_{(C)}$ became the major species with about 100% of total concentration at pH range from 5 to 12, while at pH 11, $UO_2(OH)_3^-$ and at pH 13 and $UO_2(OH)_4^{2-}$ became the major species with nearly 100% of the total concentration.

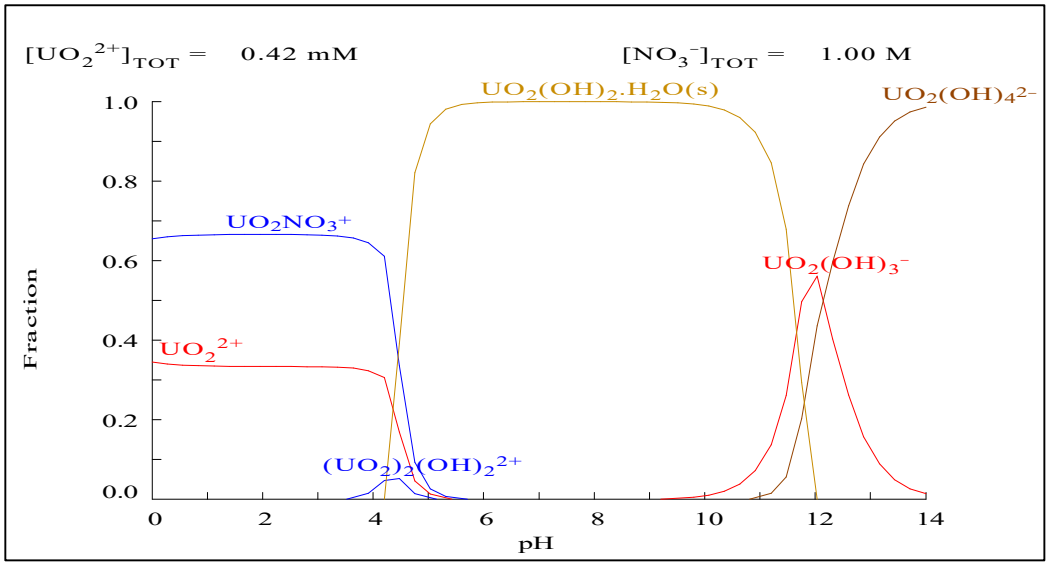

FIG. 2.4. Expected aqueous speciations of U(VI) as a function of pH calculated using the hydra-medusa equilibrium calculation program.

The effect of the initial uranium concentration on the uranium adsorption of the grafted kaolinite was determined, using the fixed mass of grafted kaolinite (0.01 g), and a fixed volume (15 mL) of prepared standard uranium solution (100 mg/L) at 25°C for 90 min. A volume phase ratio of 0.66 g grafted kaolinite per litre solution was chosen.

The studied initial uranium concentrations ranged from 100 mg/L to 600 mg/L. The obtained results are shown in Fig. 2.5. The uranium adsorption efficiency decreases significantly with an increasing initial uranium concentration. For the efficient use of the grafted kaolinite material, the initial uranium concentration in a liquid waste best does not exceed 100 mg/L. The obtained data further indicates that the capacity of the grafted kaolinite adsorbent is approximately 100 mg uranium per g.

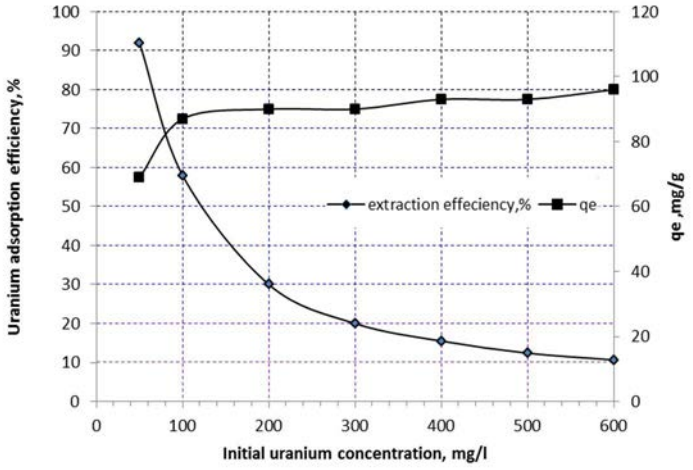

Fig. 2.5. Effect of the initial uranium concentration on the uranium adsorption efficiency.

Several common adsorption isotherm models were considered to fit the attained isotherm data under the equilibrium adsorption of the grafted kaolinites. Most common examples of these models are Langmuir, Freundlich and Dubinin-Radushkevich (D-R) isotherms. The Langmuir model assumes that the adsorption occurs uniformly on the active sites of the sorbent, and

once a sorbate occupies a site, no further sorption can take place at this site. The Langmuir model is commonly expressed by Eq. (2.4) [2.26–2.28].

$$\frac{C_e}{q_e} = \frac{1}{bQ_0} + \frac{C_e}{Q_0} \tag{2.4}$$

where

Q_o and b the Langmuir constants, are the saturated monolayer sorption capacity and the sorption equilibrium constant, respectively.

A plot of C_e/q_e versus C_e would result in a straight line with a slope of $(1/Q_o)$ and intercept of $1/bQ_o$ as shown in Fig. 2.6. The Langmuir parameters given in Table 2.3 can be used to predict the affinity between the sorbate and sorbent using the dimensionless separation factor R_L that is provided in Eq. (2.5).

$$R_L = \frac{1}{1+b_{\ 0}} \tag{2.5}$$

The R_L value indicates the type of isotherm to be irreversible ($R_L = 0$), favourable ($0<R_L<1$), linear ($R_L = 1$) and unfavourable ($R_L>1$). The values of R_L for the adsorption of uranium (VI) onto the grafted kaolinite material are shown in Fig. 2.6. Results shown in Fig. 2.7 indicate that the adsorption of uranium (VI) is more favourable at higher initial uranium (VI) concentrations than at lower concentrations.

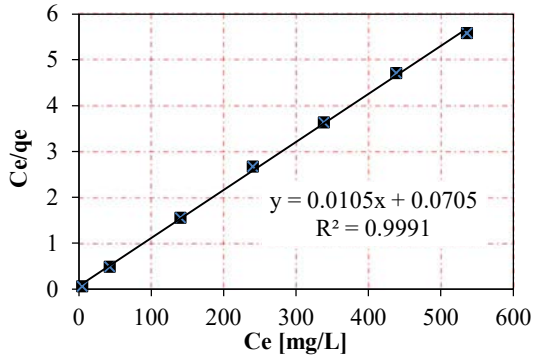

FIG. 2.6. Langmuir isotherm indicating the adsorption of uranium on the grafted kaolinite material.

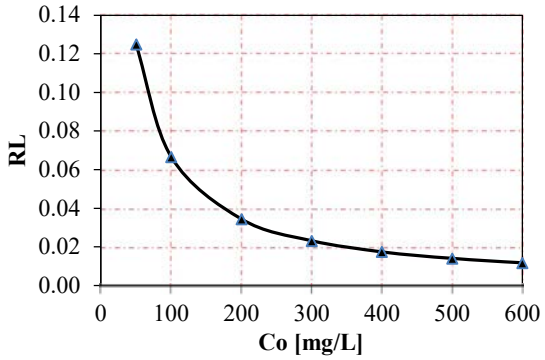

FIG. 2.7. Separation factor R_L of uranium (VI) adsorbed on the grafted kaolinite material.

In the Freundlich isotherm the adsorbed solute at equilibrium, q_e, is related to the concentration of solute in the solution, C_e, as shown in Eq. (2.6):

$$q_e = K_F C_e^{\,1/n} \tag{2.6}$$

This expression can be linearized as following:

$$\log q_e = \log K_F + \left(\frac{1}{n}\right) \log C_e \tag{2.7}$$

where

K_F and n are the Freundlich constants which represent sorption capacity and sorption intensity.

A plot of ($logq_e$) versus ($logC_e$) would result in a straight line with a slope of $1/n$ and intercept of log K_F as shown in Fig. 2.8. The respective Freundlich constants are also provided in Table 2.3.

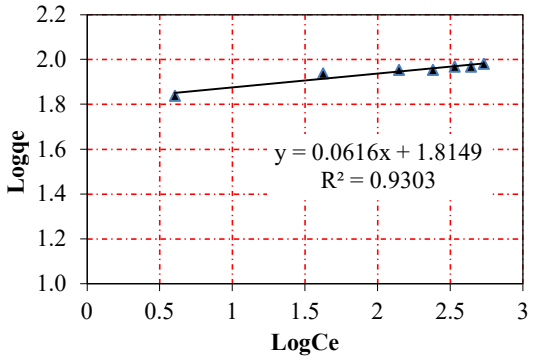

FIG. 2.8. Freundlich isotherm for adsorption of uranium on the grafted kaolinite material.

The Dubinin-Radushkevich (D-R) isotherm model was applied to the data, to better understand the heterogeneity of the surface energies of adsorption and the characteristic porosity of the adsorbent. The linear form of the D-R isotherm is given by the following equation:

$$ln\, q_e = ln\, q_m - \beta\, \varepsilon^2 \tag{2.8}$$

where

q_m is the maximum mass of ions that can be sorbed onto a unit weight of the grafted kaolinite material, i.e. sorption capacity (mg/kg);

β is the constant related to the sorption energy (mol^2/kJ^2);

ε is the polanyi potential = RT ln(1 + 1/Ce);

R is the gas constant (mol/kJ);

T is the absolute temperature (K).

The mean free energy of sorption can be calculated using the following equation:

$$Ea = \frac{1}{\frac{1}{2}(-2\beta)} \tag{2.9}$$

The D-R plots of $\ln q_e$ versus ε^2 for the sorption of uranium ions on the grafted kaolinite are shown in Fig. 2.9. Linear regression analysis using pairs of $\ln q_e$ and ε^2 resulted in the derivation of q_m, β and the correlation factor (R^2). These parameters are listed in Table 2.3.

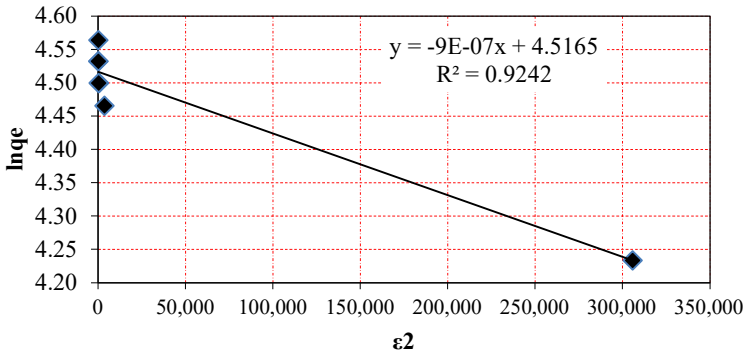

FIG. 2.9. Dubinin-Radushkevich (D-R) isotherm for adsorption of uranium on the grafted kaolinite material.

When comparing the determined isotherms with the experimental data, the Langmuir provided the best fit, followed by the D-R isotherm and the Freundlich isotherm.

TABLE 2.3. LANGMUIR, FREUNDLICH AND DUBININ-RADUSHKEVICH (D-R) ISOTHERM PARAMETERS FOR URANIUM ADSORPTION ON THE GRAFTED KAOLINITE MATERIAL.

Langmuir model parameters			**Freundlich model parameters**			**D-R model parameters**			
Q_0 [mg/g]	**b [L/mg]**	**R^2**	**1/n**	**K_f [mg/g]**	**R^2**	**β [mol²/kJ²]**	**Q_m [mg/kg]**	**E_{ads} [kJmol⁻¹]**	**R^2**
95.23	0.14	0.99	0.06	65.29	0.93	9×10^{-7}	91.51	1	0.92

The effect of the temperature on the uranium adsorption of the grafted kaolinite was determined using the fixed mass of grafted kaolinite (0.01 g) in a fixed volume (15 mL) of prepared standard uranium solution (100 mg/L) at 25°C for 90 min. Again, a volume phase ratio of 0.66 g grafted kaolinite per litre solution was chosen. Several experiments were carried out at different temperatures ranging from 25 to 60°C. The experimental results are presented in Fig. 2.10. The obtained results indicate that the uranium adsorption efficiency was not affected by the applied temperatures.

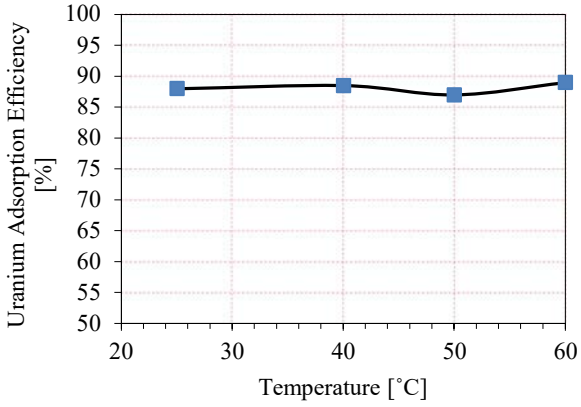

FIG. 2.10. Effect of temperature on the uranium adsorption efficiency.

From an economic point of view, it is desirable to use as little adsorbent material as possible. The influence of the adsorbent amount on the uranium uptake is shown in Fig. 2.11. A series of adsorption experiments was conducted, using different adsorbent doses ranging from 0.25 g to 2.66 g grafted kaolinite per litre solution. The uranium standard solution (100 mg U/L at room temperature with 90 min shaking time and pH = 4) from previous experiments was used again for this analysis. The obtained results show that the adsorption efficiency decreases with an increasing adsorbent amount (adsorbent dose). This observation is most likely the result of increased aggregation. Consequently, the available adsorptive capacity of adsorbent is not fully utilized at higher adsorbent doses.

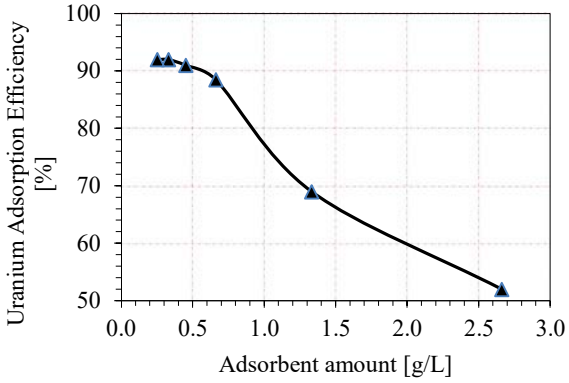

FIG. 2.11. Effect of the adsorbent amount on the uranium adsorption efficiency.

Desorption (elution) of uranium from the loaded grafted kaolinite material was studied by contacting a loaded amount (0.01 g) of loaded grafted kaolinite with ascorbic acid, NaCl acidified with H_2SO_4, HCl, water and citric acid. The elution efficiency was calculated by the change between the initial and the final concentration of uranium. The results of desorption experiments are shown in Fig. 2.12. Ascorbic acid achieved the best results eluting about 95% of the loaded uranium.

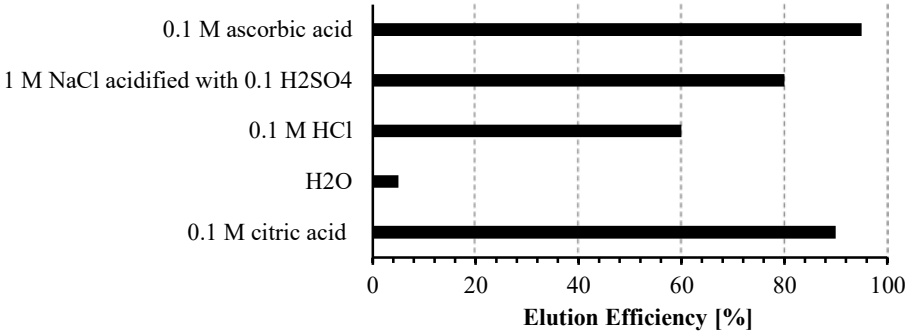

FIG. 2.12. Elution yields using different eluent reagents.

The Fourier-transform infrared spectroscopy (FT-IR) patterns of the grafted kaolinites before and after uranium (VI) adsorption are compared in Fig. 2.13. Before the uranium adsorption, the O–H stretching vibration transpired at 3775.72 and 3515.93 cm^{-1}. This may be credited to the silanol (Si–OH) group and water molecules (H–O–H) on the surface. The band at 1598.99 cm^{-1} for the bending of Al–O–H and the stretching occurred in the band at 1081.1 cm^{-1}. The bands for Al–O–Si stretching and bending vibrations were at 818.9 and 460.1 cm^{-1} [2.29]. After the adsorption of uranium (VI), the bands of most groups had changed in their amplitudes and locations. The O–H stretching vibration bands shifted from 3515.9 to

3485.62. In the meantime, the adsorption intensity greatly decreased which indicates that the –OH group played an important role in the creation of the uranium bonds. We further observed that a new peak appeared at 1384.5 cm^{-1}. This may be the characteristic peak of the uranyl ions adsorbed onto the grafted kaolinite material [2.30].

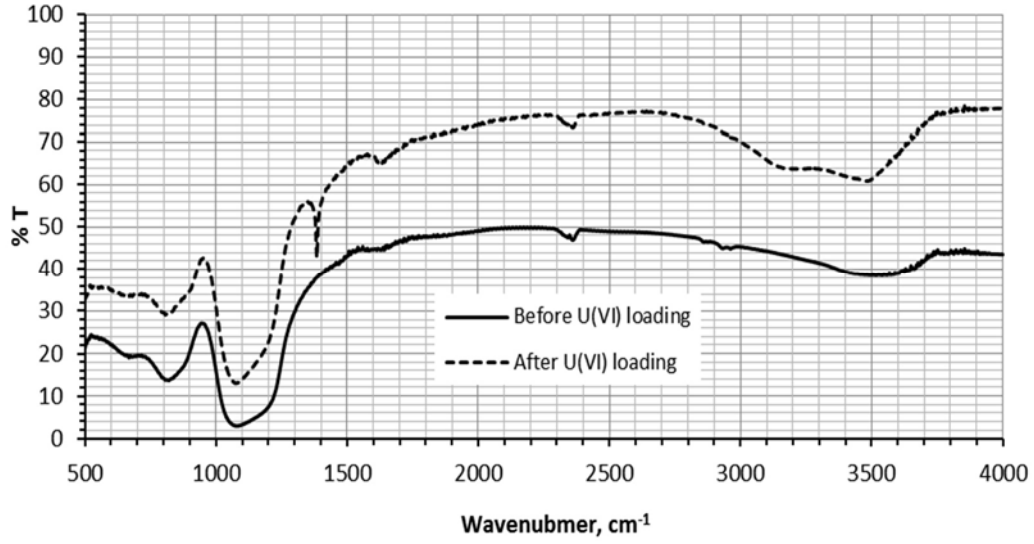

FIG. 2.13. Fourier-transform infrared spectroscopy (FTIR) analysis of the grafted kaolinites before and after uranium adsorption experiments.

Scanning electron microscope (SEM) images of the grafted kaolinites before and after uranium (VI) adsorption are presented in Fig. 2.14. Before uranium (VI) adsorption (Fig. 2.14a on the lefthand side) the surface of the grafted kaolinite was smooth and can be described as neat and uniform. After uranium (VI) adsorption (Fig. 2.14b on the righthand side) the surface became lumpy and covered with materials containing uranium. We also observed that there were some cleavages and small openings after adsorption. The latter observations may be due to the rehydration of the grafted kaolinite in the aqueous solution which resulted in the improvement of the d-spacing [2.31].

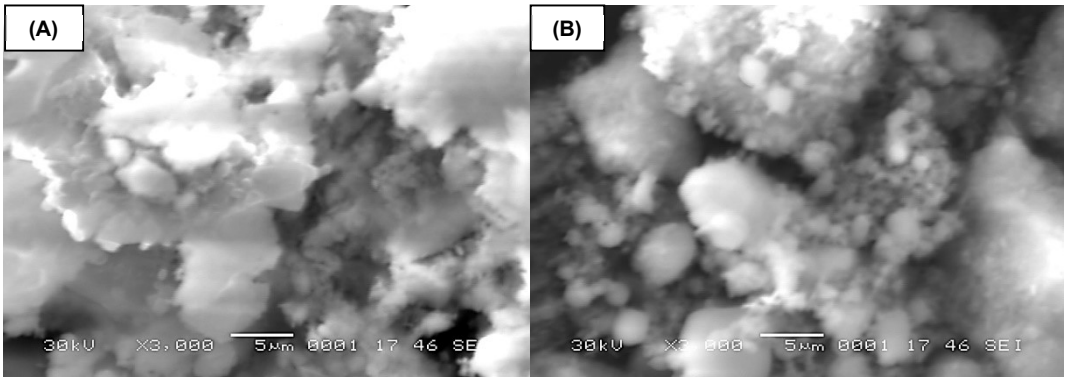

FIG. 2.14. Scanning electron microscope (SEM) analysis of the grafted kaolinites before (A) and after (B) uranium adsorption experiments.

The reliability of the attained data on the successive usage of the adsorbent was confirmed by equilibrating 0.5 g of the grafted kaolinite with a 400 mg/L uranium solution under improved

experimental conditions. The desorption was carried out (using 0.1 M ascorbic acid) and the uranium concentration was assessed in each case. The results attained on a successive usage of the same grafted kaolinite sample showed reproducible results with a standard deviation of -3.89% after eight adsorption-desorption cycles. The obtained data suggest very good reusability of grafted kaolinite adsorbent. Based on the obtained results, optimum adsorption conditions for the grafted kaolinite material are summarized in Table 2.4. Such optimum adsorption conditions may be most valuable for an economic assessment of using the grafted kaolinite adsorbent for liquid waste treatment.

TABLE 2.4. PREFERRED PROCESS CONDITIONS FOR URANIUM ADSORPTION USING THE GRAFTED KAOLINITES

Parameters	**Optimum conditions**
pH	4
Contact time	90 min
Initial uranium concentration	100 mg/L
Adsorbent mass	0.25 g/L
Temperature	25ºC
Capacity	95.23 mg/g
Desorption	By using 0.1 M ascorbic acid
Reusability	Up to eight cycles with R.S.D. of -3.89%

The prepared kaolinite adsorbent showed a good uranium adsorption capacity of about 95 mg U/g adsorbent in laboratory tests. A first case study conducted with a liquid waste sample provided by the Nuclear Materials Authority in Egypt is used to test the kaolinite adsorbent's performance in a more realistic setting. A batch experiment was performed by contacting 0.1 g of the grafted kaolinite with 200 mL of the raffinate solution for 90 min. Subsequent analysis of the effluent samples showed that only 59 mg U/g adsorbent or 62% of the theoretical adsorption capacity could be reached. This is not unusual and can be explained through a competition of different ions present in the liquid waste samples. In this case specifically iron ions. Using the 0.1 M ascorbic acid as an eluent was found effective for uranium desorption of the loaded kaolinite adsorbent bed. About 96% uranium or 56 mg U/g adsorbent were eluted in total.

The results of this study indicate that kaolinite clay could be converted into an efficient adsorbent material for uranium removal from aqueous solution by aluminium oxide grafting. The maximum adsorption capacity of the modified kaolinite clay for uranium is approximately 95 mg/g using the uranium standard solution. This is much higher than the absorption capacity of the untreated kaolinite clay and may be explained as a result of the increase in negative surface charge. A high pH value is preferred for uranium adsorption on the modified kaolinite clay since this increases the negative surface charge. Adsorption isotherms indicate that the uranium adsorption onto the modified kaolinite clay is a monolayer adsorption process. First experiments with an exemplary liquid waste sample indicate reduced adsorption efficiencies as other heavy metal ions are present.

2.2 MOROCCO: URANIUM EXTRACTION FROM WET PHOSPHORIC ACID WITH ARGAN NUTSHELL (ANS) SAWDUST

The argan nut is used in Morocco for the production of argan oil. Large quantities of argan nut shells (ANS) are produced and largely disposed of every year. This chapter describes how ANS can be used to produce a bio-sorbent for the extraction of uranium from phosphoric acid, or other solutions. Today sustainable development is recognized as an emerging trend and multifaceted methodology comprizing environmental, ecological, scientific, economic, social and political issues of global significance. Two of the key aspects of sustainable development from an energy and chemical perspective, are to develop more renewable forms of energy and to reduce environmental pollution. Increased heavy metals pollution is one of the main challenges to sustainable production today. Uranium is one of the most hazardous pollutant metals, due to its chemical toxicity and radioactivity. Since natural radiation has permanently been part of the human environment, large amounts of uranium have been discharged into the environment through leaching from natural deposits, release from mine- and mill tailings, emissions from the nuclear industry, the combustion of coal and other fuels as well as the use of mineral fertilizers that can contain considerable amounts of accompanying natural uranium.

The presence of heavy metals such as cadmium that is already regulated [2.32, 2.33] and uranium that is not regulated yet in phosphoric acid, is a potential risk for the environment and public health. Phosphoric acid is a product of great importance in fertilizers, as well as in the chemical and food industry. Phosphoric acid is the second most produced acid in the world, after sulphuric acid. This acid is used as a raw material for the production of detergents, food products, alimentary supplies for cattle, toothpastes and fertilizers [2.34]. Phosphoric acid is manufactured using different processes. Most commonly, thermal, and wet processes are used. The thermal process produces a pure acid and requires considerable amounts of energy, while the wet process is presently considered more economic and practiced much more widely. Approximately 90% of the phosphoric acid produced worldwide, is obtained by the wet process [2.35]. The most common form of the wet process involves a digestion of the phosphate mineral [$Ca_3(PO_4)_2$] with sulphuric acid [2.36]. Phosphoric acid produced by this process contains a variety of impurities, such as calcium sulphate, fluorine, cadmium, lead, and arsenic, as well as uranium impurities. The impurities vary according to the origin of the phosphate rock mineral [2.37]. The existence of such impurities in phosphoric acid adversely affects the process performance and is detrimental to the quality of produced acid [2.37, 2.38]. For this reason, about 95% of the acid produced by the wet process is directly used almost exclusively in agriculture as fertilizers and is excluded from the use in non-fertilizer applications (food and detergent applications) where a higher-purity acid is required [2.39]. In the wet phosphoric acid (WPA) process, based on sulphuric acid dissolution, about 80–90% uranium, passes into phosphoric acid and the rest precipitates into the phosphogypsum, a byproduct of the WPA. Since phosphoric acid is used to produce fertilizers, most of the uranium transfers to the final fertilizer products.

In view of the radio toxicity, the removal of natural uranium, contained in industrial phosphoric acid, appears to be an important step for a more sustainable production of phosphoric acid and the decontamination of phosphate fertilizers [2.40, 2.41]. It is further worth noting that considerable amounts of unconventional uranium, that can substitute uranium mining elsewhere, could be produced this way. Morocco possesses considerable phosphate rock reserves [2.42] with relatively high (>100 mg/kg [2.43]) natural uranium concentrations, is one of the largest phosphate rock producing countries in the world and by far the largest exporter of phosphate rock [2.44]. Wet-acid processing of phosphate rock with unconventional uranium (and potentially also REEs) recovery could be an attractive value

proposition for Morocco. Methods for the recovery of uranium from phosphoric acid are well known and were used in the USA and, to a smaller extent, elsewhere on an industrial scale until the late 1990s, when uranium prices plummeted, making recovery uneconomic for fertilizer producing companies. Other, less expensive methods may make uranium recovery from phosphate rock viable again.

Among the various available techniques [2.45-2.47], adsorption may be an attractive candidate, since it can combine effectiveness with cheapness. Adsorption is a simple attractive process in view of its high efficiency, cost-effectiveness, easy handling and flexibility of design, environmental amiability, low energy cost, lower toxicity and safe operation method, as well as the availability of different adsorbents [2.47, 2.48]. In addition, the recovery of pure metal for recycling, as well as for reuse of the adsorbent, are other advantages. To be economical, the applied adsorbent needs to be inexpensive and efficient. It better not lead to environmental concerns. Activated carbon (AC) is a conventional material widely used for adsorption processes due to its high adsorption efficiency. High manufacturing costs and difficulty in regeneration have imposed restrictions on its use though [2.47-2.49]. The search for inexpensive and more environmentally benign materials lead to byproducts from agricultural and food processing such as: wheat bran, sawdust, tree barks and chitin [2.45]. The most popular adsorbents among them are microbial biomass and lignocellulosic materials. These are natural materials available in large quantities and, being waste products, have a low price [2.50]. Sawdust is a natural lignocellulose material and is a promising adsorbent for removing pollutants, because it is easily obtained from wood waste of carpentry, paper, and furniture industries [2.50, 2.51]. According to Dupont et al. [2.52], the rapid metal uptake by immobilized sawdust in general, can enable a large-scale application of a biosorption process by an inexpensive adsorbent in a packed column.

Argan nutshell (ANS) sawdust from the argan fruit tree maybe a suitable biosorbent. The fruit size varies from 17 to 30 mm in length and 10–17 mm in width [2.53]. It is one of the most common trees in Morocco. All parts of the argan tree are used by local people: the almond fruit, for production of argan oil for culinary and cosmetic uses [2.54, 2.55], and the fruit pulp and seed cake residue from the production of argan oil is used as cattle feed. The wood and woody shell of the fruit are burned for heating [2.56, 2.57]. Argan oil production is a major industry with exponential growth in Morocco. Estimates on the available quantities of ANS waste material vary widely. Zbair et al. [2.58] estimate that 2 700 t ANS are discharged every year, while Tatome et al. [2.59] consider this number to be as high as 60 000 t. In any case, ANS waste can be used as a secondary, renewable resource in the preparation of biosorbents for the adsorption of heavy metals similar to AC.

Previously, ANS were used for adsorption experiments of: bisphenol A and diuron by Zbair et al. [2.58, 2.60], copper by El-Boundati et al. [2.61], pharmaceutical compounds by Benjedim et al. [2.62] and triphenylmethanes by El-Khomri et al. [2.63]. A researcher from the Abdelmalek Essadi University further filed a patent for the use of ANS as a bio-sorbent [2.64] and Moussaoui et al. [2.65] investigated the adsorption behaviour of argan leaves, pulps and fruits. Besides the use as an adsorbent ANS may be used as a raw material for CO_2 capture [2.66] or battery production [2.54, 2.67].

The raw ANS used in this work was collected in rural areas of the southwestern Morocco (Souss Massa). The ANS was used as received, without any additional treatment, such as washing or drying, and were converted into sawdust with a mortar grinder type Retsch RM 200. The sawdust was then sieved (for more homogeneity) to various particle sizes ranging from 125 to 350 μm.

A stock solution of uranium (1000 mg/L) was prepared in Milli-Q ultra-pure water. The adsorption experiments were performed in 10 mL water with a 10 mg/L uranium concentration. Different working solutions were prepared by proper dilution, using Milli-Q ultra-pure water. Since single toxic metallic species rarely exist, a synthetic solution of several heavy metals based on their concentrations in phosphoric acid was prepared. The synthetic solution (10 mL) was prepared with 20 mg/L As, 20 mg/L Cd, 250 mg/L U, 110 mg/L Al and 50 mg/L Th. All other working solutions with varying concentrations were obtained by successive dilution. Commercial phosphoric acid (85% purity, density = 1.57 and molecular weight M = 98 g/mol, 0.007% heavy metals) was used to determine the chemical resistance of the ANS sawdust in aggressive acidic media. Commercial phosphoric acid was obtained from Sigma-Aldrich. Water was added to obtain 0.85% and 8.5% dilution. These dilutions were chosen to reduce the viscosity and density effects in the exchange capacity. The contaminated solutions of phosphoric acid were prepared by adding uranium. Milli-Q ultra-pure water was used in all the experiments. The industrial phosphoric acid under investigation was a 54% P_2O_5 (about 12 M H_3PO_4) solution, containing numerous elements. Among them, the behaviour of uranium was investigated for the adsorption studies. The chemical analysis of the exemplary industrial phosphoric acid was performed by ICP-MS and the results are depicted in Table 2.5. The experiments were done, using a 10 mL phosphoric acid solution.

TABLE 2.5. CHEMICAL ANALYSIS OF EXEMPLARY CRUDE PHOSPHORIC ACID PRODUCED IN MOROCCO

Component	**Concentration**	**Component**	**Concentration**
P_2O_5	54 wt%	Cd	15 mg/kg
CaO	0.56 wt%	Zn	90 mg/kg
Al_2O_3	0.1 wt%	As	14 mg/kg
MgO	0.97 wt%	V	144 mg/kg
Fe_2O_3	0.48 wt%	Cr	197 mg/kg
K_2O	0.68 wt%	U	156 mg/kg
Ni	48 mg/kg	Th	44 mg/kg

Adsorption experiments were performed in a glass column of 20 mm diameter and 250 mm height. Glass wool was placed at the bottom of the column to prevent leaching of the adsorbent. About 1 g of the ANS sawdust-substrate was packed into the column. The sawdust was repeatedly washed with double distilled water (until no brown colouration was visible) to remove surface impurities. For each run, the adsorption experiments were carried out by passing a given solution (10 mL) of a desired concentration of uranium through the column. The flow rate of the eluent was controlled to be about 1 mL/min. The flow rate was determined by preliminary experiments to ensure that no plugging occurs during the elution of the metal solution. At the column outflow, the eluents were collected in plastic bottles. The concentrations of the residual metals were determined by ICP-MS. All the experiments were conducted at room temperature. To ensure high accuracy, reliability and reproducibility of the collected data, all batch experiments were carried out three times. The mean values of the three data sets are presented here.

The adsorption efficiency was expressed as a percentage of adsorbed metal, compared to initial metal concentrations. The per cent adsorption by the ANS sawdust was determined as following [2.58]:

$$A(\%) = \frac{C_0 - C}{C_0} 100 \quad (2.10)$$

where

C_0 and C (mg/L) are the initial and residual concentrations of the respective metal ions.

Adsorption isotherms have traditionally been used for preliminary investigations and fixations of the operating parameters. Information gained from the isotherms can, however, not be used to accurately scale up the system. To know the practical applicability of ANS sawdust, column operations have been investigated on the adsorption of uranium to obtain a factual design model. The adsorbent dose is 1 g/L. The inlet concentration is 10 mg/L. The flow rate is 1 mL/min. The results were used to build the breakthrough curve and to determine the breaking point.

For any adsorption process, the most important factors are the recovery of the metal ions adsorbed and the regeneration capacity of the adsorbent. To make the adsorption process more economical and also to obtain practical information on the recovery of uranium, desorption of adsorbed uranium from exhausted ANS sawdust was studied using organic acid. The procedure was carried out using 50 mL of 1 M, 0.5 M and 0.1 M citric acid as elution solution. A solution of each acid with a pre-determined uranium concentration was passed though the column of the pre-adsorbed ANS sawdust. The desorbed solution of the column was again collected for later analysis. The adsorbent was washed twice with double distilled water, before each measurement, to remove loosely adhered uranium. The desorption percentage, D (%) was determined using Eq. (2.11) [2.47]:

$$D(\%) = \frac{The\ concentration\ of\ desorbed\ meta\ \ (mg.L^{-1})}{The\ concentration\ of\ adsorbed\ metal\ (mg.L^{-1})} 100 \quad (2.11)$$

The recyclability of an adsorbent is of crucial importance in industrial practice for heavy metal removal. To test the suitability and the stability of the adsorbent, it is necessary to regenerate the spent adsorbent. To regenerate the spent adsorbent, it was subjected to successive adsorption and desorption cycles. The spent ANS sawdust was again washed with double distilled water to remove any unadsorbed metal ions. Adsorption onto ANS sawdust was easily regenerated adding 30 mL heated (75℃) Milli-Q ultra-pure water. Elemental analysis was conducted using ICP-MS with a Thermo Scientific XSERIES 2 (Thermo Fisher Scientific, Bremen, Germany). SEM images were recorded using a Quanta 200, manufactured by the FEI Company. SEM was used to analyse the surface morphology of the ANS sawdust. The samples were cryo-fractured under liquid nitrogen. Since the sawdust itself is not conductive, a thin gold coating was applied, using sputtering. FTIR spectra were acquired using a TWO spectrometer to identify functional groups on the bio-sorbent surface. FTIR spectral analysis was performed within the wave number range of 100–4000 cm^{-1} and a resolution of 4 cm^{-1}. The results of the ICP-MS analyses are shown in Table 2.6. These results indicate the presence of Ca and Zn. The analysis further shows the presence of Fe.

TABLE 2.6. CHEMICAL ANALYSIS OF THE ANS SAWDUST

Element	Concentration [mg/kg]	Element	Concentration [mg/kg]
Al	142	Na	25.43
Mg	214	Ca	1524
P	562	Mn	6
S	288	Fe	186
Cl	663	Ni	0.47
K	1771	Cu	2
Zn	7	As	0.43
Br	2	Se	100

The surface morphology of the raw ANS sawdust was determined, using SEM with different magnifications. The SEM images shown in Fig. 2.14 reveal that the morphology of this material can facilitate the adsorption of metals, due to the irregular rough surfaces with tangles and microfibrils that form a coarse fibrous texture. This makes the surface amenable for the attachment of reactive functional groups such as metal ions.

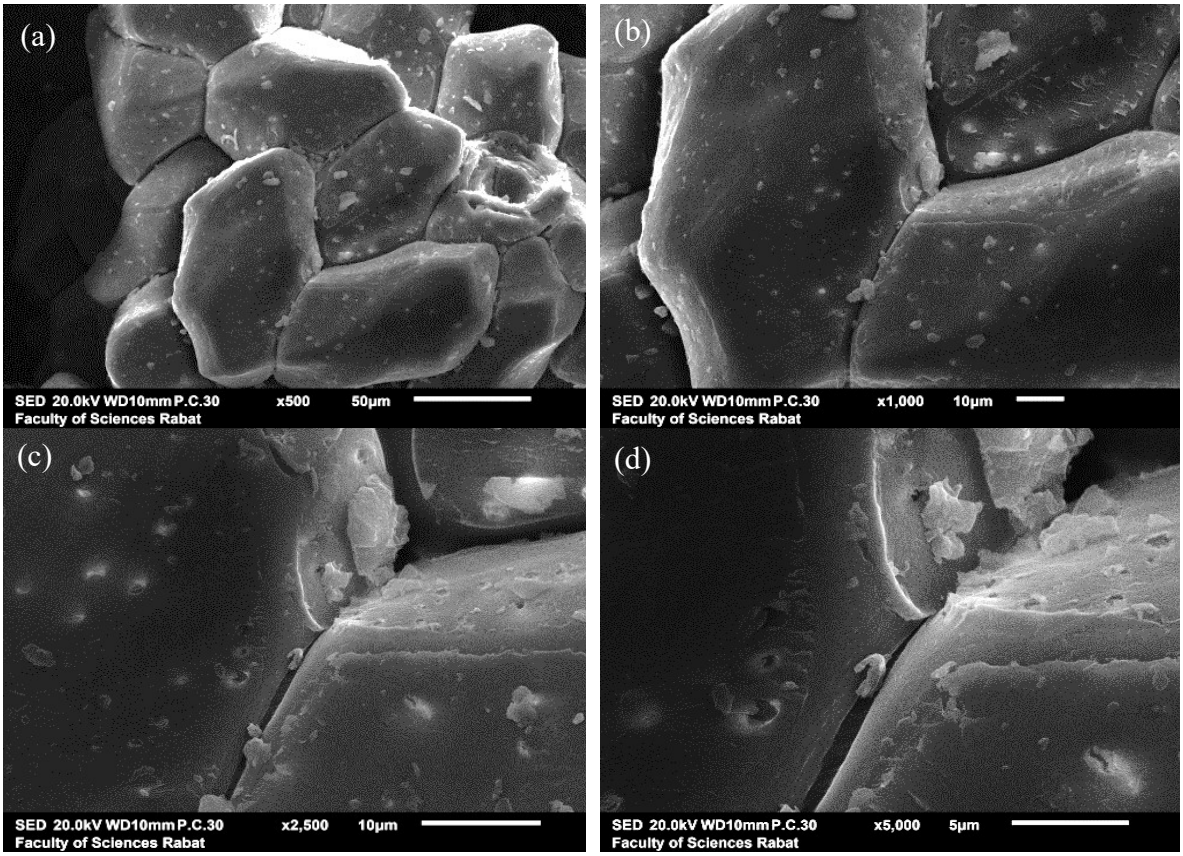

FIG. 2.14. SEM images of ANS sawdust at different magnifications: (a): 500,(b): 1000, (c): 2500 and (d): 5000.

To determine which functional groups were responsible for metal uptake, FTIR analysis in solid phase was performed on the ANS sawdust. FTIR spectra of adsorbent solid samples before and after the adsorption process are shown in Fig. 2.15.

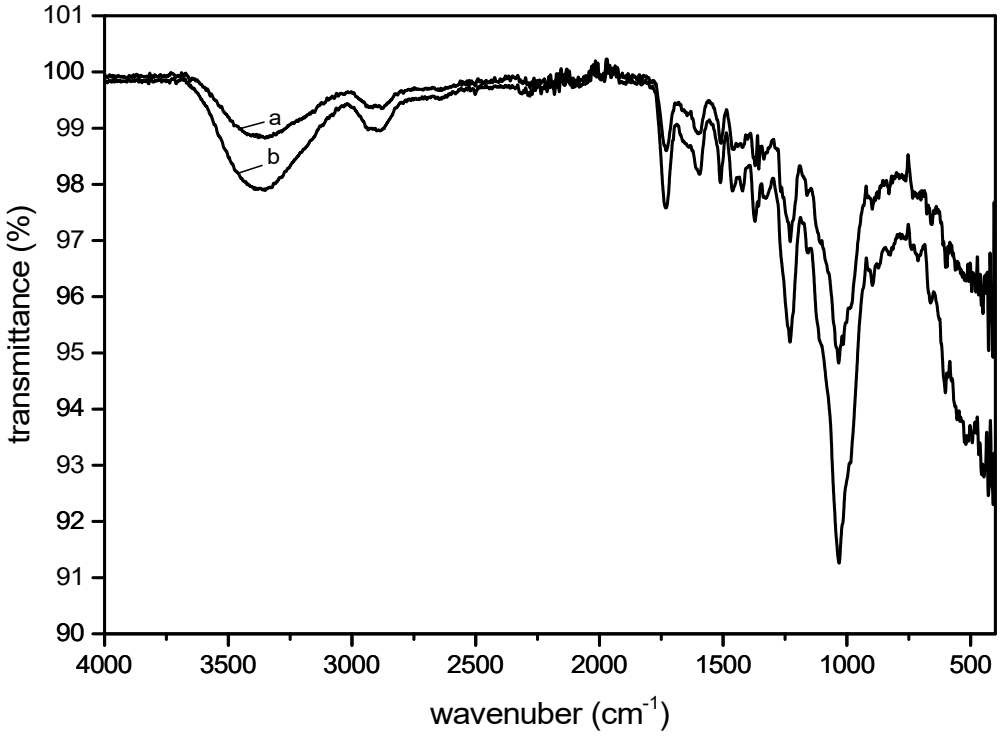

FIG. 2.15. FTIR spectra of ANS sawdust in a raw form (a) and in adsorbed form (b).

The FTIR spectrum of particles shows characteristic absorption bands associated with the chemical groups of lignocellulosic compounds: cellulose, hemicellulose and lignin [2.17]. Such components are mainly composed of alkenes and aromatic groups.

It can be seen in Fig. 2.15a, that an absorption band is observed at wave number 3350 cm^{-1}, that is representative of the characteristic O–H stretching vibration and hydrogen bond of hydroxyl functional groups on the surface [2.70, 2.71]. The absorption peak observed at 2873 cm^{-1} is the characteristic band for the C–H stretching vibration from CH and CH_2 in cellulose and hemicellulose components [2.72, 2.73]. Absorption at the wave number of 1727 cm^{-1} is attributed to the carbonyl C=O stretching vibration of the linkage of carboxylic acid in a lignin or ester group in hemicellulose [2.74-2.76]. The carboxylic groups may also be present in the particle as traces of fatty acids in oils [2.77]. The peak around 1600 cm^{-1} is ascribed to the C=C stretching that can be attributed to the lignin aromatic groups [2.48]. The peak located at 1512 cm^{-1} is assigned to the C=C ring stretch of aromatic rings [2.58]. The sharp peak seen at 1230 cm^{-1} is due to the C–O stretching vibration of the acetyl group in lignin and the hemicellulose component, respectively [2.77-2.80]. The sharp strong peak seen at 1033 cm^{-1} is assigned to the CO and O–H stretching vibration, which belongs to polysaccharide in cellulose [2.81, 2.82]. It was evident from the FTIR spectrum, that carboxyl and hydroxyl groups are present in abundance. These groups may function as proton donors. Hence, deprotonated hydroxyl and carboxyl groups may be involved in coordination and action with metal ions.

Spectral analysis before (see Fig. 2.15a) and after (see Fig. 2.15b) uranium adsorption were compared. A major increase in peak intensity at 3350 cm^{-1}, 1730 cm^{-1}, 1230 cm^{-1} and 1033 cm^{-1} appeared in the spectrum of heavy metals loaded with ANS sawdust, indicating the involvement of –OH groups, C=O, C–O and C–C in binding with the heavy metals in the adsorption process. These functional groups substitute hydrogen ions for metal ions in a solution or donation of an electron pair to form complexes with the metal ions in solutions. Due to abundant binding groups, ANS sawdust has a large heavy metal adsorption potential. Preliminary adsorption tests on ANS sawdust were performed to determine the uranium adsorption capability. The ANS sawdust demonstrated outstanding metal removal capabilities with 99.58% adsorption efficiency. The high efficiency can be explained with cellulose, hemicellulose and lignin that contain surface functional groups such as carboxylic, carbonyl and hydroxyl. These groups possess a high affinity for heavy metal ions [2.83, 2.84]. Accordingly, the metal uptake by the adsorbent might occur through a sorption process, involving these surface functional groups.

The adsorption efficiency of the ANS sawdust was compared with the adsorption efficiency of conventional AC. In the experiments, ANS sawdust had a slightly higher uranium adsorption potential than the conventional AC used. Industrial phosphoric acid contains numerous impurities and heavy metals, so that single metals adsorption tests are only of limited use. Table 2.7 depicts the per cent adsorption of As, Cd, U, Al and Th. The 1 g sample of ANS sawdust was able to simultaneously remove 77% Th, 52% U, 42% As, 36% Cd and 24% Al. This limited adsorption effectiveness can be explained by the loss of accessible sites to other metal ions.

TABLE 2.7. PER CENT ADSORPTION OF As, Cd, U, Al AND Th

Element	**C_0 [mg/ℓ]**	**C_t [mg/ℓ]**	**A (%)**
As	19.21	11.00	42.73
Cd	20.02	12.77	36.21
U	250.5	119.40	52.33
Al	109.5	82.73	24.45
Th	49.43	11.25	77.24

The percentage of removal was higher at the beginning of the experiments. This can again be explained by the larger surface area of the ANS sawdust being available for the metal ion adsorption at the beginning of the experiments. As the surface adsorption sites become exhausted, the uptake rate is controlled by the rate at which the adsorbate is transported from the exterior to the interior sites of the adsorbent particles.

The breakthrough curve was obtained by plotting C/C_0 over the total throughput in mL. It can be observed that the breakthrough volume is at 50 mL. The saturation volumes (V_x) were found to be at 250 mL after 250 min (t_x). The maximum capacity of the removal of uranium ions in columns is given by Eq. (2.12) [106]. The values of Q are 0.18 mg/g. Operational column parameters are helpful in designing a fixed adsorbent for uranium removal:

$$Q = \frac{C_0 \times V}{m_s} \int_{t=0}^{t=x} \left(1 - \frac{C}{C_0}\right) dt \qquad (2.12)$$

where

Q is the maximum adsorption capacity [mg/g];

C_0 and C initial uranium concentrations [mg/L];

m_s adsorbent mass [g];

V flow rate [L/min].

Length of the unused adsorbent column or bed (LUB) calculated using Eq. (2.13) [106]:

$$LUB = L \times (1 - \frac{V_b}{V^x}) \quad (2.13)$$

where

L is the height of the bed [cm];

V_b is the breakthrough volume [mL];

V^x is the stoichiometric volume [mL], which corresponds to less than half the saturation volume (V^x). The value of LUB is 0.68 cm here.

Desorption experiments were performed to ensure that the adsorbed uranium ions can also easily be separated from the ANS sawdust adsorbent, so that the uranium can be sold, and the adsorbent can be further used. The per cent of desorption (D) of uranium is provided in Table 2.8. The desorption studies were conducted, using citric and oxalic acid. 1 M citric acid reached higher desorption rates.

TABLE 2.8. PER CENT DESORPTION OF URANIUM FROM ANS SAWDUST USING OXALIC- AND CITRIC ACID

Desorption agent	**Adsorbed concentration [mg/ℓ]**	**Desorbed concentration [mg/ℓ]**	**D [%]**
1 M Oxalic acid	9.5	1.69	17.79
1 M Citric acid	9.5	2.66	28.00

After the initial tests with 1 M oxalic- and citric acid, further experiments with changed concentrations of the citric acid were conducted. Specifically, the citric acid concentrations were 1.0 M, 0.5 M and 0.1 M. The results of the experiments are shown in Table 2.9 and revealed that the desorption percentage was found to be the highest in the case of 0.1 M citric acid (99.16%) followed by 0.5 M citric acid (65.60%). Least desorption was observed in the case of 1 M citric acid (28%).

TABLE 2.9. REAGENT USED FOR THE DESORPTION OF URANIUM

Desorption agent	**Adsorbed concentration (mg/ℓ)**	**Desorbed concentration (mg/ℓ)**	**D (%)**
1 M Citric acid	9.5	2.66	28.00
0.5 M Citric acid	9.5	6.18	65.60
0.1 M Citric acid	9.5	9.42	99.16

The used column requires only 50 mL of 0.1 M citric acid ($C_6H_8O_7$) for each desorption cycle and no weight loss per cycle was considered. Figure 2.16 shows the elution curve of ANS sawdust with 0.1 M citric acid.

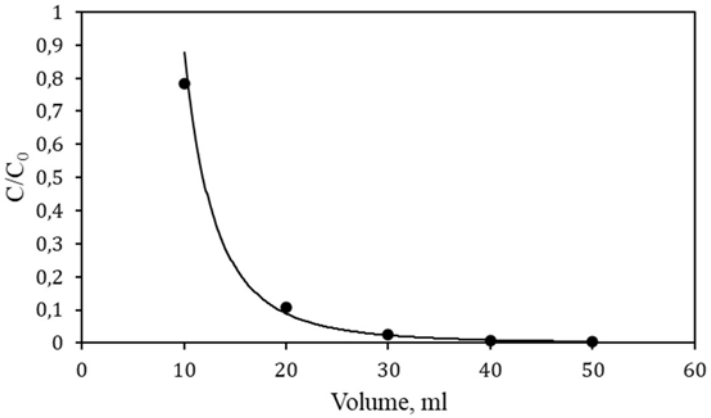

FIG. 2.16. Elution curve of ANS sawdust using 0.1 M citric acid ($C_6H_8O_7$).

The reusability of the adsorbent is of high importance for an economic and sustainable utilization. In Table 2.10, results of not regenerated (fresh) and regenerated adsorption studies are compared. The regenerated adsorbent was heated in Milli-Q ultra-pure water at 75°C. It could be observed that the heated Milli-Q ultra-pure water was a suitable regenerating solution that allowed for a per cent adsorption as high as 92%. The not regenerated adsorbent in contrast was able to adsorb 62% of the uranium in solution.

TABLE 2.10. PER CENT URANIUM ADSORPTION OF REGENERATED (TREATED WITH HEATED MILLI-Q ULTRA-PURE WATER) AND NOT REGENERATED (UNTREATED) ANS SAWDUST

Type of adsorbent	**C_0 [mg/ℓ]**	**C [mg/ℓ]**	**A [%]**
Not regenerated	10.19	3.92	61.55
Regenerated	10.03	0.71	92.92

The ANS sawdust column was used directly for the adsorption of uranium from commercial phosphoric acid with an mg/L uranium concentration. The ANS sawdust was tested with different acid concentrations (0.85%, 8.5% and 85%). The obtained results are shown in Table 2.11. It was found that the ANS sawdust adsorbed at least 99.5% of the uranium, independent of the concentration of commercial phosphoric acid used.

TABLE 2.11. PER CENT ADSORPTION (A) OF URANIUM FROM COMMERCIAL PHOSPHORIC ACID AT DIFFERENT PHOSPHORIC ACID CONCENTRATIONS

Type of adsorbate	**C_0 [mg/L]**	**C [mg/L]**	**A [%]**
Commercial phosphoric acid (0.85%)	10.18	0.05	99.50
Commercial phosphoric acid (8.5%)	9.96	0.09	99.09
Commercial phosphoric acid (85%)	10.08	0.10	99.00

After passing commercial phosphoric acid of various concentrations through the ANS sawdust, no damage or degradation was observed in the used sawdust. It can be concluded

that the visible structure of ANS sawdust remained unchanged, even in concentrated acid solutions. Besides, its adsorption capacity did not vary significantly with different phosphoric acid concentrations and remained within the experimentally determined error.

The release of uranium adsorbed from commercial phosphoric acid in ANS sawdust was carried out using 0.1 M citric acid, which previously showed the highest effectiveness. The results obtained are shown in Table 2.12. These results indicate that 0.1 M citric acid was effective to desorb about 98% of the uranium. Citric acid proved to be effective in desorbing uranium ions from spent ANS sawdust in an eco-friendly manner. Organic acids are considered as mild acids that are biodegradable and create little or no environmental pollution which makes them an ideal agent for desorption use on industrial scale.

TABLE 2.12. PER CENT DESORPTION (D) OF URANIUM ADSORBED FROM COMMERCIAL PHOSPHORIC ACID USING 0.1 M CITRIC ACID

Type of adsorbate	**Adsorbed concentration [mg/L]**	**Desorbed concentration [mg/L]**	**D [%]**
Commercial phosphoric acid (0.85%)	10.13	9.97	98.42
Commercial phosphoric acid (8.5%)	9.87	9.61	97.36
Commercial phosphoric acid (85%)	9.98	9.90	99.19

The regeneration of the ANS sawdust after desorption experiments was performed using 30 mL heated Milli-Q ultra-pure water (75°C). The results are shown in Table 2.13. It was observed that the heated Milli-Q ultra-pure water was able to regenerate the ANS sawdust used in several cycles. The per cent of adsorption of uranium ions after the regeneration process of the adsorbent was about 94%. The not regenerated adsorbent still managed adsorbing 61% of the uranium ions from commercial phosphoric acid, regardless of the concentration of commercial phosphoric acid used. The method used for the regeneration process can be considered an effective green method for recycling hazardous spent adsorbent waste.

TABLE 2.13. COMPARISON OF PER CENT ADSORPTION OF URANIUM FROM COMMERCIAL PHOSPHORIC ACID USING REGENERATED AND NOT REGENERATED ANS SAWDUST

Type of adsorbate	**Type of adsorbent**	**C_0 [mg/L]**	**C [mg/L]**	**A [%]**
Commercial phosphoric acid (0.85%)	Not regenerated	10.22	3.98	61.05
	Regenerated	10.07	0.63	93.74
Commercial phosphoric acid (8.5%)	Not regenerated	10.54	4.01	61.95
	Regenerated	10.36	0.52	94.98
Commercial phosphoric acid (85%)	Not regenerated	10.16	4.33	57.38
	Regenerated	10.01	0.57	94.30

The ANS sawdust column was used for the purification of exemplary industrial phosphoric acid produced in Morocco. Tests were conducted at different acid concentrations (5%, 30%

and 54%). The results are depicted in Table 2.14. These results revealed that the ANS sawdust was effective in considerably purifying industrial phosphoric acid. It was found that for a concentration of 5% P_2O_5 the ANS sawdust was able to reduce the concentration of uranium by 54%. In a similar attempt, the amount of uranium in a concentration of 30% P_2O_5 dropped from 87 mg/L to 40 mg/L, resulting in an adsorption efficiency of 54% as well. At an acid concentration of 54%, the ANS sawdust still adsorbed 54% of the uranium. The ANS sawdust column did not visibly decrease with the increase in the phosphoric acid concentration and viscosity. ANS sawdust seems to remain stable at any phosphoric acid concentration tested, proving that it can withstand aggressive solutions. It was further noticed that the green colour of the phosphoric acid, that is a result of metallic impurities, became noticeably clearer after the adsorption experiments.

TABLE 2.14. PER CENT ADSORPTION (A) OF URANIUM FROM INDUSTRIAL PHOSPHORIC ACID

Type of adsorbate	**C_0 [mg/L]**	**C [mg/L]**	**A [%]**
Industrial phosphoric acid (5%)	15.32	7.12	53.52
Industrial phosphoric acid (30%)	87.05	40	54.02
Industrial phosphoric acid (54%)	156.40	71.49	54.29

Real industrial phosphoric acid contains a number of heavy metals rather than a single metal. The presence of one heavy metal may hinder the adsorption of other heavy metals. In our studies, the removal of uranium by ANS sawdust in single metal solutions (99%) were higher than that of a multi-metal solution (54%). This effect can be attributed to the competition between cations and the sufficient adsorption sites available for adsorption of the heavy metal ions. The difference in per cent adsorption of different uranium ions at the same initial concentration, adsorbent mass (1 g) and flow rate (1 mL/min) may be attributed to the difference in their chemical affinity and ion exchange capacity with respect to the chemical functional group on the surface of the adsorbent [2.85]. The adsorption of uranium by this adsorbent might be attributed to their proteins, carbohydrates and phenolic compounds which have carboxyl, hydroxyl, sulphate, phosphate and amino groups that can bind metal ions [2.86]. The desorption process was again carried out using 0.1 M citric acid. The results are depicted in Table 2.15.

TABLE 2.15. PER CENT DESORPTION (D) OF URANIUM ADSORBED FROM INDUSTRIAL PHOSPHORIC ACID USING 0.1 M CITRIC ACID

Type of adsorbate	**Adsorbed concentration [mg/L]**	**Desorbed concentration [mg/L]**	**D [%]**
Industrial phosphoric acid (5%)	8.2	0.03	0.03
Industrial phosphoric acid (30%)	47.05	0.55	0.68
Industrial phosphoric acid (54%)	84.91	1.2	1.48

The ANS sawdust used in the adsorption of uranium ions from industrial phosphoric acid was regenerated using heated Milli-Q ultra-pure water (75°C). The results are shown in Table 2.16.

TABLE 2.16. COMPARISON OF PER CENT ADSORPTION (A) OF URANIUM FROM INDUSTRIAL PHOSPHORIC ACID USING REGENERATED AND NOT REGENERATED ANS SAWDUST

Type of adsorbate	Type of adsorbent	C_0 (mg/L)	C (mg/L)	A (%)
Industrial phosphoric acid (5%)	Not regenerated	15.46	9.45	38.87
	Regenerated	15.07	6.93	54.01
Industrial phosphoric acid (30%)	Not regenerated	86.79	54.58	37.11
	Regenerated	87.45	40.61	53.56
Industrial phosphoric acid (54%)	Not regenerated	156.36	97.95	37.35
	Regenerated	157.05	70.33	55.58

The by-product from argan oil production, specifically argan nut shells (ANS), were used to produce a biosorbent in the form of fine sawdust, for the recovery of uranium from phosphoric acid. Laboratory scale experiments were conducted with a packed column of 10 mm diameter and 250 mm length. Three different solutions: a synthetic heavy metals solution with 250 mg/L uranium content, a commercial phosphoric acid (0.85%, 8.5% and 85%) solution with 250 mg/L uranium content and an exemplary industrial phosphoric acid (5%, 30% and 54%) solution produced in Morocco with 156 mg/kg uranium content were used for adsorption, desorption, and regeneration studies. All the solutions were sent through the packed column at a flow rate of 1 mL/min. The ANS sawdust successfully adsorbed 99% of the uranium from the synthetic heavy metal solution. The ANS sawdust further managed to adsorb more than half (53–54%) of the uranium in the exemplary industrial phosphoric acid. Desorption studies with 0.1 M citric acid indicate very high desorption rates (97–99%) of uranium, in the case of the synthetic solution and the commercial phosphoric acid and very low desorption rates (1–2%) of uranium, in the case of the exemplary industrial phosphoric acid. The ANS sawdust adsorbent may thus only be used for the extraction/detoxification and not for the recovery of uranium (and other heavy metals) from phosphoric acid, or other solutions. In conclusion, this work opens a new way to valourize ANS, which is generally disposed of unused at present. A first step to the production and commercialization of a low-cost, sustainable, and renewable substitute for commercial AC is presented.

REFERENCES TO CHAPTER 2

[2.1] YANG, Z., WANG, C., LIU, D., YANG, S., LI, Y., NING, Y., A quantitative evaluation of uranium mobility and potential environment, J. Hazard. Mater. **381** (2020) 120977.

[2.2] HANEKLAUS, N., BAYOK, A., FEDCHENKO, V. KELLEY, R., Phosphate rocks and nuclear proliferation, Sci. Glob. Secur. **25** (2017) 143–158.

[2.3] PAYNE, T.E., DAVIS, J.A., LUMPKIN, G.R., CHISARI, R., WAITE, T.D., Surface complexation model of uranyl sorption on Georgia kaolinite, Appl. Clay Sci. **26** (2004) 151–162.

[2.4] KREPELOVA, A., SACHS, S., BERNHARD, G., Uranium(VI) sorption onto kaolinite in the presence and absence of humic acid, Radiochim. Acta **94** (2006) 825–833.

[2.5] SACHS, S., BERNHARD, G., Sorption of U(VI) onto an artificial humic substance-kaolinite-associate, Chemosphere **72** (2008) 1441–1447.

[2.6] GUERRA, D.L., LEIDENS, V.L., AIROLDI, C., VIANA, R.R., Application of Brazilian kaolinite clay as adsorbent to removal of U(VI) from aqueous solution : Kinetic and thermodynamic of cation-basic interactions, J. Solid State Chem. **183** (2010) 1141–1149.

[2.7] GUERRA, D.L., LEIDENS, V.L., VIANA, R.R., AIROLDI, C., Amazon kaolinite functionalized with diethylenetriamine moieties for U(VI) removal: Thermodynamic of cation-basic interactions, J. Hazard. Mater. **180** (2010) 683–692.

[2.8] CAMPOS, B., AGUILAR-CARRILLO, J., ALGARRA, M., GONÇALVES, M.A., RODRÍGUEZ-CASTELLÓN, E., ESTEVES DA SILVA, J.C.G., BOBOS, I., Adsorption of uranyl ions on kaolinite, montmorillonite, humic acid and composite clay material, Appl. Clay Sci. **85** (2013) 53–63.

[2.9] METWALLY, S.S., HASSAN, R.S., EL-MASRY, E.H., BORAI, E.H., Gamma-induced radiation polymerization of kaolin composite for sorption of lanthanum, europium and uranium ions from low- grade monazite leachate, J. Radioanal. Nucl. Chem. **315** (2018) 39–49.

[2.10] REINOSO-MASET, E., LY, J., Study of uranium(VI) and radium(II) sorption at trace level on kaolinite using a multisite ion exchange model, J. Environ. Radioact. **157** (2016) 136–148.

[2.11] ZHANG, H., LIU, Z., HU, P., LIU, T., WU, W., Adsorption of U(VI) onto kaolin studied by batch method, J. Radioanal. Nucl. Chem. **297** (2013) 1–12.

[2.12] EVANS, N., WARWICK, P., LEWIS, T., BRYAN, N., Influence of humic acid on the sorption of uranium (IV) to kaolin, Environ. Chem. Lett. **9** (2011) 25–30.

[2.13] BARGER, M., KORETSKY, C.M., The influence of citric acid, EDTA, and fulvic acid on U(VI) sorption onto kaolinite, Appl. Geochem. **26** (2011) S158–S161.

[2.14] BACHMAF, S., MERKEL, B., Sorption of uranium(VI) at the clay mineral-water interface, Environ. Earth Sci. **63** (2011) 925–934.

[2.15] WANGGH, G., WANG, X., CHAI, X., LIU, J., DENG, N., Adsorption of uranium (VI) from aqueous solution on calcined and acid-activated kaolin, Appl. Clay Sci. **47** (2010) 448–451.

[2.16] OHNUKI, T., YOSHIDA, T., OZAKI, T., SAMADFAM, M., KOJAI, N., YUBUTA, K., MITSUAGASHIRA, T., KASAMA, T., FRANCIS, A.J., Interactions of uranium with bacteria and kaolinite clay, Chem. Geol. **220** (2005) 237–243.

[2.17] GAO, L., YANG, Z., SHI, K., WANG, X., U(VI) sorption on kaolinite: effects of pH, U(VI) concentration and oxyanions, J. Radioanal. Nucl. Chem. **284** (2010) 519–526.

[2.18] TAHA, M.H., EL-MAADAWY, M.M., HUSSEIN, A.E.M., YOUSSEF, W.M., Uranium sorption from commercial phosphoric acid using kaolinite and metakaolinite, J. Radioanal. Nucl. Chem. **317** (2018) 685–699.

[2.19] MARCZENKO, Z., Separation and Spectrophotometric Determination of Elements, Ellis Horwood Series of Analytical Chemistry, USA (1986).

[2.20] DING, D.H., LEI, Z.F., YANG, Y.N., FENG, C.P., ZHANG, Z.Y., Nickel oxide grafted andic soil for efficient cesium removal from aqueous solution: Adsorption behavior and mechanisms, ACS Appl. Mater. Interfaces **5** (2013) 10151–10158.

[2.21] FANHUAJIE, F., DING, H., BAI, J., WU, X., LEI, F., TIAN, W., WANG, Y., QIN, Z., Sorption of uranium(VI) from aqueous solution onto magnesium silicate hollow spheres, J. Radioanal. Nucl. Chem. **289** (2011) 367–374.

[2.22] SHUIBO, X., CHUN, Z., XINGHUO, Z., JING, Y., XIAOJIAN, Z., JINGSONG, W., Removal of uranium (VI) from aqueous solution by adsorption of hematite, J. Environ. Radioact. **100** (2009) 162–166.

[2.23] PARAB, H., JOSHI, S., SHENOY, N., VERMA, R., LALI, A., SUDERSANAN, M., Uranium removal from aqueous solution by coir pith: equilibrium and kinetic studies, Bioresour. Technol. **96** (2005) 1241–1248.

[2.24] ARAMI, M., LIMAEE, N.Y., MAHMOODI, N.M., TABRIZI, N.S., Removal of dyes from colored textile wastewater by orange peel adsorbent : Equilibrium and kinetic studies, J. Colloid Interface Sci. **288** (2005) 371–376.

[2.25] MISAELIDES, P., GODELITSAS, A., FILIPPIDIS, A., CHARISTOS, D., ANOUSIS, I., Thorium and uranium uptake by natural zeolitic materials, Sci. Total Environ. **173–174** (1995) 237–246.

[2.26] SHENG, L., ZHOU, L., HUANG, Z., Facile synthesis of magnetic chitosan nano-particles functionalized with N/O-containing groups for efficient adsorption of U(VI) from aqueous solution, J. Radioanal. Nucl. Chem. **310** (2016) 1361–1371.

[2.27] LI, L., DING, D., HU, N., FU, P., XIN, X., WANG, Y., Adsorption of U(VI) ions from low concentration uranium solution by thermally activated sodium feldspar, J. Radioanal. Nucl. Chem. **299** (2014) 681–690.

[2.28] LATOUR, R.A., The Langmuir isotherm: A commonly applied but misleading approach for the analysis of protein adsorption behavior, J. Biomed. Mater. Res. **103** (2015) 949–958.

[2.29] ZHU, W., LIU, Z., CHEN, L., Sorption of uranium(VI) on Na-attapulgite as a function of contact time, solid content, pH, ionic strength, temperature and humic acid, J. Radioanal. Nucl. Chem. **289** (2011) 781–788.

[2.30] LIU, M., DONG, F., YAN, X., ZENG, W., HOU, L., PANG, X., Biosorption of uranium by Saccharomyces cerevisiae and surface interactions under culture conditions, Bioresour. Technol. **101** (2010) 8573–8580.

[2.31] MUKHOPADHYAY, B., WALTHER, J., Acid-base chemistry of albite surfaces in aqueous solutions at standard temperature and pressure, Chem. Geol. **174** (2001) 415–443.

[2.32] GILBERT, B.N., European Union Debates Controversial Plans to Limit Cadmium in Fertilizer, http;//www.sciencemag.org/news/2018/04/european-union-debates-controversial-plans-limit-cadmium-fertilizer (Accessed on 18 July 2018).

[2.33] ULRICH, A.E., Cadmium governance in Europe's phosphate fertilizers: Not so fast? Sci. Total Environ. **650** (2019) 541–545.

[2.34] GONZALEZ, M.P., NAVARRO, R., SAUCEDO, I., AVILA, M., REVILLA, J., BOUCHARD, C., Purification of phosphoric acid solutions by reverse osmosis and nanofiltration, Desalination **147** (2002) 315–320.

[2.35] MOUSA, M.A., GADO, H.S., ABDELFATTAH, M.M.G., MADI, A.E., TAHA, M.H., ROSHDY, O.E., Removal of uranium from crude phosphoric acid by precipitation technique, Arab J. Nucl. Sci. Appl. **46** (2013) 38–47.

[2.36] QAMOUCHE, K., CHETAINE, A., ELYAHYAOUI, A., MOUSSAIF, A., TOUZANI, R., BENKDAD, A., AMSIL, H., Radiological characterization of phosphate rocks , phosphogypsum, phosphoric acid and phosphate fertilizers in Morocco: An assessment of the radiological hazard impact on the environment, Mater. Today Proc. **27** (2020**)**.

[2.37] MONSER, L., BEN AMOR, M., KSIBI, M., Purification of wet phosphoric acid using modified activated carbon, Chem. Eng. Process. **38** (1999) 267–271.

[2.38] DAIFULLAH, A.A.M., AWWAD, N.S., EL-REEFY, S.A., Purification of wet phosphoric acid from ferric ions using modified rice husk, Chem. Eng. Process. **43** (2004) 193–201.

[2.39] NASR, B.B., HEDI, B., ABDELLATIF, G., RODRIGO, M.A., Purification of wet-process phosphoric acid by hydrogen peroxide oxidation, activated carbon adsorption and electrooxidation, Chem. Eng. Technol, **28** (2005) 193–198.

[2.40] EL-ASMY, A.A., SERAG, H.M., MAHDY, M.A., AMIN, M.I., Purification of phosphoric acid by minimizing iron, copper, cadmium and fluoride, Sep. Purif. Technol. **61** (2008) 287–292.

[2.41] ZERMANE, S., MENIAI, A.H., Experimental study of competitive adsorption of heavy metals and organic matter for the phosphoric acid purification, Energy Procedia **18** (2012) 888–895.

[2.42] GEISSLER, B., STEINER, G., MEW, M.C., Clearing the fog on phosphate rock data — Uncertainties, fuzziness, and misunderstandings, Sci. Total Environ. **642** (2018) 250–263.

[2.43] VAN KAUWENBERGH, S.J., Cadmium and other Minor Elements in World Resources of Phosphate Rock (Proc. Fertiliser Society No. 400) (1997).

[2.44] USGS Phosphate Rock Statistics and Information; National Minerals Information Center (2020).

[2.45] BULUT, Y., TEZ, Z., Removal of heavy metals from aqueous solution by sawdust adsorption, J. Environ. Sci. **19** (2007) 160–166.

[2.46] MEENA, A.K., KADIRVELU, K., MISHRA, G.K., RAJAGOPAL, C., NAGAR, P.N., Adsorptive removal of heavy metals from aqueous solution by treated sawdust (Acacia arabica), J. Hazard. Mater. **150** (2007) 604–611.

[2.47] SHAKOOR, S., NASAR, A., Adsorptive decontamination of synthetic wastewater containing crystal violet dye by employing Terminalia Arjuna sawdust waste, Ground Water Sustain. Dev. **7** (2018) 30–38.

[2.48] CHEN, X., XU, R., XU, Y., HU, H., PAN, S., PAN, H., Natural adsorbent based on sawdust for removing impurities in waste lubricants, J. Hazard. Mater. **350** (2018) 38–45.

[2.49] ALIDADI, H., DOLATABADI, M., DAVOUDI, M., BARJASTEH-ASKARI, F., JAMALI-BEHNAM, F., HOSSEINZADEH, A., Enhanced removal of tetracycline using modified sawdust: Optimization, isotherm, kinetics, and regeneration studies, Chem. Process Saf. Environ. Prot. (2018).

[2.50] SĆIBAN, M., RADETIĆ, B., KEVRESAN, Z., KLASNJA, M., Adsorption of heavy metals from electroplating wastewater by wood sawdust, Bioresour. Technol. **98** (2006) 402–409.

[2.51] SĆIBAN, M., KLASNJA, M., SKRBIĆ, B., Modified softwood sawdust as adsorbent of heavy metal ions from water, J. Hazard. Mater. **136** (2006) 266–271.

[2.52] DUPONT, L., BOUANDA, J., DUMONCEAU, J., APLINCOURT, M., Biosorption of Cu(II) and Zn(II) onto a lignocellulosic substrate extracted from wheat bran, Environ. Chem. Lett. (2005) 165–168.

[2.53] BOUQBIS, L., DAOUD, S., KOYRO, H.W., KAMMANN, C.I., AINLHOUT, L.F.Z., HARROUNI, M.C., Biochar from argan shells: production and characterization, Int. J. Recycl. Org. Waste Agric. **5** (2016) 361–365.

[2.54] ELMOUWAHIDI, A., ZAPATA-BENABITHE, Z., CARRASCO-MARÍN, F., MORENO-CASTILLA, C., Activated carbons from KOH-activation of argan (Argania spinosa) seed shells as supercapacitor electrodes, Bioresour. Technol. **111** (2012) 185–190.

[2.55] QAISS, A., BOUHFID, R., ESSABIR, H., Characterization and use of coir, almond, apricot, argan, shells, and wood as reinforcement in the polymeric matrix in order to valorize these products, Agric.Biomass Based Potential Mater. (2015) 305–339.

[2.56] CHARROUF, Z., HILALI, M., JAUREGUI, O., SOUFIAOUI, M., GUILLAUME, D., Separation and characterization of phenolic compounds in argan fruit pulp using liquid chromatography-negative electrospray ionization tandem mass spectroscopy, Food Chem. **100** (2007) 1398–1401.

[2.57] ESSABIR, H., ACHABY, M., HILALI, E., BOUHFID, R., QAISS, A., Morphological, structural, thermal and tensile properties of high density polyethylene composites reinforced with treated argan nut shell particles, J. Bionic Eng. **12** (2015) 129–141.

[2.58] ZBAIR, M., AINASSAARI, K., DRIF, A., OJALA, S., BOTTLINGER, M., PIRILÄ, M., KEISKI, R.L., BENSITEL, M., BRAHMI, R., Toward new benchmark adsorbents: preparation and characterization of activated carbon from argan nut shell for bisphenol A removal, Environ. Sci. Pollut. Res. Int. **25** (2017) 1869–1882.

[2.59] TATANE, M., ELMINOR, H., AYEB, M., LACHERAI, A., Effect of argan nut shell powder on thermal and mechanical behavior of compressed earth blocks, Int. J. Appl. Eng. Res. **13** (2018) 4740–4750.

[2.60] ZBAIR, M., BOTTLINGER, M., AINASSAARI, K., OJALA, S., STEIN, O., KEISKI, R.L., BENSITEL, M., BRAHMI, R., Hydrothermal carbonization of argan nut shell: Functional mesoporous carbon with excellent performance in the adsorption of

bisphenol A and diuron, Waste Biomass Valorization **11** (2020) 1565–1584.

[2.61] EL BOUNDATI, Y., ZIAT, K., NAJI, A., SAIDI, M., Generalized fractal-like adsorption kinetic models: Application to adsorption of copper on argan nut shell, J. Mol. Liq. **276** (2019) 15–26.

[2.62] BENJEDIM, S., ROMERO-CANO, L.A., PÉREZ-CADENAS, A.F., BAUTISTA-TOLEDO, M.I., LOTFI, E.M., CARRASCO-MARIN, F., Removal of emerging pollutants present in water using an E-coli biofilm supported onto activated carbons prepared from argan wastes: Adsorption studies in batch and fixed bed, Sci. Total Environ. **720** (2020) 137491.

[2.63] EL-KHOMRI, M., EL-MESSAOUDI, N., BENTAHAR, S., DBIK, A., LACHERAI, A., Removal of cationic dye from aqueous solution using agricultural wastes: Argan and almond shells, Iran. J. Energy Environ. **9** (2018) 255–262.

[2.64] CHAFIK, T., Nanoporous Carbonated Materials prepared from the Shell of the Argan Fruit, Patent WO/2012/050411 a1 2012.

[2.65] MOUSSAOUI, H., BAHAMMOU, Y., IDLIMAM, A., LAMHARRAR, A., ABDENOURI, N., Investigation of hygroscopic equilibrium and modeling sorption isotherms of the argan products: A comparative study of leaves, pulps, and fruits, Food Bioprod. Process. **114** (2018) 12–22.

[2.66] BOUJIBAR, O., SOUIKNY, A., GHAMOUSS, F., ACHAK, O., DAHBI, M., CHAFIK, T., CO2 capture using N-containing nanoporous activated carbon obtained from argan fruit shells, J. Environ. Chem. Eng. **6** (2018) 1995–2002.

[2.67] DHABI, M., KISO, M., KUBOTA, K., HORIBA, T., CHAFIK, T., HIDA, K., MATSUYAMA, T., KOMABA, S., Synthesis of hard carbon from argan shells for Na-ion batteries, J. Mater. Chem. A **5** (2017) 9917–9928.

[2.68] ALY, M.M., MOUSA, M.A., TAHA, M.H., KANDIL, K.M., EL-ZOGHBY, A.A., Kinetics and thermodynamics of uranium adsorption from commercial di-hydrate phosphoric acid using D 2 EHPA-impregnated charcoal, Arab J. Nucl. Sci. Appl. **46** (2013) 29–37.

[2.69] YANG, H., YAN, R., CHEN, H., LEE, D.H., ZHENG, C., Characteristics of hemicellulose, cellulose and lignin pyrolysis, Fuel **86** (2007) 1781–1788.

[2.70] BELLO, O.S., AHMAD, M.A., AHMAD, N., Adsorptive features of banana (Musa paradisiaca) stalk-based activated carbon for malachite green dye removal, Chem. Ecol. **28** (2012) 153–167.

[2.71] MUSIĆ, S., KREHULA, S., POPOVIĆ, S., SKOKO, Ž., Some factors influencing forced hydrolysis of $FeCl_3$ solutions, Mater. Lett. **57** (2003) 1096–1102.

[2.72] DÁVILA-JIMÉNEZ, M.M., ELIZALDE-GONZÁLEZ, M.P., PELÁEZ-CID, A.A., Adsorption interaction between natural adsorbents and textile dyes in aqueous solution. Physicochemical and engineering aspects, Colloids Surf. A **254** (2005) 107–114.

[2.73] GUPTA, V.K., RASTOGI, A., Sorption and desorption studies of chromium(VI) from nonviable cyanobacterium Nostoc muscorum biomass, J. Hazard. Mater. **154** (2008) 347–354.

[2.74] GAO, Y., LI, Y., ZHANG, L., HUANG, H., HU, J., SHAH, S.M., SU, X., Adsorption and removal of tetracycline antibiotics from aqueous solution by graphene oxide, J. Colloid Interface Sci. **368** (2011) 540–546.

[2.75] GARCÍA-ROSALES, G., COLÍN-CRUZ, A., Biosorption of lead by maize (Zea mays) stalk sponge, J. Environ. Manage. **91** (2010) 2079–2086.

[2.76] WANG, Y., LIU, R., Comparison of characteristics of twenty-one types of biochar and their ability to remove multi-heavy metals and methylene blue in solution, Fuel Process. Technol. **160** (2017) 55–63.

[2.77] MWAIKAMBO, L.Y., ANSELL, M.P., Chemical modification of hemp, sisal, jute, and kapok fibers by alkalization, J. Appl. Polym. Sci. (2002) 2222–2234.

[2.78] AHMARUZZAMAN, M., GUPTA, V.K., Rice husk and its ash as low-cost adsorbents in water and wastewater treatment, Ind. Eng. Chem. Res. **50** (2011) 13589–13613.

[2.79] RICORDEL, S., TAHA, S., CISSE, I., DORANGE, G., Heavy metals removal by adsorption onto peanut husks carbon: Characterization, kinetic study and modeling, Sep. Purif. Technol. **24** (2001) 389–401.

[2.80] SRIVASTAVA, V.C., MALL, I.D., MISHRA, I.M., Characterization of mesoporous rice husk ash (RHA) and adsorption kinetics of metal ions from aqueous solution onto RHA, J. Hazard. Mater. **134** (2006) 257–267.

[2.81] LIU, D., HAN, G., HUANG, J., ZHANG, Y., Composition and structure study of natural Nelumbo nucifera fiber, Carbohydr. Polym. **75** (2009) 39–43.

[2.82] ESSABIR, H., HILALI, E., ELGHARAD, A., EL MINOR, H., IMAD, A., ELAMRAOUI, A., AL GAOUDI, O., Mechanical and thermal properties of bio-composites based on polypropylene reinforced with nut-shells of argan particles, Mater. Des. **49** (2013) 442–448.

[2.83] KURNIAWAN, T.A., CHAN, G.Y.S., LO, W.-H., BABEL, S., Comparisons of low-cost adsorbents for treating wastewaters laden with heavy metals, Sci. Total Environ. **366** (2006) 409–426.

[2.84] TAN, W.T., OOI, S.T., LEE, C.K., Removal of chromium(VI) from solution by coconut husk and palm pressed fibres, Environ. Technol. **14** (2008) 277–282.

[2.85] GIRI, A.K., PATEL, R., MANDAL, S., Removal of Cr (VI) from aqueous solution by Eichhornia Crassipes root biomass-derived activated carbon, Chem. Eng. J. **185–186**, (2012) 71–81.

[2.86] PATHAK, A., VINOBA, M., KOTHARI, R., Emerging role of organic acids in leaching of valuable metals from refinery-spent hydroprocessing catalysts, and potential techno-economic challenges: A review, Crit. Rev. Environ. Sci. Technol. **0** (2020) 1–43.

CHAPTER 3 CASE STUDIES ON THERMAL MINERAL ORE PROCESSING

3.1 INDIA: THERMAL TREATMENT OF LOW GRADE INDIAN URANIUM ORES

Investigations have been carried out on the potential use of thermal processes for developing low grade Indian uranium ores. Ores from Tummalapalle, Rohil-Ghateswar and Jaduguda have been considered in this study. Thermal characterization studies on the carbonate uranium ores using thermo gravimetry and differential thermal analysis (TG-DTA) techniques were coupled with evolved gas analysis, XRD and SEM analyses. The samples of the study included: pure pyrite, actual ore and float concentrate (enriched in pyrite) obtained from the ore.

Roasting of pure pyrite revealed that it oxidises between 405°C and 700°C, whereas calcination of ore at temperatures beyond about 550°C indicated the formation of a new phase ($CaSO_4$) along with other chemical compounds associated with the calcination. The occurrence of chemical reactions has been ascertained by the various peaks observed by the TG-DTA curves in conjunction with XRD analyses of products at intermediate temperatures. The oxidative roasting of crushed ore before grinding, at an optimum temperature of 585°C, for a residence time of 5 hour, resulted in the lowering of the work index from 13 to 7.7 kwh/t, and a cleaner leach liquor with a reduction of 30% lower sulphate concentration for further recovery of uranium by precipitation. It was found that the energy that can be utilized from a nuclear power reactor from the uranium present in the ore, is several orders higher than the energy spent for thermal pre-treatment of the ore. The results of this study did thus actively support the idea of energy neutral mineral processing.

The present study also includes the recovery of by-products from the tailings of a metasomatite uranium ore of Indian origin, containing 1400, 270 and 240 ppm Cu, Mo and Ni respectively as sulphides, along with 400 ppm U_3O_8 and 77% SiO_2 as the main gangue material. The leach residue after the removal of uranium from the ore was subjected to froth flotation for separation and concentrations of sulphide minerals containing Cu, Mo and Ni. It is proposed that the sulphide rich flotation concentrate be subjected to sulphation roasting at about 550°C, followed by mild acid and alkaline leaching for the recovery of Cu and Mo.

A study was carried out on the roasting of the bulk sulphide byproduct obtained by flotation of the uranium ore from Jaduguda, Jharkhand. Results showed the feasibility of recovering Cu, Ni, Co and Mo with yields of 98%, 65%, 93% and 93% respectively, at an optimum roasting temperature of 550°C for 4 hours residence time, using 12 wt% alkali sulphate as additive.

The department of Atomic Energy in India is engaged in the development of nuclear power technology, including exploration, mining and processing of nuclear minerals, applications of radiation technologies in the fields of agriculture, medicine, industry, and basic research. At present, about 7.5 GWe is generated in India with 23 nuclear power reactors which contribute 2.2% of the total electricity generated in the country. It is planned to increase this to about 64 GWe by the year 2032, comprizing mainly of pressurized heavy water reactors (PHWRs) and light water reactors (LWRs) with a minor contribution from a fast breeder reactor (500 MWe) and an advanced heavy water reactor (300 MWe) [3.1]. To operate its nuclear reactors, India requires currently about 1000 t of uranium per year. Of this amount the indigenous supply can cover 385 t uranium per year. The demand for uranium in India is envisaged to increase exponentially to about 2915 t per year by 2035, according to the Indian nuclear power program plan [3.2-3.4]. In a pursuit to bridge the uranium supply demand gap in India, extensive R&D

studies are being carried out on the extraction of uranium from complex and refractory ores of lean tenor and/or high carbonate content.

Thermal processing of ores has taken a backseat in the last two decades, due to a variety of reasons chiefly, the high capital cost of calcination plants, the energy extensive operation, the low reactivity of calcined products and the release of environmentally harmful gases. However, the advent of flash calcination technology (FCT), prevalent in modern green cement production, addressed some inherent drawbacks of the conventional calcination process [3.5]. The unique advantages of FCT, such as the very short retention times in high temperature zones, high heat transfer rates, good oxygen contact and rapid cooling, would be significantly useful for processing carbonate rich uranium ores of very- or ultra-fine size mineralization.

The thermal treatment of the carbonate type of ores yields incidental concentration of the uranium content due to a release of CO_2 from the material processed, which is beneficial for ores of lean tenor. The increased porosity aids in reducing energy input for comminution and improves leach recovery. With regards to CO_2 released during calcination, that is obviously one of the non-desirable aspects, the mineral industry is now using specially designed calciners that have in-built design features for capturing and yielding potential food grade CO_2 [3.6]. The utilization of surplus heat and/or part of the electricity generated by HTRs can possibly make thermal processing an attractive and sustainable option for processing complex carbonate uranium ores, particularly those of lean tenor, in which the uranium mineral is finely disseminated and contained in refractory minerals.

The Tummalapalle uranium ore is a phosphatic, silicious calcitic dolostone, in which the uranium values are finely disseminated and intimately associated with the reactive gangue mineral, pyrite. The ore contains 0.03–0.04% U_3O_8, 1.24% pyrite and 80% carbonates (mostly dolostone) by weight. Mineralogical studies have indicated that about 5–8% uranium values are intimately associated with pyrite. Though hydrometallurgical processing under alkaline conditions is an established option for such uranium ore [3.7], simultaneous dissolution of sulphide minerals pyrite, pyrrhotite, chalcopyrite, etc. results in the co-existence of sulphate ions in the leach liquor along with uranium. The complex mineralogy of the ore necessitates aggressive leaching conditions, resulting in high total dissolved solids (TDS) of about 150 g/L in the leach liquor. The high TDS content in the leach liquor does not favour concentration and purification of uranium values by the ion exchange process in the downstream. A presence of high concentrations of other anionic species like CO_3^{2-}, HCO_3^- and SO_4^{2-} in comparison to $[UO_2(CO_3)_3]^{4-}$, results in an inefficiency of ion exchange (IX) purification [3.8]. The processing of uranium ores containing more than 1.5% S causes problems in both leaching of uranium and a subsequent IX process [3.9]. This in effect leaves sub-stoichiometric quantities of these reagents for effective uranium minerals solubilization, thereby decreasing the overall leachability [3.9]. Moreover, the lean grade of the ore in question calls for a complex process flow chart, including the recycling of part of the leach liquor, to build up the concentration of uranium before the precipitation of yellow cake.

Thermal pretreatment of the ore at an appropriate temperature is one of the ways of minimizing the solubilization of sulphides during leaching and thereby reducing the deleterious effect of sulphates on downstream hydrometallurgical processes. Thermal treatment of ore aids the conversion of sulphides to respective oxides, which are not leachable under alkaline conditions. Besides, it is expected that micro cracks developed in composite particles due to the heat treatment of ore, will not only lower the energy required for comminution but also improve the accessibility of the uranium grains to leachants, owing to the increased porosity and higher liberation. Thermal treatment of carbonate rocks results in

the release of CO_2 gas and increases the surface area due to increased porosity. Considering the above benefits, the option of thermal pre-treatment of Tummalapalle uranium ore is considered. A differential thermal pre-treatment of the ore, including the removal of sulphur from pyrite, followed by the decomposition of carbonates, has been attempted to address the above issues. The thermal treatment, prior to alkaline leaching of the ore, would have advantages of (1) reducing the work index of the ore which lowers the energy during the grinding of the ore, (2) allowing for leach liquor (with lower TDS) to be suitable for the purification by an IX process, as sulphur is removed by the oxidation of pyrite to iron oxide. Lastly, (3) the uranium leaching efficiency may increase due to an increased porosity of the carbonate ore.

Besides Tummalapalle uranium ore, a promising new metasomatite type of uranium deposit was discovered in the Rohil-Ghateshwar area located in the Sikar district of Rajasthan. The host rocks of this deposit are albitized biotite schists of the Delhi fold belt [3.10]. The predominant presence of siliceous minerals in the Rohil ore, necessitated an acid leaching route for the extraction of uranium values. However, the presence of significant amounts of sulphides of Fe, Cu, Ni and Mo in the ore, calls for their removal/recovery from the ore before discharging it back into the environment. The comprehensive process scheme developed for this ore consists of the removal of Fe sulphides by magnetic separation, recovery of uranium by acid leaching and recovery of Cu, Ni and Mo from the leach residue by froth flotation, followed by sulphatizing roasting and water leaching [3.11]. Studies presented in this publication, include the development of a process scheme for the recovery of byproducts such as Cu, Ni and Mo from the leach residue by a pyrometallurgical route.

The first uranium mine in India is operating at Jaduguda, Jharkhand since 1967. The process flow chart, to produce uranium concentrate as a magnesium diuranate, can be referred to in the publication by Suri et al. [3.12]. The chlorite-biotite schist type of ore contained sulphides of Cu, Mo, Ni and Fe. The ore was crushed and ground in a rod and pebble mill. The ground ore slurry was subjected to froth flotation to separate out the sulphides as float. The flotation sink was dewatered using a high rate thickener, followed by a disk filter. The filter cake was repulped to about 50 wt% solids and then leached in air using agitated leaching tanks, known as Pachucas. Leaching was carried out using dilute sulphuric acid (at a pH of about 1.6–1.8) as leachant and pyrolusite as the oxidant. The leach slurry was filtered and clarified, to get the uranium bearing mother liquor. This liquor was purified and concentrated by ion exchange, using an anionic exchange resin. The uranium values from the resin are eluted by an acidified brine solution, which is treated with lime to increase the pH to about 3.5. The excess iron and sulphate, present in the system, is then removed as iron-gypsum cake and recycled back to the re-pulping stage, before leaching. H_2O_2 is added to the iron-free eluate after ion exchange to precipitate uranium peroxide. NH_3 is added to maintain the acidity (pH = 3.5). The waste solid and liquid streams are neutralized by limestone to precipitate radionuclides along with heavy metals like Mn, Fe, Cu, and others. The waste slurry is then classified in a hydro cyclone. The cyclone underflow is sent back for mine-backfill and the overflow is sent to a tailings pond. The tailings pond effluent is treated with barium chloride and lime to precipitate radionuclides before being returned to the tailings pond.

The bulk sulphide float produced from the ore, was studied for the recovery of Cu, Ni, Co and Mo by thermal processing. The scope for recovering by sulphatizing roasting followed by leaching was published by Anand Rao et al. [3.13]. A brief account of these studies is given in this publication, showing the importance and scope of thermal processing for the recovery of Cu, Ni, Co and Mo as byproducts.

A pure iron pyrite sample was purchased from M/s Jainson laboratories, Meerut, India. The purity of the pyrite powder was found to be >99%, from the analysis carried out by an inductively coupled plasma-optical emission spectrometry (ICP-OES). The whole rock analysis of uranium ore samples, used in the investigations, is given in Table 3.1.

TABLE 3.1 WHOLE ROCK ANALYSIS OF THE THREE URANIUM ORE SAMPLES INVESTIGATED

Analyte	**Tummalapalle**	**Rohil-Ghateshwar**	**Jaduguda**
U_3O_8	0.048	0.04	0.06
SiO_2	19.4	58.9	67.2
CaO	24.7	3.1	5.4
MgO	13.7	3.6	2.2
Loss on Ignition	32	4.2	
S (Total)	0.8	4.3	0.8
Fe (Total)	1.5	10	10.5
Ni	Traces	0.024	0.1
P_2O_5	2.8	0.06	1.4
MnO	0.2	0.04	
Mo	-	0.024	0.02
Na_2O	0.2	4.3	
K_2O	1.8	1.04	
TiO_2	0.1	0.28	0.66
Al_2O_3	2.2	9.1	5.5

Thermal characterization of pure pyrite, Tummalapalle ore and the flotation concentrate (sulphide concentrate), separated from the Tummalapalle ore, was carried out using simultaneous thermogravimetric analysis (TGA) and differential thermal analysis (DTA) in a commercial unit (Leinseis STA PT-1600) with about 50 mg charge heated at 10°C/min rate in an alumina cup under air flow (20 mL/min) and with alumina as the reference material. The equipment was provided with an evolved gas analysis attachment. The roasted samples were characterized with respect to morphology and microstructure by scanning electron microscopy (SEM, Camscan MV2300CT/100, UK). Phase identification was carried out by XRD in an Inel-make unit (model MPD) with Cr-K_α radiation at 30 mA, 40 KV using a curved position-sensitive detector, thereby observing the diffraction data in a complete 2θ range of interest simultaneously. Uranium and sulphur in the ores and heat treated products, were chemically analysed by ICP-OES, following the standard procedures as described by Ray et al. [3.14].

The Bond work index (BWI) is an inherent property of material and is independent of the head feed granulometry. Development of micro cracks and changes in the structure of the rock, due to decomposition reactions, are envisaged during the thermal treatment of ores, carbonates in

particular, which reduces the BWI of the ore. The BWI of the ore before and after thermal treatment was determined using the standard procedure and calculated using Eq. (3.1) [3.15].

$$W_i = \frac{4.45}{P_i^{0.23} G^{0.82} P^{0.5} F^{0.5}} \tag{3.1}$$

where

W_i is the work index;

P_i is the mesh of grind = (75 microns in this case) (mm);

G is the grindability (grams/revolution);

F is the 80% passing feed size (mm);

P is the 80% passing product size (mm).

The Tummalapalle ore samples were crushed in a jaw crusher, followed by a roll crusher and then ground in a wet ball mill to get to the required particle size. A sulphide concentrate was separated from the ore, in order to understand the effect of sulphide on roasting of the remaining ore. Floatation of the ground ore was carried out to produce pyrite concentrate at optimized parameters: Size = 85% passing 100#, In situ pH = 8.5, 0.125 kg/t of sodium isopropyl xanthate ($C_4H_7NaOS_2$) as collector, 0.025 kg/t of sodium silicate as dispersant, 0.1 kg/t of amyl alcohol as frother. The flotation concentrate assayed 4.18% S. The flotation experiments were carried out in a 3 L Denver flotation cell.

Split core bore-hole samples from the Rohil-Ghateswar ore were prepared by mixing. XRD and optical microscopic analyzis indicated uraninite as the major uranium bearing phase with smaller amounts of brannerite and davidite. The other minerals that were identified were: chalcopyrite, molybdenite, pyrite, pyrrhotite, riebeckite, quartz, traces of albite, biotite, boulangerite, chlorite, covellite and goethite. Amongst the sulphides, the pyrrhotite content is about 10% and pyrite is 1.1%. Uraninite is mostly liberated, however occasionally uraninite of a very fine size is associated with non pyrrhotite sulphides. The process flow chart for preparing the feed for roasting for the recovery of Cu and Mo as byproducts, is given in Fig. 3.1. After size reduction stages, the ground ore was leached for uranium, using sulphuric acid, maintaining a pH of 1.5, and an oxidation potential of 400–420 mV using MnO_2, 50 wt% solids at 40–45°C for 6 hours. Pyrrhotite was removed from the leach residue by magnetic separation at about 2 kGauss, using a wet high intensity magnetic separator. The non magnetic fraction was subjected to a two stage (Rougher followed by Cleaner) froth flotation using 0.5 kg/t sodium isopropyl xanthate as collector, 0.5 kg/t sodium silicate as dispersant and 0.2 kg/t amyl alcohol as frother. About 80% and 92% Cu and Mo values present in the ore could be recovered in the float product which assayed 20% S, 2.2% Cu and 0.4% Mo. This sulphide float was used as feed for subsequent sulphation roasting experiments.

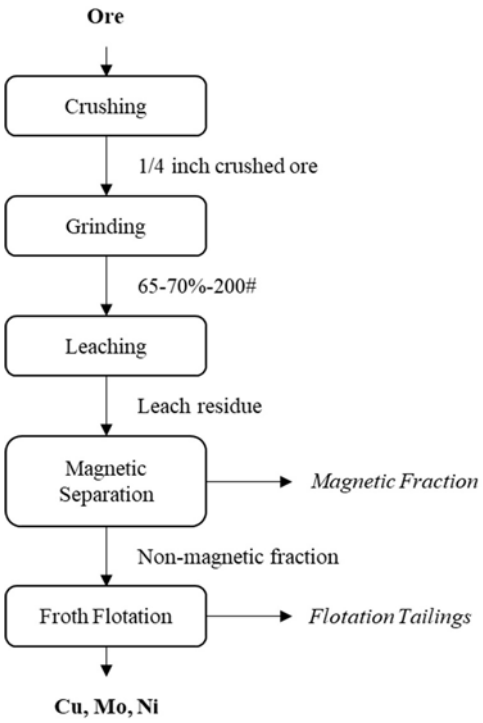

FIG. 3.1. Process scheme followed for the preparation of feed for roasting experiments for the recovery of Cu, Mo and Ni.

A bulk sulphide float was being produced at the Jaduguda uranium mill, by the flotation of sulphides from the ground ore, using cresylic acid, creosote, soda and light diesel oil as flotation reagents; their details are reported elsewhere [3.13]. The bulk sulphide float contained 11% Cu, 7% Ni, 0.4% Co, 3% Mo, 0.17% Pb and 0.26% Fe as their respective sulphide minerals. The size of this product was 60%, passing 75 μm.

The Tummalapalle ore, sulphide float concentrates and pure pyrite samples were placed in a silica crucible (size: 15.6 × 9.8 × 15.6 mm) with a powder thickness of 2 mm and then subjected to oxidative roasting in a muffle furnace at pre set temperatures for 5 hours duration. The calcines obtained, were subsequently taken out from the furnace, and naturally cooled in air to room temperature. The sulphide concentrates samples obtained by the flotation of the uranium ore were subjected to sulphatizing roasting, following the same procedure as above, except that the Na_2SO_4 was added as additive to improve the conversion of sulphides to sulphates of Cu and Mo. The bulk sulphide float obtained from Jaduguda ore was subjected to sulphatizing roasting in a muffle furnace already heated to the desired temperature as reported earlier [3.13].

Calcines of Tummalapalle ore obtained after roasting were air cooled and subjected to leaching studies in a stainless steel autoclave reactor (1 L capacity) equipped with the necessary instrumentation and controls to maintain a pre set temperature, overpressure, gas sparging and agitation speed of the impeller. All the experiments were conducted at optimum conditions, as they were determined in earlier studies. The calcines of Rohil-Ghateswar and Jaduguda samples were subjected to plain water leaching for recovery of Cu, Mo, Ni and Co into the liquid phase.

The identification of process steps and the temperature range in which pyrite in the ore decomposes, are important with reference to the liberation of uranium as mentioned earlier. As the pyrite content (1.6%) in the original ore is quite low, the sulphide flotation concentrate (assaying 8% pyrite) was obtained from the ore for getting accentuated effects during the thermal study. The TG-DTA data of both the original ore and the sulphide flotation concentrate separated from the ore, were compared to the oxidation of pure pyrite, to understand the pyrite decomposition event appropriately.

The TGA-DTA curves of Tummalapalle ore showed a broad exothermic peak, starting at 394°C. In the flotation concentrate of the ore, the same peak is more pronounced, showing clearly resolved double exothermic peaks. When these exothermic peaks were compared with the oxidation peaks of pure pyrite, it could be seen that the events starting at around 394°C in the ore and that of the flotation concentrate, are due to the oxidation of pyrite to FeS and the subsequent oxidation of FeS to Fe_2O_3 as indicated in the reactions below.

$$FeS_2 + O_2 = FeS + SO_2$$

$$4FeS + 7O_2 = 2Fe_2O_3 + 4SO_2$$

The evolved gas analysis at 438°C indicated SO_2 gas emission, thereby confirming the occurrence of oxidation reactions as seen below.

$$4FeS + 4CaCO_3 + 9O_2 = 2Fe_2O_3 + 4CO_2 + 4CaSO_4$$

$$2FeS_2 + 4CaCO_3 + 7.5O_2 = Fe_2O_3 + 4CO_2 + 4CaSO_4$$

The mass change was observed in the TG-DTA curve of the actual ore between 473°C and 557°C, which is the result of two competing reactions, occurring simultaneously. First was the reaction of FeS/FeS_2 (unreacted) with calcium carbonate of dolomite forming Fe_2O_3 and $CaSO_4$ and the second was the simple oxidation of FeS.

The XRD of products taken out at various temperatures (for the flotation ore sample) are shown in Fig. 3.2. The reaction product at 585°C shows a slight decrease in dolomite peak intensity and the formation of $CaSO_4$, thereby confirming the reactions.

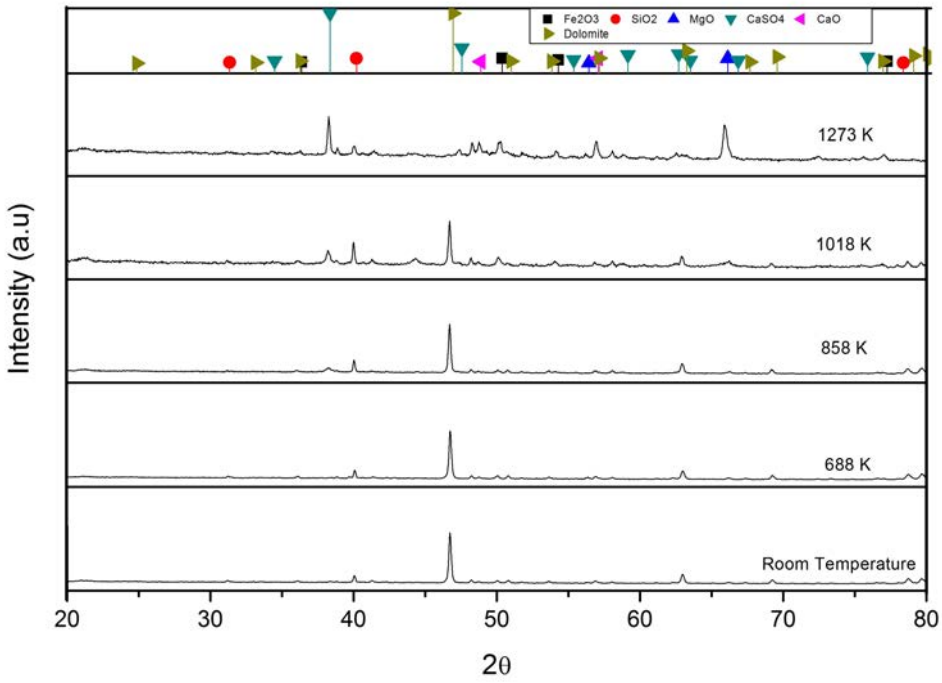

FIG. 3.2. XRD patterns obtained after heating floatation concentrate of Tummalapalle ore to various temperatures.

Beyond 557°C unreacted dolomite in the ore decomposes. There is large mass loss commencing at around 682°C . The occurrence of the reaction can also be confirmed from the evolved gas analysis showing CO_2 liberation at 764°C. It could also be observed that silica in the ore remains unreacted. The final products of heating the ore at 1000°C were thus $CaSO_4$, Fe_2O_3, MgO, CaO and unreacted SiO_2.

$$MgCa(CO_3)_2 = MgO + CaO + CO_2$$

The BWI of the Tummalapalle uranium ore was estimated to be 15.7 KWh/t. The BWI of the same ore after heat treatment at 900°C was found to be 7 KWh/t or less than half of the original BWI. Significant reduction in the BWI was found for calcined uranium ore. The results obtained indicate important improvements in the BWI, due to calcination. Calcination of ore created micro fractures at intergranular and transgranular level, caused by differential heating and subsequent thermal expansion between the mineral phases. This was supported by scanning electron microscopy (Fig. 3.3) which shows the formation of fractures during calcination.

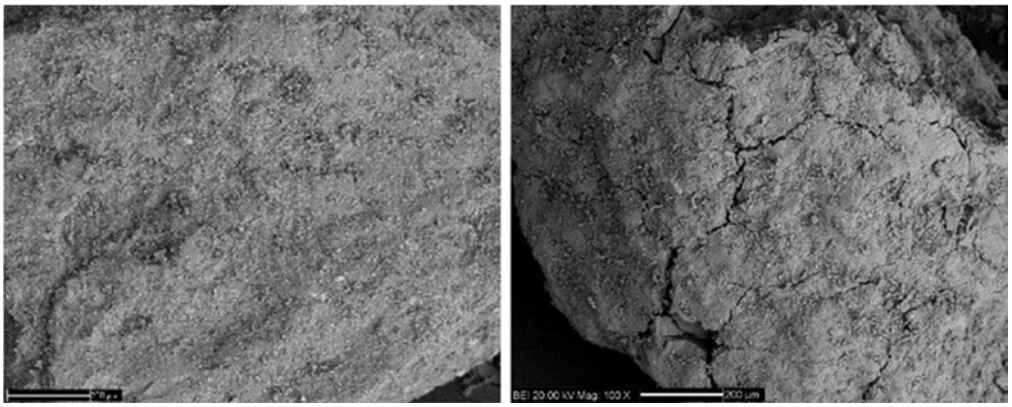

FIG. 3.3. SEM images of the ore (a) before and (b) after calcination at 900°C.

Based on the TG-DTA analysis of the floatation concentrate obtained from Tummalapalle uranium ore, three roasting temperatures at 450°C, 585°C and 900°C were chosen, to study the effect of thermal pretreatment on the leachability of uranium and the leach liquor chemistry.

The ground ore was ultimately leached in a batch autoclave reactor at previously achieved optimum process conditions described by Suri [3.16], namely Na_2CO_3 45 g/L, $NaHCO_3$ 45 g/L, PO_2 7 kg cm^{-2}, a temperature of 125°C, contact time of 4 hours and a solid concentration of 50 wt%. The uranium leachability obtained in pressure leaching was about 77%. The reactive nature of sulphide minerals, particularly pyrite, led to a high consumption of lixiviants and oxidants. The $[SO_4]^{2-}$content obtained in the single stage leach solution was about 27 g/L, due to the aggressive leaching conditions, resulting in near complete dissolution of reactive gangue, pyrite (FeS_2) present in the ore. $[SO_4]^{2-}$ content in the leach solution is a point of concern as it takes away the sodium hydroxide added along with it in the form of counter ion $[Na]^{+1}$, requiring a fresh supplement and there are further strict limits on the $[SO_4]^{2-}$ concentration levels in the mill effluents.

Precipitation of sulphate as calcium salt is not at all efficient under prevailing alkaline conditions (pH: 9.8–10) of the leach liquor. Hence, to the extent possible, the parameters during leaching of uranium are manipulated so that the dissolution of pyrite is within manageable limits.

XRD analysis of thermally treated flotation concentrate at 585°C showed that the products of the oxidizing reaction of pyrite in the presence of flowing air were Fe_2O_3 and $CaSO_4$. Keeping this in mind, roasting of the Tummalapalle ore was carried out in a muffle furnace at 585 °C for 5 hours. The resulting calcine was then subjected to leaching in a batch autoclave reactor at the same process condition as applied to untreated calcine. The leachability of the uranium values was about 72%. An interesting observation was the drop in the sodium sulphate content of the leach liquor to 19 g/L, which shows a clear 30% decrease, in comparison to that present in the leach liquor generated from untreated ore under identical experimental conditions. Since uranyl carbonate is an anionic complex, presence of excessive sulphate ions in leach liquor would critically affect the loading capacity of the anionic exchange resins. A drop in the sulphate ion concentration in the leach liquor would therefore show a positive impact on enhancing the ion exchange performance.

Though the TG-DTA and XRD analysis of Tummallapalle uranium ore showed that the ore undergoes thermal decomposition to form CaO, MgO and CO_2 at temperatures ranging from 720°C to 848°C and results in increased porosity due to gas release and other cracks enabling better diffusion and transport of the reactants and products in the leaching process, the leachability of uranium was substantially low. Results of the leaching experiments carried out on the ore treated at 585°C and 900°C along with that of untreated ore are given in Table 3.2. Poor extraction of uranium from roasted calcines can be attributed to a higher pH, a pH of about 12, of resulting leach slurry due to the formation of calcium hydroxide. The conducive pH for good leaching of uranium with sodium carbonate and sodium bicarbonate under oxidizing conditions is pH 9–10. Thus, the solution pH of the resulting calcine slurry explains the suboptimal leachability of uranium values.

TABLE 3.2. LEACHING RESULTS OF CALCINE OBTAINED AFTER CALCINING AT 585°C AND 900°C FOR 5 HOURS

Fixed parameters: scale of experiment = 250 g; MOG (-200#) = 77%; Solid concentration = 50% (by weight); Temperature = 125°C; Contact time = 4 hours; Na_2CO_3 = 45 kg/t; $NaHCO_3$ = 45 kg/t; Oxidant = oxygen; Reaction pressure = 7 kg/cm^2

	Leachability (%)		Leach liquor
	Uranium	**Sulphur**	**Na_2SO_4(g/L)**
Unroasted	77.2	79.23	27.18
585°C	72	79.6	19
900°C	0	81.7	19.5

The effect of roasting temperature on the extraction of metals (Cu and Mo) by sulphation roasting water leaching technique from Rohil-Ghateswar uranium ore was further investigated. In each roasting experiment, the sulphide float and the Na_2SO_4 additive were mixed uniformly (Feed: Na_2SO_4 = 2:1) and roasted at various temperatures: 400 °C, 500 °C, 600 °C and 650 °C. Then roasted products were leached with hot water (90–95°C) for 6 hours. The results are given in Fig. 3.4. The leachability of Cu is about 82% and that of Mo is only about 1.8%. This could be due to Cu getting converted to $CuSO_4$ and Mo to MoO_3 during roasting and MoO_3 is not soluble in plain water. Hence, leaching of the calcine produced at 650 °C was carried out with dilute acidified water (5% H_2SO_4 by volume). The leachabilities of Cu and Mo have been found to increase to 98% and 80% respectively.

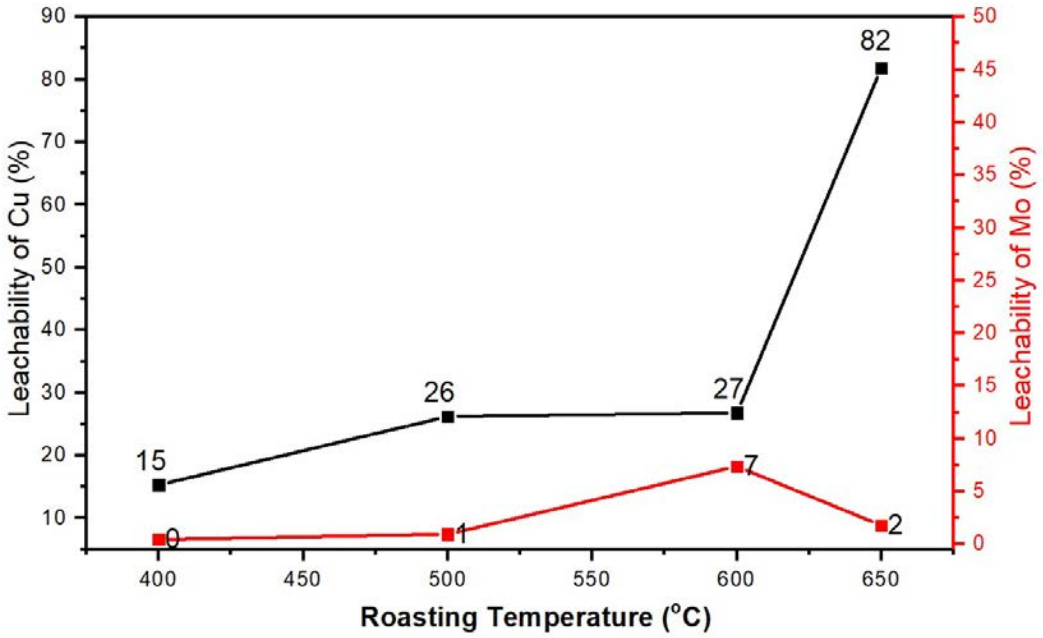

FIG. 3.4. Effect of temperature on the recovery of Cu and Mo values from the Rohil-Ghateswar uranium ore.

The chemical reactions during the roasting of bulk sulphide float are as follows:

$$MeS(s) + \frac{3}{2}O_2(g) \leftrightarrow MeO(s) + SO_2(g)$$

$$SO_2(g) + \frac{1}{2}O_2(g) \leftrightarrow SO_3(g)$$

$$MeO(s) + SO_3(g) \leftrightarrow MeSO_4(g)$$

$$2MeSO_4(s) \leftrightarrow 2MeSO(s) + 2SO_2(g) + O_2(g)$$

where Me stands for Cu, Ni, Co and Fe.

Several basic principles concerning sulphate roasting include the theoretical decomposition points of metal sulphates according to the chemical reactions above, the effect of the partial pressure of sulphur dioxide on these decomposition points and the theoretical selectivity of the sulphation reactions [3.17]. The metals Cu, Ni and Co can be effectively separated from Fe by controlling the temperature, as the decomposition temperature of $FeSO_4$ is much lower than the sulphates of Cu, Ni and Co. The following reactions take place in the case of MoS_2:

$$MoS_2(s) + 3O_2(g) \leftrightarrow MoO_2(s) + 2SO_2$$

$$2MoO_2(s) + O_2(g) \leftrightarrow 2MoO_3(s)$$

The roasted material was leached with plain water twice, for 30 minutes each time, at 333 K, maintaining 30–40% solids by weight to obtain Cu, Ni, Co and Mo in the aqueous phase. However, only some of the MoO_3 reports in leach solution due to its low solubility at acidic pH. Hence, the leach residue was releached at alkaline pH (adjusted using NaOH) for recovering the remaining MoO_3 values.

The factorial design scheme of the roasting experiments were carried out varying the roasting temperature in the range of 500°C to 650°C, residence time between 4 and 6 hours, addition of percentage quartz from 0 to 14 and an addition of per cent alkali sulphate between 0 and 6 details of which were reported in earlier studies [3.13]. Fisher's test indicated that the temperature, per cent alkali addition and their interaction effect are effective for recovering Ni and Co in that order whereas temperature alone was significant for recovering Cu. The results indicated the possibility of recovering Cu, Ni, Co and Mo with corresponding overall yields of 98%, 65%, 93% and 93% respectively by roasting at a temperature of 550°C for 4 hours residence time by adding 12wt% Li_2SO_4 before roasting.

The heat required for thermal decomposition of simplified Tummalapalle ore at 350°C can be estimated as following:

$$MgCO_3 = MgO + CO_2$$

$$(\Delta H^o)_R = (\Delta Hf^o)_{MgO} + (\Delta Hf^o)_{CO_2} - (\Delta Hf^o)_{MgCO_3} = 116.58\, kJ/mol$$

$$(\Delta_{623K})_R = (\Delta H^o)_R + \int_{298K}^{623K} (Cp)_{MgO} + (Cp)_{CO_2} - (Cp)_{MgCO_3} dT$$
$$= 115{,}204.67\, J/mol - K$$

The total heat required for $MgCO_3$ = (Sensible Heat from 25°C to 350°C)$_{Reactants}$ + Heat of reaction at 350°C + (Sensible Heat from 350°C to 727°C)$_{Products}$ = 2194.54 kJ/kg ($MgCO_3$).

In addition, decomposition of FeS_2 at 427°C needs to be considered:

$$2FeS_2 + 5.5O_2 = Fe_2O_3 + 4SO_2 = -6{,}020.52\,kJ/kg\ (FeS_2)$$

$CaCO_3$ decomposition is considered to take place at 727°C.

$$CaCO_3 = CaO + CO_2 = 2{,}505.75\,kJ/kg\ (CaCO_3)$$

It is assumed that SiO_2 undergoes no reaction and requires only sensible heat.

$$\int_{298}^{847K} (Cp)_{SiO_2} dT + \int_{847K}^{1{,}000K} (Cp)_{SiO_2} dT = 743.98\ kJ/kg(SiO_2)$$

The total heat required to raise 1 kg Tummalapalle uranium ore to 727°C was estimated to be 0.48 (heat required due to $CaCO_3$) + 0.32 (heat required due to $MgCO_3$) + 0.15 (heat required due to SiO_2) + 0.015 (heat required due to FeS_2) = 2007.6 kJ/kg.

The energy that could be utilized in a compact high temperature reactor (CHTR), a HTGR designed in India, from the contained uranium present in the Tummalapalle ore, is for example, several orders higher than the energy spent for thermal pretreatment of the ore. Similar calculations would show that the energy required, would be 1252 kJ/kg of simulated ore, for roasting at 585ºC (optimum roasting temperature found for thermal treatment of Tummalapalle ore in the present study). The energy that would be produced in a nuclear reactor from the uranium present in Tummalpalle ore is as high as 174 182 kJ/kg, which is much higher than the energy required for thermal pretreatment. The heat for thermal pretreatment of the ore can be obtained from the waste steam, generated from the nuclear power reactor. A similar advantage can obviously be drawn from the thermal treatment of Rohil Ghateshwar uranium ore for the recovering of Cu and Mo as byproducts and Jaduguda uranium ore for recovering Cu, Ni, Co and Mo as byproducts.

A carbonate ore, containing pyrite, has been chosen for the evaluation of energy neutral mineral processing with sustainable comprehensive extraction by incorporation of a thermal pretreatment stage in the current plant practice. Studies were carried out on thermal characterization of the pure constituents of the lean grade pyritic carbonate uranium ore by TG DTG DTA techniques. The investigations on pure constituents have helped to get a better understanding of the thermal pretreatment of actual ore. These analyses have been followed by TG DTG DTA of different size fractions of actual ore. Together with these analyses, evolved gas analysis has confirmed that the ore undergoes active oxidation of pyrite at about 427ºC and active decomposition of calcite at about 727ºC. It was further observed that the size of the ore has no significant effect on the oxidation and decomposition of pyrite and carbonate minerals respectively. The optimum temperature for oxidative roasting is found to be 585ºC. Thermal pretreatment by oxidative roasting of the crushed ore (before grinding) is useful and results in a reduction of the work index during grinding from 13 to 7.7 kwh/t ore. This amounts to savings of 19 kJ/kg ore. A new phase of $CaSO_4$ was identified during the thermal pretreatment at the optimum temperature. This is the reason for not being able to completely avoid a sulphur concentration in the leach liquor. The other new phase formed during roasting are CaO, MgO and Fe_2O_3. The first estimate of the heat requirement for differential thermal pretreatment of the ore has been obtained through heat balance calculations. There is also a reduction of about 30% in the sulphate concentration of leach liquor due to the oxidation of pyrite to Fe_2O_3 during roasting at 858 K. This helps in producing cleaner leach liquor for the extraction of uranium in downstream processing.

The recovery of copper and molybdenum from a non magnetic fraction of leach residue of Rohil uranium ore, indicated the possibility of recovering 79% Cu and 76% Mo values

respectively by sulphation roasting (optimum conditions: temperature = 550°C, time = 6 hours, mesh of grind 65 wt% passing a 200 mesh) followed by dilute sulphuric acid (5 vol% 98% concentrated H_2SO_4) leaching at 80-90°C for 6 hours time at 50 wt% solids. The process scheme developed, not only recovers the valuable metals (Cu, Mo and Ni) as byproducts, but also reduces acid mine drainage that would be posed by disposing of leach residue without the removal of sulphide.

The studies on the roasting of bulk sulphide float under static bed conditions (optimum parameters: T = 350°C, Residence time = 4 hours, % addition of Li_2SO_4 = 12) have revealed the feasibility of converting the valuable metals Cu, Ni and Co into water soluble sulphate forms and Mo into MoO_3.

3.2 INDONESIA: THERMAL PROCESSING OF TIN SLAG

Eastern Sumatra is part of the South East Asian tin belt and has large resources of cassiterite (SnO_2) that are mostly concentrated in the Bangka Belitung Island in Indonesia. With a total amount of 800 000 t of tin, Indonesia ranks 2nd in the list of countries regarding world tin reserves. Cassiterite is commonly associated with naturally radioactive minerals, such as monazite and xenotime, that also contain REEs. Consequently, the smelting process of tin concentrate also produces a radioactive waste called tin slag that, since it is categorized as low level radioactive waste as indicated in Fig. 3.5, needs to be stored properly.

FIG. 3.5. Tin slag stockpile.

Radioactive elements are present in tin slag, since the smelting process use tin concentrate with approximately 30% impurities, that means the associated minerals such as monazite and xenotime also involved in the smelting process, end up in the tin slag. The recovery of uranium, thorium and REEs from tin slag is of interest to Indonesia and first studies developed a process that constitutes a combined pyrometallurgical and hydrometallurgical method that will be introduced in this chapter. Tin slag processing requires external energy in the form of heat. This process heat could be provided directly, using greenhouse gas lean energy sources. Nuclear energy could be an interesting solution for providing heat for tin slag processing. The HTGR is a nuclear reactor type that can provide process heat in addition to electricity at relatively high temperatures (>750°C). Indonesia is looking into the possibility of constructing a HTGR prototype with a 10 MWth capacity, so that using process heat from HTGRs may in fact be of particular interest for Indonesia. This project was aimed at studying the possibility of the utilization of nuclear heat, generated from a HTGR for mineral processing, particularly tin slag and monazite processing (see next chapter). Figure 3.6 shows the general flow chart used for tin ore processing in PT Timah, the national tin producing company in Indonesia.

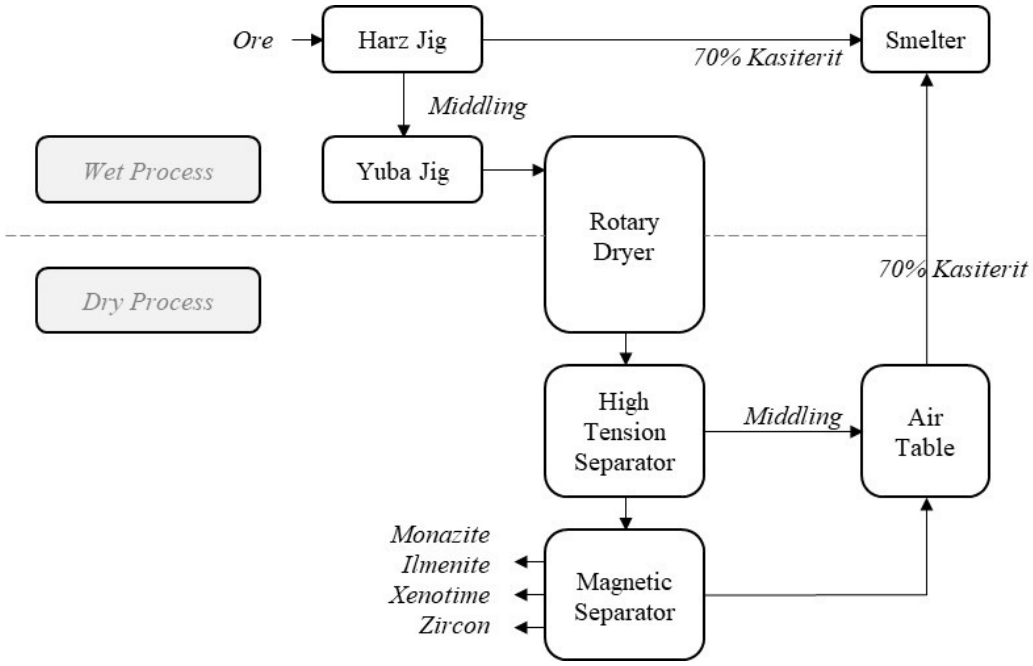

FIG. 3.6. Beneficiation of tin ore in PT Timah.

Tin ore processing at PT Timah produces considerable amounts of monazites (high grade and low grade) and xenotimes, which are currently stored on site and are available as secondary or unconventional resources for further processing. Table 3.3 shows the amounts of high-grade monazite, low grade monazite and xenotime produced in 2008.

TABLE 3.3. MONAZITE AND XENOTIME PRODUCTION FROM PT TIMAH AT THE END OF OCTOBER 2008

No	Mineral	Initial stock	Total production	Total	Output	Final stock
1.	**High grade monazite**					
	Number (drums)	0	0	0	0	0
	Weight (t)	408 820	0	408 820	0	408 820
	Minimum concentration (%)	88.31	0	78.31	0	78.31
	Minimum weight (t)	320 163	0	320 163	0	320 163
	Low grade monazite					
	Number (drums)	(13 Jb + 117 d)	0	(13 Jb + 117 d)	0	(13 Jb + 117 d)
	Weight (t)	549 683	0	549 683	0	549 683
	Minimum concentration (%)	35.09	0	35.09	0	35.09
	Minimum weight (t)	192 894	0	192 894	0	192 894
2.	**Xenotime**					
	Number (drums)	345	0	345	0	345
	Weight (t)	88 389	0	88 389	0	88 389
	Minimum concentration (%)	65.04	0	65.04	0	65.04
	Minimum weight (t)	57 488	0	57 488	0	57 488

Various slags are produced as byproducts in metallurgical processes or as residues in incineration processes. According to the origins and the characteristics, the main slags can be classified into three categories: ferrous slags, non ferrous slags and incineration slags.

Slags usually contain a quantity of valuable metals and notable amounts of harmful or heavy metals. The release of these metals may cause environmental problems. The conventional method for the disposal of slags is dumping. The increasing dump of slags not only occupies plenty of land, but also wastes resources and can potentially have an impact on the environment, as heavy metals can leach and pollute the environment, specifically water bodies. It is therefore desirable to recover metals from slags and to utilize the slags this way.

Tin slag is generated during smelting of tin concentrates through the fusion of ferrous silicate with limestone flux. Slag is collected when molten tin is tapped into a settler. Tin oxide (SnO_2) from cassiterite is reduced to tin metal through the smelting process. At PT Timah on Bangka Island, the concentration of tin in the cassiterite that is smelted has a concentration of approximately 70%, while the impurity minerals comprise 30%. During the smelting process, the impurity minerals are separated from molten tin metal and collected in the slag phase. Tin slag is processing waste with a density of 3076 kg/m^3 and contains Sn and Si, as well as other valuable elements such as the radioactive elements uranium and thorium, and rare earth metals. Until now, the tin slag has not been utilized further and was dumped in a stockpile area.

The Regulation of the Head of the Nuclear Energy Regulatory Agency No. 16/2013 on radiation safety in the storage of technologically enhanced naturally occurring radioactive material (TENORM) states that the value of the radioactivity of uranium and thorium series allowed has to be below 1 Bq/g or equivalent to 81 ppm for uranium and 246 ppm for thorium. Based on these data, the radioactive elements in tin slag have to be separated first, before tin slag can be stored or released into the environment. The tin slag produced at PT Timah is characterized in Table 3.4 below. As discussed earlier, the tin slag shows elevated concentrations of thorium and uranium (>1 Bq/g) that classify it as TENORM and require further processing before it can be safely stored or released into the environment.

TABLE 3.4. CHARACTERIZATION OF TIN SLAG IN INDONESIA

Material	Concentration
Th (ppm)	2.028
U (ppm)	276
SiO_2 (%)	34.26
CaO (%)	15.44
TiO_2 (%)	11.92
Al_2O_3 (%)	11.70
Fe_2O_3 (%)	8.84
ZrO_2 (%)	4.78
Other minor oxides (%)	12.06

Tin slag is an example of a non ferrous slag byproduct, which is economically important. The tin ore obtained from the mine site is beneficiated into tin concentrate, middling and tin tailings. After the beneficiation of tin ore to obtain tin concentrate, tin tailings are collected as waste from the process. This so called waste accounts for about 25% of the total weight of the beneficiated ore. Based on economics as well as environmental related issues, enormous efforts have been directed worldwide towards tin tailings management issues. These efforts consider utilization, storage and disposal of the tin tailings.

China and Brazil are the world's largest producers of tin, followed by Indonesia and Bolivia. These countries account for 77% of tin imports into the USA. A tin smelting plant, Cia. Estanifera do Brazil, which is perhaps one of the most integrated units in the world, is described here as an example of advanced tin production. The plant is unique in its ability to treat a wide variety of relatively pure ores from Thailand, relatively impure ores from Africa and Bolivia, as well as ores from various provinces of Brazil. This is a feature that makes the Brazilian plant stand out, if compared to other tin processing plants in the world. Besides the mentioned ores, a wide range of residues, drosses and tin containing materials can also be processed. The entire smelting operation, including ore treatment, primary smelting, slag treatment and electrolytic refining are described in detail in Fig. 3.7.

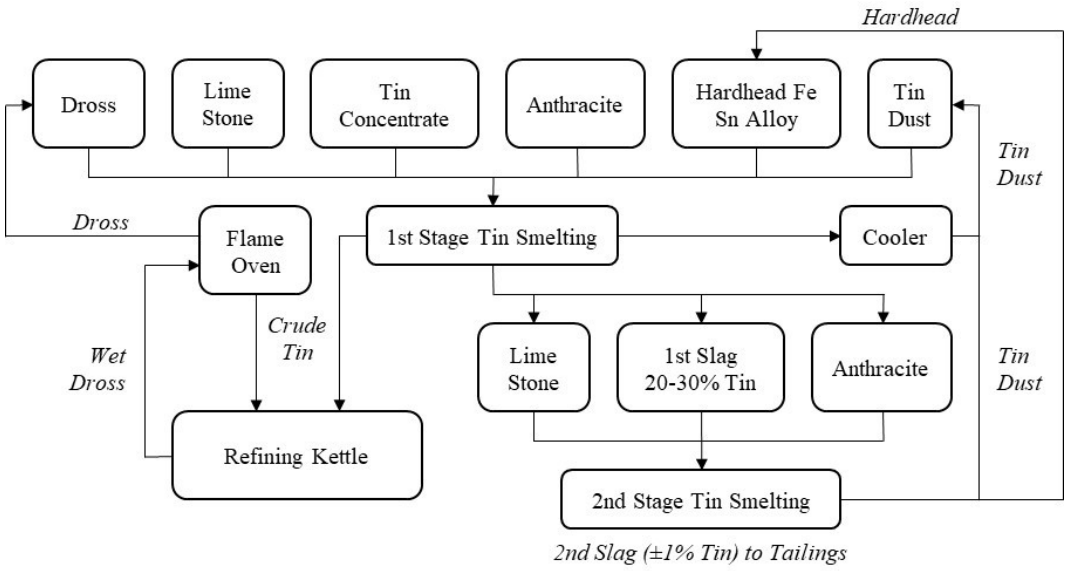

FIG. 3.7. Advanced tin processing in Brazil.

Tin slag has long been known as a source of the relatively scarce metals such as tantalum and niobium. Common sources for such tin slags are the Congo, Malaysia and Thailand. Various techniques are known for the extraction of tantalum and niobium and other metals present in tin slags. Table 3.5 shows characteristic elements in tin slag from Thailand.

TABLE 3.5. CONCENTRATIONS OF RELEVANT ELEMENTS IN THAILAND TIN SLAG

Material	**Concentration (%)**
Ta_2O_5	10.69
Nb_2O_5	-
Fe_2O_3	6.68
SnO_2	-
TiO_2	10.99
SiO_2	20.14
Al_2O_3	12.99
CaO	16.10
MgO	-
WO_3	-
ZrO_2	3.21

The Malaysia Smelting Corporation (MSC) operates two plants, one in Butterworth in Penang and another one near the city centre of Penang Island. The plants are among the largest in the world, each having a capability of processing some 60 000 t of ore concentrate per year. The plants cater for the need of local tin ore suppliers. Both plants were established a decade ago and have contributed much to the growth of the city. About 10% of the initial feed weight,

normally ends up as tin slag. A simplified flow chart of tin smelting operations in these plants is shown in Fig. 3.8. Not many modifications have been made to the plants since they first started operating. Tin slag can be classified in three different grades: high grade slag, low grade slag and very low grade slag. These gradings usually refer to the niobium and tantalum content. A high grade slag shows >8% combined niobium and tantalum content. Very low grades show <5% of these elements, and in low grade slag the content usually ranges from 5 to 8%.

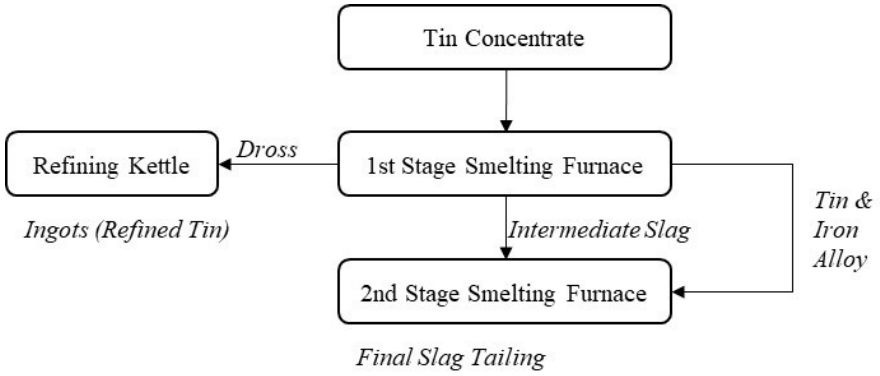

FIG. 3.8. Simplified flow diagram of the tin-smelting process in Penang, Malaysia.

Even with a market for the high grade slag, low and very low grade slags are still being discarded as they have been before. These slags are normally dumped on the premises of the smelting plant. Because of their earlier start of operation, both tin processing plants in Penang are located in densely populated areas. Table 3.6 shows an analysis of tin slag from Penang with M1 (very low grade tin slag from MSC), M2 (low grade tin slag from DKS), M3 (high grade tin slag from MSC) and M4 (very low grade tin slag from DKS).

TABLE 3.6. ANALYSIS OF TIN SLAG FROM PENANG

Sample	Ta_2O_5 (wt%)	Nb_2O_5 (wt%)	U (mg/kg)	Th (mg/kg)
M1	0.69	1.33	361.33 ± 17.06	358.25 ± 7.41
M2	2.34	3.07	268.50 ± 5.94	1275.50 ± 64.72
M3	8.16	5.57	505.50 ± 13.75	2807.79 ± 38.03
M4	0.55	1.33	244.0 ± 7.06	517.00 ± 50.43

Niobium and tantalum are known to co-occur with cassiterite deposits. During the process of extraction of tin by cassiterite smelting, these metals join the slag phase, and the slag is processed for the recovery of niobium and tantalum. The tin slag used in the present studies was of Malaysian origin. Chemical analysis of a typical sample is shown in Table 3.7. Sodium hydroxide, hydrochloric acid and other chemicals used in these studies were of an analytical reagent grade.

TABLE 3.7. CHEMICAL ANALYSIS OF TIN SLAG (AS OXIDES IN WT%)

Material	**Concentration (wt%)**
SnO_2	1.33
Nb_2O_5	3.43
Ta_2O_5	3.05
SiO_2	23.07
Al_2O_3	10.42
Fe_2O_3	22.77
CaO	13.12
TiO_2	7.97

Contents of the tin slag can be grouped into three categories: Refractory metals (Nb, Ta, Ti), acid solubles (Fe, Ca, Mn, Al) and acid insoluble oxides (SiO_2, Al_2O_3). The flow chart developed, essentially consists of a combination of alkali and acid processing steps to separate the impurities, and obtain a product enriched in Nb-Ta values which could serve as a suitable starting material for the extraction of niobium and tantalum by hydrofluoric acid.

A hydrometallurgical processing scheme has been developed to extract niobium and tantalum from low grade tin slag. The different steps of the processing scheme are shown in Table 3.8.

TABLE 3.8. ALKALI AND ACID PROCESSING OF MALAYSIAN TIN SLAG

Alkali Processing					
	Type	Pugging			
	Slag / NaOH	1 / 2			
	Temperature (°C)	250			
	Duration (hours)	4			
Acid Leaching					
	Strength of HCl (%)	32.5			
	Temperature (°C)	50			
	Duration (min)	15			
	Leach liquor analysis (% solubility)	Al	48	Ti	76
		Ca	45	Nb	4
		Fe	43	Ta	2
Residue					
		Analysis (%)	Recovery (%)		
	Nb_2O_5	10.6	86.5		
	Ta_2O_5	10.4	95.9		
	TiO_2	7.0	-		

The studies conducted for tin slag processing from Malaysia, resulted in the confidence that tin slag processing from Indonesia can also be possible on a larger scale. Several studies of tin smelting processing in Indonesia showed that an effective method of extraction is needed because of the presence of silica structures within the slag. The process of separation of radioactive elements and rare earth metals is carried out by various methods, including alkaline methods (using NaOH), acidic methods (using H_2SO_4), chloronization methods (using chlorine gas), and high temperature reduction methods (using supercritical carbon dioxide). Susilaningtyas [3.14] reported that alkaline and acid methods are widely used in the separation process of slags. Figure 3.9 shows the tin smelting process at the PT Timah plant in Indonesia.

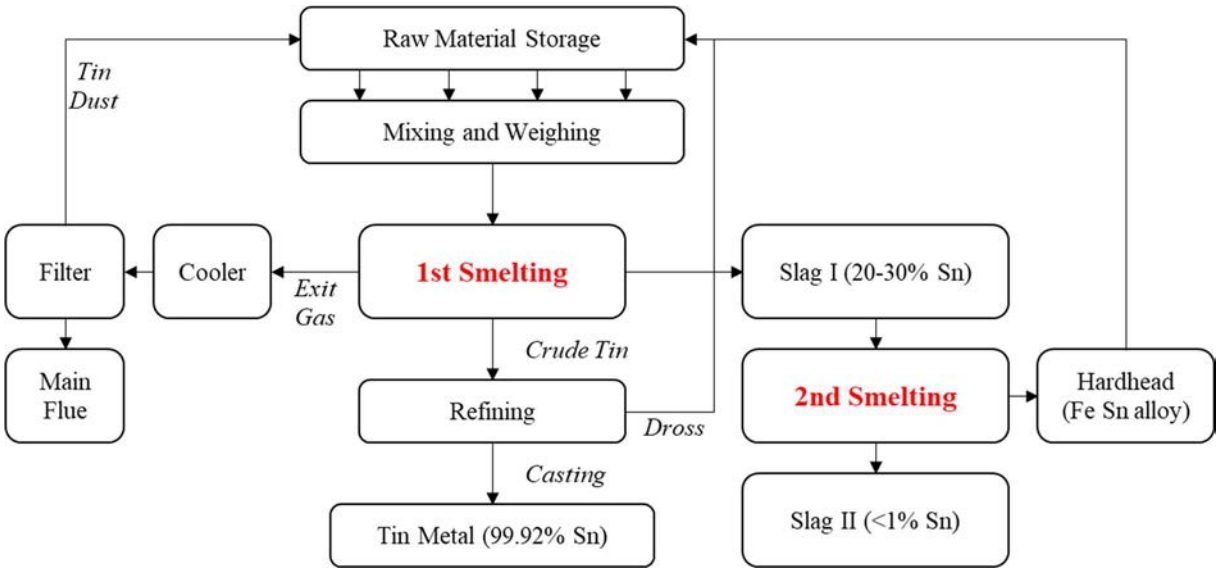

FIG. 3.9. Flow chart of tin smelting process at PT Timah plant in Indonesia.

The direct leaching process of tin slag becomes ineffective in the presence of silica structures that can block the contact between reagent and elements in the tin slag. Pre-treatment is therefore required to damage the silica structures of the slag before the leaching process. One of the methods that can be used, is alkali fusion. Alkaline fusion is a process of decomposition of tin slag by reacting at high temperatures with an alkali compound. Research conducted by Subramanian [3.15] and Anggraini [3.16] shows that at high temperatures, sodium hydroxide can decompose silica contained in tin slag into water soluble silicate compounds. According to Subramanian [3.15], slag decomposition with NaOH is effective for damaging the silica structure in slag while increasing its porosity. NaOH reacts with silica to form water soluble Na_2SiO_3. The reaction occurring between NaOH and the oxides in slag at the melting process is as follows:

$$UO_3 \cdot SiO_{2(s)} + 2NaOH_{(s)} \rightarrow UO_2(OH)_{2(s)} + Na_2SiO_{2(aq)}$$

$$ThO_2 \cdot 2SiO_{2(s)} + 4NaOH_{(s)} \rightarrow Th(OH)_{4(s)} + 2Na_2O_{3(aq)}$$

$$(REE)_2O_3 \cdot 3SiO_{2(s)} + 6NaOH_{(s)} \rightarrow 2REE(OH)_{3(s)} + 3Na_2SiO_{3(aq)}$$

The Na_2SiO_3 formed in the slag smelting process can be removed through a water leaching process of the solid or frit. The washing process is capable of dissolving Na_2SiO_3 to produce a precipitate free of silica, known as hydroxide cake. This precipitate is then further processed to extract valuable elements contained in it. Uranium and thorium which are radioactive elements can be separated from rare earth metals by dissolving them with acids. According to Susilaningtyas [3.14], acid reagents commonly used in the processing of minerals containing radioactive elements and REEs are hydrochloric acid (HCl) and sulphuric acid (H_2SO_4). The tin slag processing research conducted by the National Nuclear Energy Agency (BATAN) of Indonesia in 2013, indicates that the radioactive elements of uranium and thorium and rare earth metals in slags can be dissolved in sulphuric acid (H_2SO_4), hydrochloric acid (HCl) or nitric acid (HNO_3). According to Suharyanto et al. [3.17, 3.18], sulphuric acid (H_2SO_4) is able to dissolve the elements in slag more than hydrochloric acid (HCl). In this process, sulphuric acid is used to digest hydroxide cake, containing radioactive elements and REEs. During the reaction process with sulphuric acid, the radioactive elements will dissolve [3.19] while the rare earth metals will precipite. REEs may precipitate under alkaline sulphate conditions. The

presence of the remaining unreacted Na^+ ions with SiO_2 in the hydroxide cake and addition of sulphuric acid, creates alkaline sulphate conditions that form a precipitate of $NaREE(SO_4)_2$. The reaction that occurs between hydroxide cake and sulphuric acid is as follows:

$$Na^+ = REE^{3+} + 2SO_4^{2-} \rightarrow NaREE(SO_4)_{2(s)}$$

$$UO_2^{2+} + SO_4^{2-} \rightarrow UO_2SO_{4(aq)}$$

$$Th^{4+} + 2SO_4^{2-} \rightarrow Th(SO_4)_{2(aq)}$$

Filtrate analysis showed that uranium and thorium in hydroxide cake dissolved in sulphuric acid. Sulphuric acid can dissolve more thorium than uranium. The thorium solubility in sulphuric acid was determined to be 79.93%. This value is greater than the solubility of uranium in sulphuric acid which was determined to be 30.49%. The analysis using ICP-OES showed that the REE content was not detected in the filtrate, so it can be concluded that REEs do not dissolve in the sulphuric acid solution. The recovery of REEs by sulphuric acid was about <0.01%. Besides the sulphuric acid method, research on tin slag processing has also been performed by dissolving methods using hydrochloric acid. Hydrochloric acid is able to dissolve uranium and thorium in hydroxide cake. Besides dissolving uranium and thorium, hydrochloric acid is also capable of dissolving rare earth metals. The REE leaching reaction of tin slag is a heterogeneous reaction because it involves two phases, namely solid and liquid. Assuming that the fusion process decomposes the slag and makes the REEs in the form of a hydroxide compound, the leaching reaction that occurs by using a hydrochloric acid reagent is as follows:

$$(REE)(OH)_{3(s)} + 3HCl_{(aq)} \rightarrow (REE)Cl_{3(aq)} + 3H_2O$$

The REEs which dissolve in HCl will mix with uranium and thorium, so further processing is required to separate uranium and thorium from the REEs. Dissolved REEs in chloride solution can be precipitated into REEs hydroxide by neutralization, using sodium hydroxide or ammonium hydroxide. The analysis performed here indicate that the best percentage of LTJ extraction of 87.5% is obtained at a concentration of 2 M HCl at a temperature of 40°C. Meanwhile, it is known that the leachability selectivity of Fe, Al, Ca and Si is not good enough with a consecutive average value of 0.51, 0.50, 0.42 and 0.34. Tin slag from Indonesia contains about 2.7% $(Ta,Nb)_2O_5$. Studies presented here have revealed several alternative processes, including leaching with H_2SO_4 and HF, slag decomposition with NaOH at high temperatures or acid-base digestion combinations for the extraction of tantalum and niobium from tin slag.

The successful tests lead to a flow chart for tin slag processing at a batch process pilot plant with a 50 kg tin slag capacity in Indonesia. Figure 3.10 provides an overview of the process.

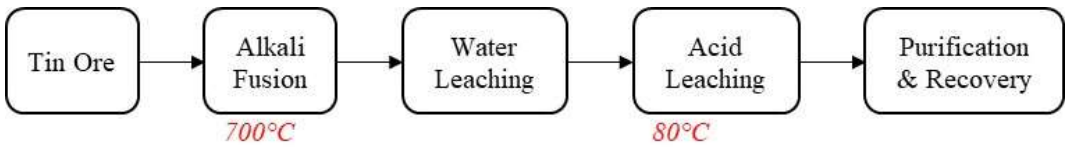

FIG. 3.10. Tin slag processing batch processing in Indonesia.

From a single batch of 50 kg tin slag, roughly 20 kg $RE(OH)_3$ and 92 g mixed uranium and thorium hydroxide could be recovered. In total there are three unit processes that require heat. The heat requirements are summarized below:

— Preheating

Mass of solid (Tin slag + NaOH)	= 150 kg/h
Initial temperature	= 30°C
Final temperature	= 250°C
Overall heat required	= 40 834.8 kJ/h
Design of heat requirement	= 49 001.8 kJ/h

— Alkali fusion

Mass of solid (Tin slag + NaOH)	= 150 kg/h
Initial temperature	= 30°C
Final temperature	= 700°C
Overall heat required	= 83 525.80 kJ/h
Design of heat requirement	= 100 230.96 kJ/h

— Dissolution of frit or acid leaching

Mass of slurry	= 156.42 kg/h
Initial temperature	= 30°C
Final temperature	= 80°C
Overall heat required	= 11 797.7 kJ/h
Design of heat requirement	= 14 157.3 kJ/h

3.3 INDONESIA: THERMAL PROCESSING OF MONAZITE

BATAN and here in particular the Center for Technology of Nuclear Ore Minerals, is the government institution that has the authority and responsibility to manage all radioactive minerals in Indonesia. To manage these minerals properly, some activities such as exploration and studies in mining and extraction technology are performed on a regular basis. For more than a decade, research and development efforts were conducted to obtain the extraction technology to produce uranium, thorium and REEs from monazite. The extraction methods have been developed up to pilot plant scale with a batch capacity of 50 kg monazite per batch. The smelting process of tin concentrate for instance is known to produce a radioactive waste, called tin slag, as described in the previous chapter. These radioactive elements can be present in tin slag, because the smelting process use tin concentrate with approximately 30% impurities content. This means that associated minerals such as monazite and xenotime are also involved in the smelting process and end up in the tin slag. The study of uranium, thorium and REEs extraction from tin slag has resulted in a process stage that combines a pyrometallurgical and hydrometallurgical process. The element concentration of monazites from Bangka in Indonesia is provided in Table 3.9.

TABLE 3.9. REPRESENTATIVE ANALYSIS OF OXIDES FOUND IN BANGKA MONAZITE CONCENTRATE (GRADE 94%) IN INDONESIA

Number	Oxide	Concentration
1	CeO_2	31 506±0.075
2	La_2O_3	13 165±0.038
3	Nd_2O_3	11 025±0.062
4	ThO_2	6283±0.022
5	Y_2O_3	3931±0.024
6	Pr_6O_{11}	2984±0.022
7	P_2O_5	19 109±0.102
8	SnO_2	1034±0.004
9	Sm_2O_3	1956±0.005
10	Gd_2O_3	1981±0.003
11	Dy_2O_3	1029±0.011
12	SiO_2	1295±0.021
13	U_3O_8	0.298±0.005
14	Fe_2O_3	0.770±0.012
15	TiO_2	0.043±0.001
16	Yb_2O_3	0.310±0.004
17	Er_2O_3	0.412±0.005
18	Al_2O_3	0.826±0.021
19	CaO	0.219±0.006
20	ZrO_2	0.177±0.005

Monazite minerals in Indonesia are generally obtained as a byproduct from tin mining. Monazite contains REEs and radioactive elements so that they need to be safely stored. Currently these minerals have not been treated and are only stockpiled in a special place to prevent the spread of radioactive material. Monazite can, depending on the accompanied elements, different chemical formula that are depicted in Table 3.10.

TABLE 3.10. CHEMICAL FORMULA OF MONAZITE

Name	Chemical formula
MONASIT - (Ce)	$(Ce, La, Nd, Th, Y)PO_4$
MONASIT - (La)	$(La, Ce, Nd)PO_4$
MONASIT - (Nd)	$(Nd, La, Ce)PO_4$

Monazite in Indonesia is located on Bangka Belitung Island. The monazite mineral is a by-product of mining and beneficiation of tin ore. PT Timah and PT Koba Tin are processing plants which produce tin in Indonesia. Tin processing at Bangka produces about 7290 t to 8505 t monazite per year. Beneficiation of tin ore in PT Timah is described in the previous chapter and Table 3.11 provides a representative characterization of monazite ore from Indonesia with regards to REEs and other materials of interest.

TABLE 3.11. CHARACTERIZATION OF MONAZITE IN INDONESIA

Elements	**Element concentration %**	**Phosphat concentration %**
La	11.34	19.10
Ce	18.27	30.67
Nd	8.64	14.33
Pr	0.54	0.91
Th	6.47	10.00
Others (Si, Zr, Sn, Y, Sm, Gd, Dy, U)	-	24.99

Monazite is a common beach sand mineral, present in acidic igneous rocks and vein deposits and usually contains 4–12% ThO_2, 20–30% Ce_2O_3 and 10–40% La_2O_3. The resource estimates of monazite in inland placer deposits, stands at 10.21 million t in 2005. India holds only 3% of the world reserves as compared to 36% by China and 13% by the USA. In placer deposits, monazite occurs as a minor constituent, while the major minerals are ilmenite, rutile, zircon, and quartz. Beneficiation processes of beach sand minerals vary from location to location, depending on their mineralogical and chemical composition. Monazite concentrate is usually further processed under different conditions with time, temperature, and acid/alkaline concentration being the main process parameters. Monazites are usually processed by thermal treatment, followed by REEs recovery under optimized conditions of leaching and an extraction process via solvent extraction and precipitation to produce salts and a concentrate of radioactive materials and REEs from the leach liquor. Sulphuric acid has been used most extensively for the leaching of monazites, where the sulphate ion (SO_4^{2-}) of H_2SO_4 acts as a ligand that reacts at high temperature as follows:

$$2REEPO_4 + 3H_2SO_4 \rightarrow REE_2(SO_4)_3 + 2H_3PO_4$$

$$2H_3PO_4 \leftrightarrow H_4P_2O_7 + H_2O$$

$$ThO_2 + 2H_2SO_4 \leftrightarrow Th(SO_4)_2 + 2H_2O$$

$$Th(SO_4)_2 + H_4P_2O_7 \leftrightarrow ThP_2O_7 + 2H_2SO_4$$

Under high temperature, phosphate reacts with H_2SO_4 to form H_3PO_4 which then dehydrates to pyrophosphoric acid. Thorium oxide reacts with H_2SO_4 first to form thorium sulphate, and then reacts with pyrophosphoric acid to form thorium pyrophosphate which is insoluble even in a strong acid solution. While rare earths are leached from the acid-roasted concentrate, water and thorium remain in the solid residue, resulting in good separation of rare earths from thorium. Thorium is further removed from the leach solution by precipitation with oxalate anions. The oxalate precipitate that contains thorium and REE-oxides is dissolved in nitric acid, followed by a selective extraction of REEs with tributyl phosphate (TBP) from the nitrate

solution. A flow chart for monazite processing with sulphuric acid leaching is shown in Fig. 3.11. The depicted process is used in the USA for the selective solubilization of either thorium or REEs from monazites, under controlled conditions, on industrial scale.

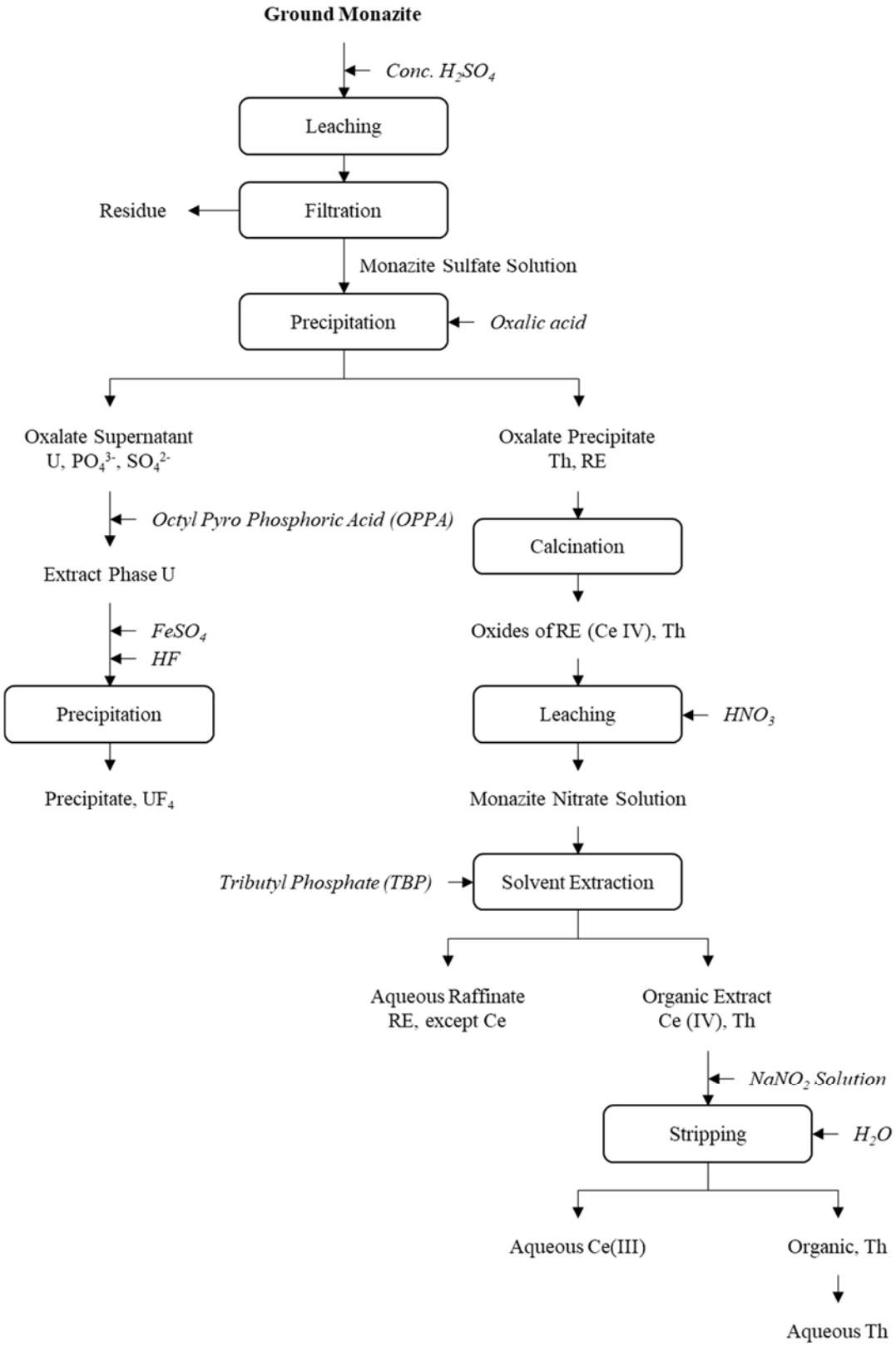

FIG. 3.11. Flow diagram for the leaching of monazite by an acidic method.

Alkaline leaching of monazite is most preferable and widely used as it has many advantages. The most important of these advantages is the simultaneous removal of phosphorous during leaching, the production of a useful byproduct (sodium phosphate) that can be used as fertilizer and the regeneration of alkali. Sodium hydroxide is most used as a reagent on monazite alkaline leaching. Monazite alkaline leaching with sodium hydroxide takes place at 140°C and can be described with the following reaction:

$$2REEPO_4 + 6NaOH \rightarrow 2RE(OH)_3 + 2Na_3PO_4$$

$$Th_3(PO_4)_4 + 12NaOH \rightarrow 3Th(OH)_4 + 4Na_3PO_4$$

The hydroxide cake obtained from alkaline processing of monazite is leached with ammonium carbonate–bicarbonate solutions and the reactions denote as following:

$$Th(OH)_4 + 5(NH_4)_2CO_3 \rightarrow (NH_4)_6(Th(CO_3)_5) + 4NH_4OH$$

$$UO_2(OH)_2 + 3(NH_4)_2CO_3 \rightarrow (NH_4)_4(UO_2(CO_3)_3) + 2NH_4OH$$

$$2REE(OH)_3 + 4(NH_4)_2CO_3 \rightarrow REE_2(CO_3)_3 + 6NH_4OH$$

$$NH_4OH + NH_4HCO_3 \rightarrow (NH_4)_2CO_3 + H_2O$$

The thorium concentrate produced by ammonium carbonate leaching is less contaminated with silica. Sodium carbonate that can also be used for leaching actively reacts with the silicate mineral impurities. Furthermore, ammonia and carbon dioxide from the decomposition of carbonate solutions can be recycled and used for the regeneration of ammonium carbonate. This process has mostly been used in India and Brazil. An exemplary flow chart is provided in Fig. 3.12.

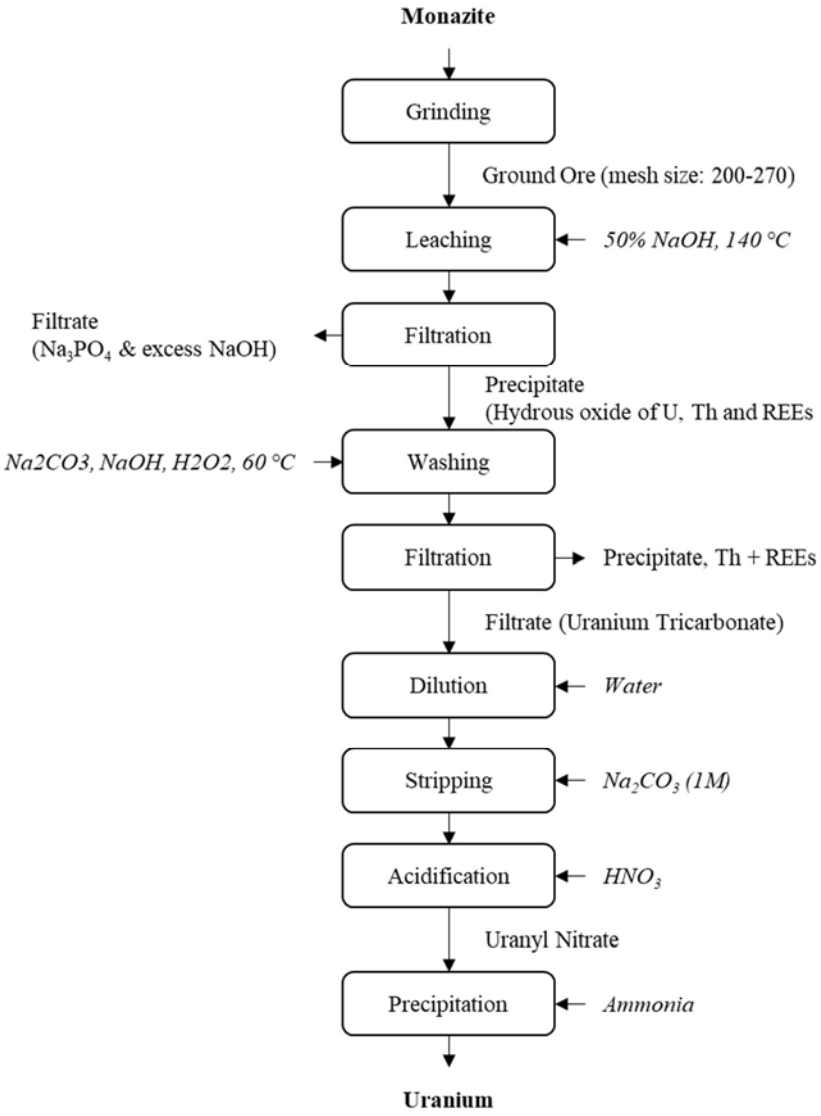

FIG. 3.12. Exemplary flow chart for the leaching of monazite with the alkaline method.

Monazite as a byproduct from tin mining contains radioactive elements such as uranium and thorium. Tin slag further contains valuable REEs that are widely used as raw materials in numerous industries. Besides, different forms of phosphate, the raw material for mineral fertilizers can be recovered. The concentrated monazite minerals in Indonesia contain REEs (about 50–68%), phosphates (18–30%), uranium (0.15–0.30%) and thorium (2.5–3.6%). BATAN as a government institution that has a responsibility to manage radioactive materials in Indonesia, has developed process technology for uranium and thorium removal from monazites with special focus on Bangka Monazite (see Fig. 3.13). The technology does not only produce ammonium diuranate or ADU ($(NH_4)_2U_2O_7$) and thorium dioxide (ThO_2), but also tri-sodium phosphate (Na_3PO_4) and rare earth hydroxide ($RE(OH)_3$). The developed technology has already been applied at pilot plant scale with a batch size of approximately 50 kg monazite per batch.

FIG. 3.13. Bangka monazite.

The hydrometallurgy process was used to extract uranium, thorium and REEs from monazite. There are two main processes of monazite processing namely the $RE(OH)_3$ extraction process and the uranium and thorium extraction process. The $RE(OH)_3$ extraction process consists of milling, alkaline leaching, selective dissolution, and multistage precipitation, while the uranium and thorium extraction process uses a solvent extraction method. The size of the monazite's particles has to be reduced to give a greater surface area allowing for better contact between the reagent and the ore. Types of milling equipment that are commonly used are rod mills, ball mills, mortar grinders, or similar. As required for the alkaline leaching stage, milling aims at obtaining a fine size of the monazite. Some studies show that alkaline leaching gives a satisfying result in -325 mesh of particle size. The alkaline leaching using sodium hydroxide (NaOH) to dissolve phosphate and convert monazite from phosphate compounds into hydroxides, is the next step. Phosphate in aqueous phase separates from leaching residue by filtration. The phosphate bonds in monazite are broken by the sodium hydroxide solution at 140°C and result in a soluble form of phosphate while uranium, thorium and REEs are kept in a solid phase as hydroxides. The reaction mechanism can be described as follows:

$$REEPO_4 + 3NaOH \rightarrow REE(OH)_3 + Na_3PO_4$$

$$(UO_2)_3(PO_4)_2 + 6NaOH \rightarrow 3UO_2(OH)_2 + 2Na_3PO_4$$

$$Th_3(PO_4)_4 + 12NaOH \rightarrow 3Th(OH)_4 + 4Na_3PO_4$$

At this stage, more than 95% phosphate is dissolved. A crystalline phase of phosphate forms at low temperature. The separation of the phosphate solution from leaching residue best takes place at higher temperatures. The leaching residue is brought to reaction with hydrochloric acid (HCl) at 3.7 pH and 70°C temperature, to dissolve REEs selectively. The selective dissolution aims to dissolve REEs with small amounts of uranium and thorium as impurities. REEs contained in the leaching residue are dissolved using hydrochloric acid, resulting in a REE-chloride solution with small amounts of radioactive element impurities. The reaction mechanism can be described as follows:

$$REE(OH)_3 + 3HCl \rightarrow REECl_3 + 3H_2O$$

$$3UO_2(OH)_2 + HCl \rightarrow 3UO_2Cl_2 + 3H_2O$$

$$Th(OH)_4 + 4HCl \rightarrow ThCl_4 + 4H_2O$$

Approximately 70% REEs are dissolved at this stage, while 5% uranium and thorium are also dissolved in the chloride solution. The solution obtained from the selective dissolution stage needs to be purified, especially to reduce or remove radioactive elements, prior to the precipitation of the REE product. The uranium and thorium can be removed to obtain the $RE(OH)_3$ product with no radioactive impurities contained. Based on the difference of precipitation of pH between REEs and uranium as well as thorium, a multistage precipitation process can be used. REEs precipitate in a higher pH than uranium and thorium. The pH of the solution increases with the addition of ammonium hydroxide (NH_4OH). Uranium and thorium precipitate at a pH of 6.3 and can be separated from the aqueous phase using filtration methods before the precipitation pH of REEs is reached. The REEs' hydroxide product can be obtained by continuing the precipitation process into pH 8–9. The precipitation reaction can be described as follows:

$$REECl_3 + 3NH_4OH \rightarrow REE(OH)_3 + 3NH_4Cl$$

$$UO_2Cl_2 + 2NH_4OH \rightarrow UO_2(OH)_2 + 2NH_4Cl$$

$$ThCl_4 + 4NH_4OH \rightarrow Th(OH)_4 + 4NH_4Cl$$

Uranium and thorium concentrate is dissolved by HCl at 80°C, then precipitated by NH_4OH. For the uranium solvent extraction (SX) process, uranium and thorium concentrate is prepared in a sulphate solution. The precipitate is therefore dissolved by sulphuric acid (H_2SO_4). The organic phase used for uranium extraction is trioctylamine (alamine 336) which is mixed with kerosene and isodecanol. The composition of the organic phase is 5% alamine, 93% kerosen and 2% isodecanol. In the first SX unit, uranium will get into the organic phase, leaving thorium in the aqueous phase. Uranium can be stripped by H_2SO_4 and precipitated by NH_4OH in the next stage. The reaction of uranium SX can be described as follows:

$$[2R_3N]_{org} + H_2SO_4 \rightarrow [(R_3NH^+)_2SO_4^{2-}]_{org}$$

$$[(R_3NH^+)_2SO_4^{2-}]_{org} + UO_2(SO_4)_3^{4-} \rightarrow [(R_3NH^+)_4UO_2(SO_4)_3^{4-}]_{org} + 2SO_4^{2-}$$

The thorium in the aqueous phase is extracted by the mixing of tributylphosphat (TBP) and kerosene with a composition of 50% TBP and 50% kerosene in the second SX unit and is carried out in the nitrate solution. Thorium in the organic phase is stripped by nitric acid (HNO_3) and precipitated by NH_4OH to obtain thorium hydroxide. The reaction of the thorium SX denotes as follows:

$$[Th^{4+}]_{aq} + [4NO_3^-]_{aq} + n[TBP]_{org} \rightarrow [Th(NO_3)_4 \cdot nTBO]_{org}$$

FIG. 3.14. $REE(OH)_3$ product from alkaline leaching of monazite in Indonesia.

Figure 3.14 shows the product from alkaline leaching in Indonesia. The technology of monazite processing which uses an alkaline leaching method in Indonesia has been scaled up recently to pilot plant scale. The location of the pilot plant is at the Center for Nuclear Minerals Teknology – BATAN, South Jakarta. The pilot plant is named PLUTHO and has the capacity of producing about 50 kg monazite per batch.

The pilot plant has the following capacity:

Capacity of processing plant = 50 kg monazite/hr.
Product:
— 20 kg $REE(OH)_3$;
— 2.6 kg mixed uranium and thorium hydroxide;
— 1.5 kg thorium hydroxide;
— 23 kg Na_3PO_4.

There are three-unit processes that require heat, and the results of heat requirement calculations are as follow:

— Monazite digestion
  Mass of solution = 160 kg/hr
  Mass of solid = 50 kg/hr
  Mass of slurry = 210 kg/hr
  Initial temperature = 100°C
  Final temperature = 140°C
  Overall heat required = 35 514.5 kJ/hr
  Design of heat requirement = 42 617.4 kJ/hr

— Dissolution of digestion residue
  Mass of slurry = 133.8 kg/hr
  Inlet temperature = 30°C
  Outlet temperature = 70°C
  Overall heat required = 59 419.3 kJ/hr
  Design of heat requirement = 71 303.2 kJ/hr

— Dissolution of 1st precipitate and dissolution residue
  Mass of slurry = 37.2 kg/hr
  Specific heat of slurry (Cp) = 3.42 kJ/kg.K
  Inlet temperature = 30°C
  Outlet temperature = 80°C
  Overall heat required = 18 070 kJ/hr
  Design of heat requirement = 21 684 kJ/hr

Since Indonesia is actively pursuing HTR development, energy neutral mineral processing for monazite processing may become relevant [3.20].

3.4 MALAYSIA: THORIUM RECOVERY FROM MALAYSIAN MONAZITE SANDS

Malaysia has many potential mineral resources, including some REE minerals such as monazite. Monazite is a phosphate that is reddish-brown in colour, contains rare earth metal and is the source of thorium, lanthanum and cerium [3.21]. Monazites usually contain small amounts of radioactive elements such as thorium and uranium [3.22]. REEs play critical roles in the application of advanced materials [3.23]. REEs can be generally grouped into light and heavy REEs. REEs from lanthanum (La, atomic number = 57) to samarium (Sm, atomic number = 62) are categorized as light REEs (LREE), while elements from europium (Eu, atomic number = 63) to lutetium (Lu, atomic number = 71), including yttrium (Y, atomic number = 39) are considered to be heavy REEs (HREE) [3.24]. Besides, thorium is a naturally occurring radioactive material (NORM) that is four times more abundant in the earth crust than uranium. Thorium is said to be a fertile material and does not undergo fission reactions by itself, making it suitable to be utilized as an alternative fuel to replace uranium. ThO_2 can be used as nuclear fuel in heavy water reactors, HTGRs, boiling water reactors, pressurized water reactors, fast neutron reactors and molten salt reactors. Compared to uranium, ThO_2 is more advantageous in the way that it is relatively inert and shows a lower coefficient of thermal expansion than UO_2. Another property that might make ThO_2 a better fuel for nuclear reactors, is the higher thermal conductivity. Mineral phosphate monazite is the main source of thorium in Malaysia. It contains about 3.1–11.34% ThO_2 which is the highest value, compared to other minerals. Besides, monazite also contains a high amount of REEs which constitute about 54–60% of the monazite, while for uranium the quantity usually ranges between 0.2 and 0.4% [3.21]. Almost 95% of the monazite can be extracted using sizing, magnetic separation, electrostatic separation and tabling. The rare earth hydroxide can be extracted by caustic soda digestion, hydrochloric dissolution and selective precipitation while rare earth oxide can be precipitated by leaching, oxidation, precipitation and calcination from rare earth hydroxide [3.25]. Compared to bastnaesite, monazite shows wide ranges of processing parameters because of the wide variation in chemical composition and weathering profile. Modifications are needed to address the ore's characteristics, to reduce the dissolution of impurity and the consumption of acid, that can also increase rare earth extraction [3.26]. High temperature stability of a monazite concentrate under reducing conditions using coal and char, could be found useful between 1200°C and 1400°C. Here monazite decomposes to form rare earth oxides and elemental phosphorus. Sodium and calcium compounds, either alone or in combination, are known to decompose monazite at higher temperatures [3.27]. There are two main methods to separate thorium from mineral monazite: acid digestion or leaching [3.21]. The amount of thorium and uranium that can to be removed is usually limited and depends on the temperature and fineness of the grinded raw material. The extraction efficiency also appears to be a result of the passivation of the monazite by precipitation of rare earth oxalates in the inert residue shell around unreacted monazite cores. Besides, under some conditions, thorium that had been leached into solution reprecipitate, most likely acts as an acid phosphate [3.27].

The monazite sands used in this study were collected from Dengkil, Selangor, Malaysia. Some of the monazite sands were crushed using a Fritsch Pulverisette 6 classic line. The crushed monazite sands were sieved until the desired particle size was reached. Through this method, the crushed monazite sands were agitated through many meshing sieve sizes. Representative samples were accordingly organized into the assorted size portions as following: <20 μm, 20-45 μm, 45–90 μm, 90–80 μm and >180 μm.

Following sorting, chemical monazite sand cracking was done mixing monazite sands with NaOH inside a ceramic crucible, before the samples were fused in a chamber furnace at 150°C.

H_2O was added to the fused monazite sands until the samples became a slurry. This mixture was then transferred to a beaker and stirred. After that, the monazite slurry was filtered using a vacuum pump. Next, the solid samples were further leached with 6 M HCl and the filtrates were analysed. Detail observations on the effect of the particle size ranging from 20 to 220 µm and a fusion duration of 1 to 4 hours were typically used.

The monazite sands were analysed by X-ray fluorescence (XRF). Particle size analysis was performed, using a Honeywell Microtrac X100 Particle Sizer. This machine scatters light from laser beams and calculates size distribution in the sample stream ranging from 0.02 to 700 µm using a scattering theory for spherical particles. XRD is a rapid analytical technique, primarily used for phase identification of a crystalline material and can provide information on unit cell dimensions. The analysed material is finely ground, homogenized and the average bulk composition is determined by analysis of XRD patterns collected using a PANalytical X'Pert PRO MPD PW 3040/60 (Cu Kα X ray source). XRD patterns from the as synthesized and annealed materials were collected in the 2θ range of 10−80° using a step size of 0.033°. A scanning electron microscope (SEM) and field emission scanning electron microscope (FESEM) with energy dispersive spectrometer (SEM/EDX; FEI Quanta 400 and FESEM/EDX; Carl Zeiss GeminiSEM 500, Oxford Instrument X-Max 80 EDS Analyzer) was employed to evaluate the distribution of REEs in particles and the elemental composition of the samples. Thermogravimetric analyses (TGA) and differential scanning calorimetry (DSC) were performed using a Netzsch STA 449 F3 Jupiter instrument to determine phase transformation, decomposition, oxidation, and sample combustion.

According to Fig. 3.15, monazite sands were observed in most areas as grey to creamy particles, while red particles represent the feldspar phase. XRD analysis is therefore needed to determine the mineral phases of these monazite sands.

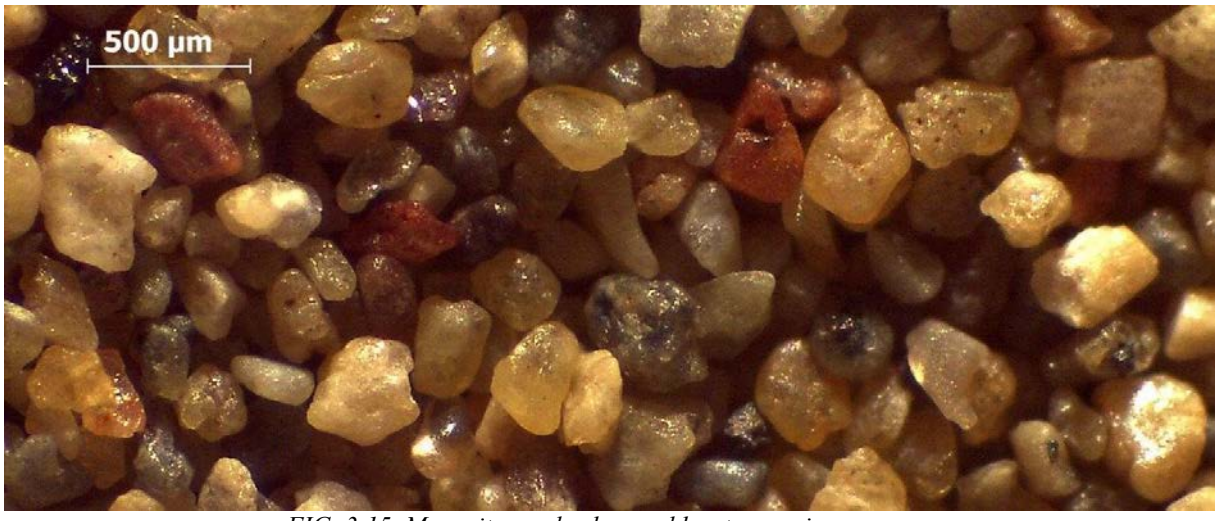

FIG. 3.15. Monazite sands observed by stereo microscope.

Table 3.12 shows the elemental content of the monazite sands. The major constituents in the monazite sands were cerium (Ce), phosphorus (P), lanthanum (La), neodymium (Nd) and thorium (Th).

TABLE 3.12. ELEMENTAL ANALYSIS OF THE RAW MONAZITE SANDS FROM MALAYSIA

Element	**Wt%**
P	19.92
Ce	39.56
La	15.48
Nd	16.86
Th	2.64
Zr	2.90
Y	2.87
U	0.089
Ca	0.68
Gd	0.59
Zn	0.20
Yb	0.17
Hf	0.16
Sn	0.11
K	0.11
Se	0.07

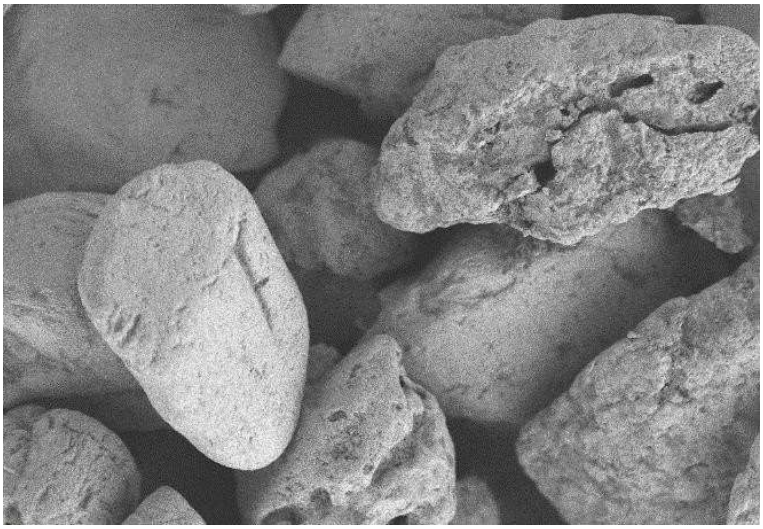

FIG. 3.16. SEM image of representative raw monazite sand from Malaysia.

A SEM image of the monazite sand with a particle size of around 170 µm is shown in Fig. 3.16. To further study the behaviour of the monazite sands, the elemental distribution maps of the monazite sands are provided in Fig. 3.17.

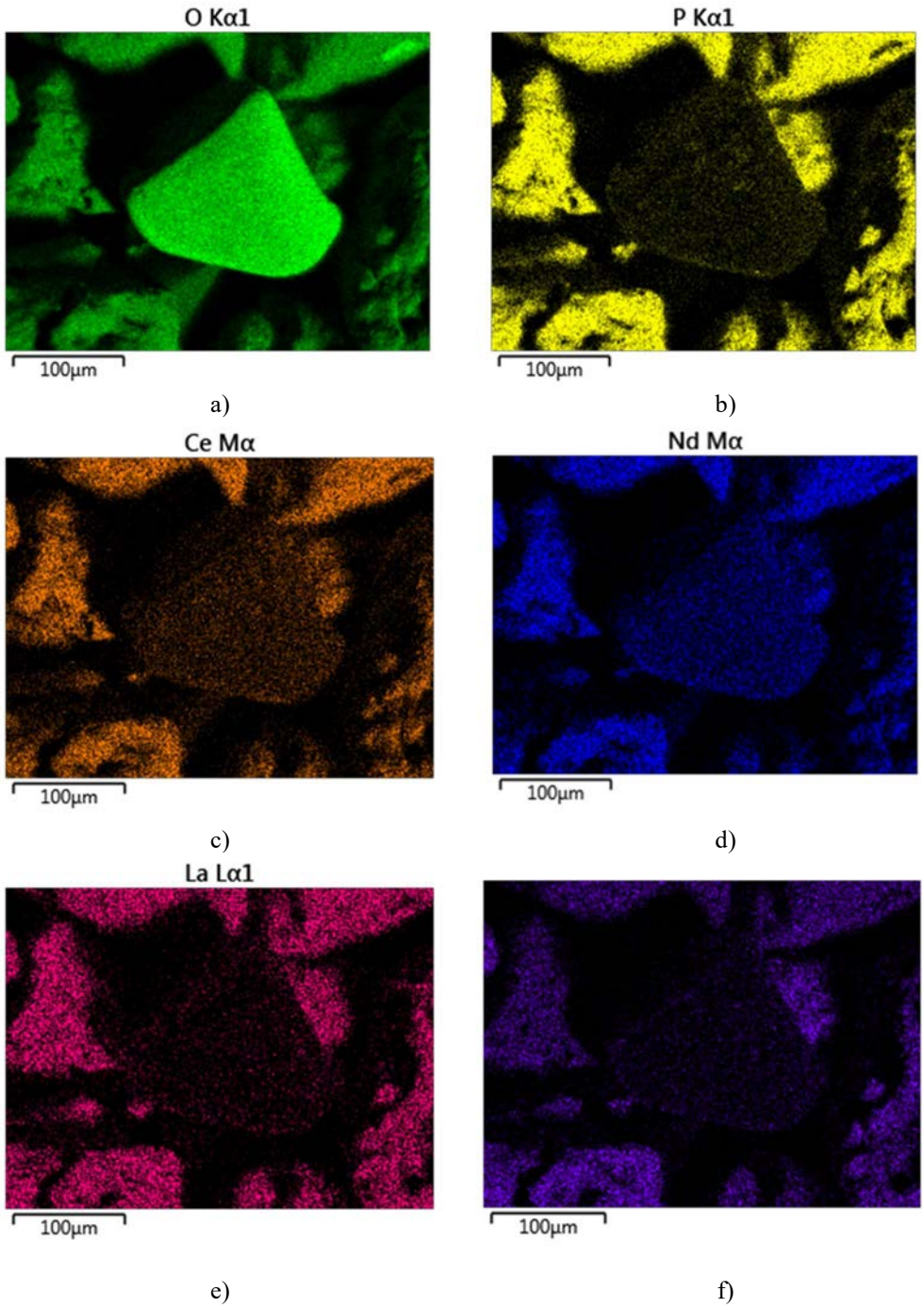

FIG. 3.17. Elemental mapping of monazite sands.

The respective images cover the major elements that exist in the monazite sands. Brighter images of particles indicate a relatively higher intensity of the analyzed elements. Fig. 3.17 clearly shows that oxide (Fig. 3.17a) and phosphate (Fig. 3.17b) are present as different particles. Ce (Fig. 3.17c) and Nd particles (Fig. 3.17d) could be identified in oxide form whereas La (Fig. 3.17e) and Th (Fig. 3.17f) occur as phosphate particles. Therefore,

beneficiation of monazite sands or physical separation is critical and needs to be done before any chemical technique can be applied for further processing.

Figure 3.18 shows an XRD pattern that identifies the qualitative mineralogy of the monazite sands. The sample consists of monazite, xenotime and feldspar. Other minerals might be present in low quantities as well but cannot be determined through XRD analysis.

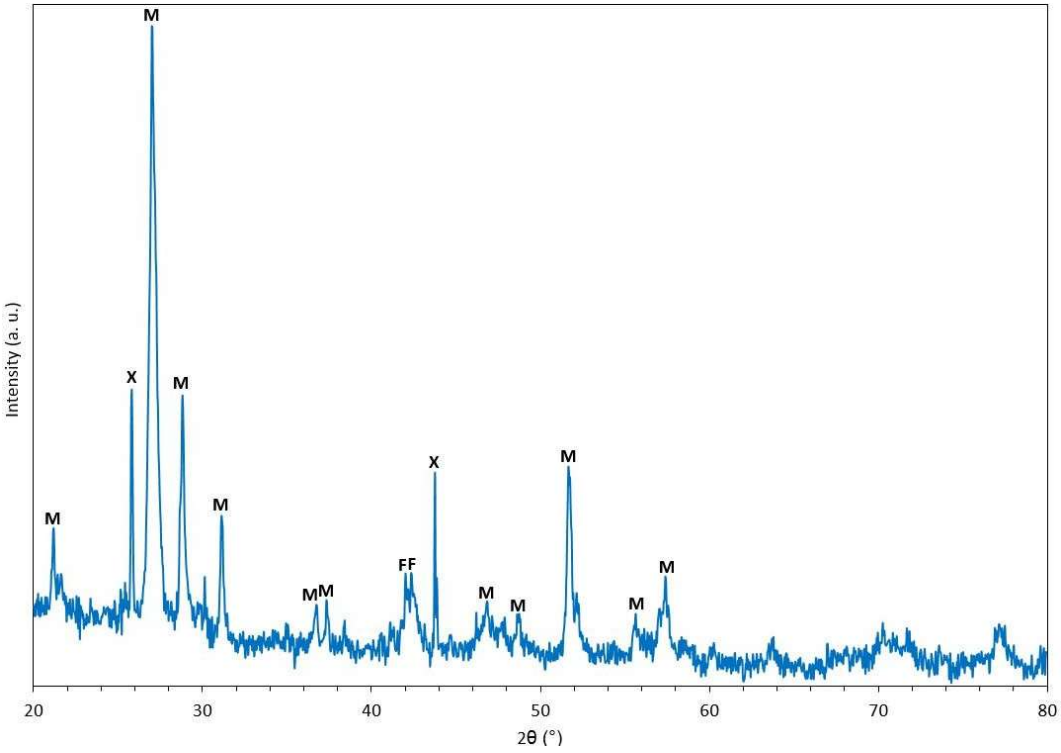

FIG. 3.18. XRD pattern of xenotime purchased for (a) demonstration plant and (b) laboratory scale. M, X and F represent monazite, xenotime and feldspar, respectively.

Thermal analysis results of monazite sands are shown in Fig. 3.19. The total mass loss was 3.05%. From the TG curve (see Fig. 3.19) it becomes clear that there are three stages of mass loss. The first stage can be attributed to vapourization of moisture that occurs from an ambient temperature to 98.5°C. No prominent mass loss occurs during the second stage. In the last stage, a slight decrease of mass can be observed, indicating a decomposition of the monazite sands itself after 1380.5°C. From the DSC curve (Fig. 3.19), it becomes further clear that the overall reaction is exothermic.

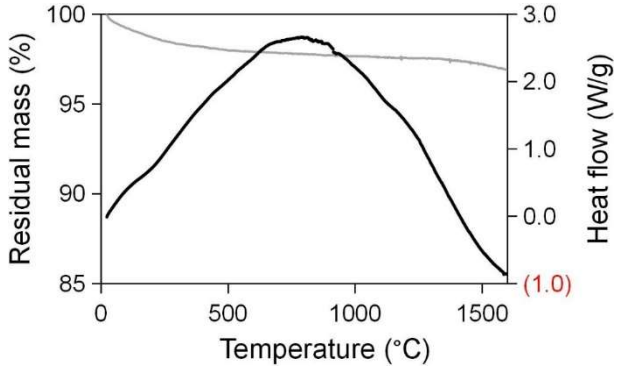

FIG. 3.19. TG (grey) and DSC (black) data recorded for monazite sands from ambient to 1600°C.

Table 3.13 shows the detailed heat capacity (Cp) of the monazite sands analysed.

TABLE 3.13. SPECIFIC HEAT CAPACITY OF THE MONAZITE SANDS

Temperature range (°C)	**CP (J $G^{-1}°C^{-1}$)**
25–164	3.535
165–219	1.165
220–649	10.372
650–794	0.806
795–832	0.268
833–872	0.195
873 - 902	0.203
903–914	0.485
915–940	0.135
941–978	0.711
979–1049	1.475
1050–1108	1.684
1109–1162	1.143
1163–1231	1.848
1232–1253	0.723
1254–1444	7.880
1445–1489	1.520
1490–1528	1.048
1529–1581	1.200
1582–1586	0.246
1587–1600	0.003

The average particle size of the monazite sands was 167 μm, shown in Fig. 3.20 and Fig. 3.21. This result is coherent with the image taken by stereo microscope that was shown before. To determine the effect of the particle size of the monazite sand, the samples were milled at different durations and speeds.

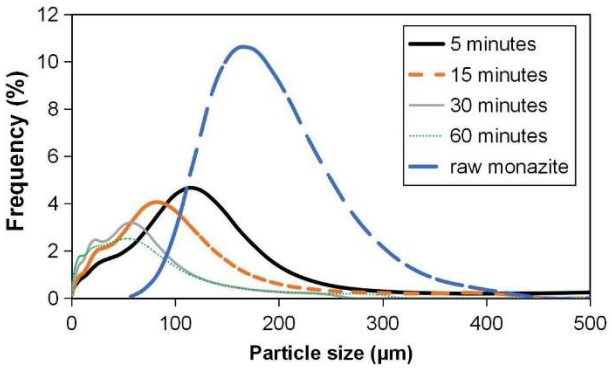

FIG. 3.20. Effect of milling duration on the monazite sands median diameter.

Upon milling at 300 rpm for 5, 15, 30 and 60 minutes, the average particle size decreases from 170 µm to 114, 88, 62 and 57 µm, respectively (see Fig. 3.20). No significant difference upon milling for 30 and 60 minutes could be observed. If the milling time is further increased, the particle size distribution becomes broader, and second peaks appear.

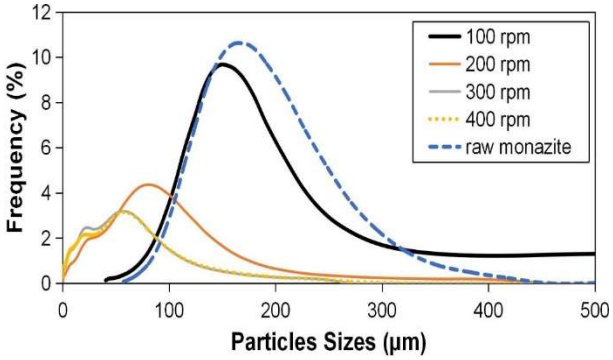

FIG. 3.21. The effect of milling speed on the monazite sands median diameter.

The particle size distribution of monazite sands after milling at different speeds is shown in Fig. 3.21. The average particle size of the monazite sand decreases from 170 µm to 148 µm and 62 µm upon increasing the speed to 100, 200 and 300 rpm, respectively. Further increase to 400 rpm did not result in further decrease of the particle size.

To study the effect of monazite sand particle sizes on the recovery of thorium, a set of experiments was performed, using different particle size ranges from 20 µm to 180 µm. The other fusion parameters were fixed at 150°C for 3 hours with a ratio of monazite sand to NaOH of 1:2. Besides, the parameters for the leaching process were fixed at 80°C for 6 hours using 6 M HCl. The obtained thorium recovery is plotted in Fig. 3.22.

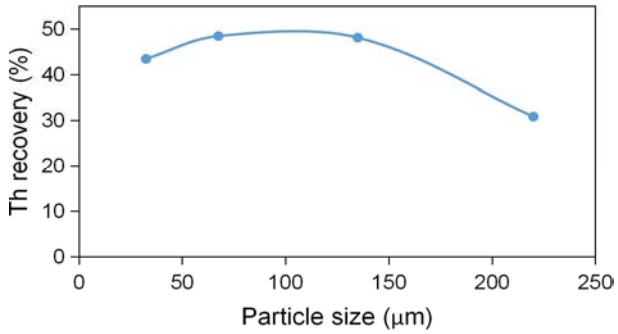

FIG. 3.22. Effect of particle size on Th recovery from monazites.

Thorium recovery increased from 30.9% to 48.1% and 48.4% by decreasing the particle size from 220 μm to 135 μm and 68 μm, respectively. A further decrease in particle size to 33 μm has an adverse effect on the thorium recovery, which then decreases to 43.4%. The decrease is most probably due to the agglomeration of smaller particles that hinder the reaction to take place.

The effect of the fusion duration on thorium recovery from monazite sands under consideration was studied for 1 to 4 hours. Data of the obtained thorium recovery is plotted in Fig. 3.23.

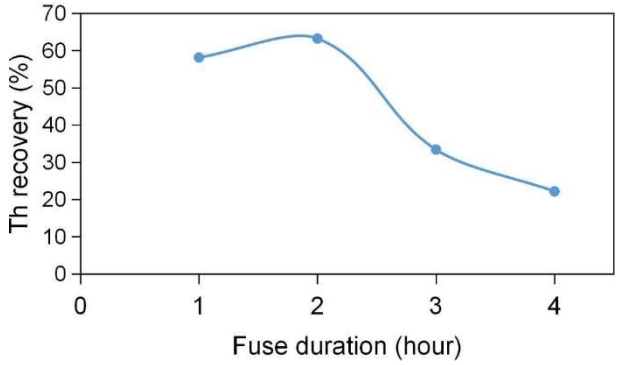

FIG. 3.23. Effect of fusion duration on thorium (Th) recovery from monazite sands.

It was concluded that the thorium recovery increases with an increase of time from 1 to 2 hours. This way the thorium recovery could be increased from 58.1% to 63.2%. Further prolonging of the fusion reaction has an adverse effect on the thorium recovery which then decreases to 33.4% and 22.2% upon fusion for 3 and 4 hours. This decrease may be due to reprecipitation of a large share of the elements contained in the monazite sands. Thus, 2 hours of fusion time would be considered an optimum value for thorium recovery in this study.

The process flow diagram of alkaline fusion on monazite sands with NaOH is shown in Fig. 3.24. The corresponding reaction is provided below. The reaction during the leaching process with HCl is also provided below. Even though the reactions are similar to the ones for xenotime minerals, the optimum parameters to recover thorium differ, due to the difference in the REE content. Each rare earth has its own unique properties such as hardness, chemical bonding, heat capacity, phases to name a only a few, making the processes significantly different from one other. For monazites most of the properties depend on the Ce or La content.

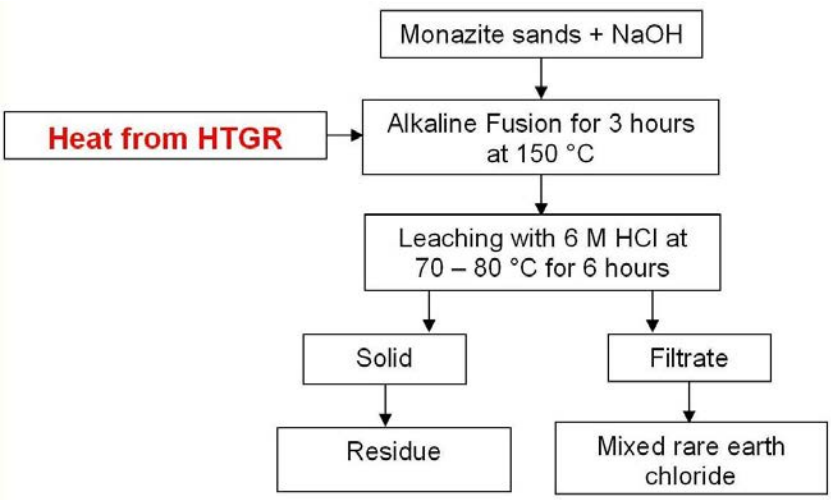

FIG. 3.24. Simplified process flow diagram of Malaysian monazite sands alkaline fusion using process heat from HTGRs.

$$REEPO_4 + 3NaOH = REE(OH)_3 + Na_3PO_4$$

$$Th_3(PO_4)_4 + 12NaOH = 3Th(OH)_4 + 4Na_3PO_4$$

$$REE(OH)_3 + 3HCl = REECl_3 + 3H_2O$$

$$Th(OH)_4 + 4HCl = ThCl_4 + 4H_2O$$

In conclusion, it can be noted that a technology for alkaline fusion for thorium recovery from Malaysian monazite sands has been developed. The latter involves fusion of monazite sands with NaOH, followed by acid leaching. The studied optimum conditions include milling monazite sands to 70 μm and fusing it for 2 hours at 150°C. It is also suggested to mill the monazite at speeds of 300 rpm for 30 minutes to get to the desired particles size. Heat generated from HTGRs could then be utilized for the alkaline fusion that takes place at elevated temperatures.

3.5 MALAYSIA: ADVANCED MATERIALS FROM MALAYSIAN ILMENITE THROUGH THERMAL PROCESSING

Thermal processes have great potential to process ilmenite more sustainably, if compared to processing with the present popular chemical route. Nowadays, ilmenite is mainly processed for its titanium content that is for instance widely used as a white pigment in paint. Nanotitania possibly produced using the thermal processing route, has many potential applications due to its greater photocatalytic activity, as a result of its high surface area.

Ilmenite or iron ore is mainly used as the source of TiO_2. It is a weakly magnetic iron black or steel grey mineral, found in metamorphic and plutonic rock [3.28]. Ilmenite is primarily found in massive ore deposits or secondary alluvial deposits that contain heavy minerals. Ilmenite is usually treated with concentrated sulphuric acid and titanium oxygen sulphate is selectively extracted and converted into titanium dioxide. During the last stage of the process, the hydrated titanium dioxide is heated to produce crystals of anatase or rutile. This process is called sulphate process.

Titanium dioxide, also known as titanium (IV) oxide or titania, is the naturally occurring oxide of titanium, with the chemical formula TiO_2. Titanium dioxide occurs in nature as rutile, anatase and brookite. Rutile is the next most abundant material and contains around 98% titanium dioxide in its ore. The metastable anatase and brookite phases convert irreversibly to the equilibrium rutile phase upon heating above temperatures in the range of 600–800°C. TiO_2 is usually a white powder that is widely used as an ingredient of white pigment, white plastic and white paper. These three products account for about 80% of the world's titanium dioxide consumption. It is also used for cosmetic products since it absorbs ultraviolet light. The rest is used in other applications such as the production of technical pure titanium, glass and glass ceramics, electrical ceramics, catalysts, electric conductors and chemicals.

Pyrometallurgical processes are used for the beneficiation of low grade iron ores and can be categorized as following: magnetizing roasting, direct reduction and smelting. Magnetizing roasting involves roasting at 600–700°C in a reducing environment. The process results in an iron-rich magnetic product such as magnetite (Fe_3O_4), maghemite (γ-Fe_2O_3) and tailings enriched with other valuable materials, such as rare earths [3.27, 3.29]. In 1989, direct reduction processing of low grade iron ores involved roasting the ores in a highly reduced atmosphere at 1000–1200°C. The process produces solid state formations of metallic iron. The reduced ore is then subjected to communation and magnetic separation. Metallic iron powder can be recovered from the process [3.30]. Smelting processes used in the treatment of iron bearing ores involve carrying out reduction using coal, char or coke at temperatures greater than 1300°C that result in iron metallization and melting of the iron and slag phases. In recent years, TiO_2 nanomaterials have also been used as semiconductor materials for photocatalytics activities [3.31-3.34].

The purpose of this project is to study photocatalyst activity of TiO_2 nanoparticles. In the synthesis part, the first stage mainly focuses on the separation of TiO_2 and Fe_2O_3, whereas in the second stage it is converting rutile into the anatase phase. The XRD analysis was done to study the properties for all the samples (commercial anatase and anatase produced in our laboratory). From the XRD analysis, the changes in the crystallite size and lattice strain of each sample powder, is compared and analysed. Then, the samples were also analysed using XRF to determine the elemental composition. XRF analysers can also determine the chemistry of a sample by measuring the fluorescent (or secondary) X-ray, emitted from a sample when it is excited by a primary X-ray source.

Ilmenite samples were collected from Bukit Beruntung, Selangor. The ilmenite samples were undergoing two stages to obtain the anatase phase. In the first stage, the ilmenite was converted into the rutile phase of TiO_2 (solid) and a filtrate containing Fe^{2+} ion which was further precipitated to get Fe_2O_3. Then in the second stage, the rutile phase samples were altered into the anatase phase. Both stages consist of alkaline fusion and acid leaching. Approximately 100 g ilmenite and 200 g NaOH were used in each fusion experiment. The temperature was varied from 550°C to 850°C with a 100°C gradient. The fusion duration was maintained for 3 hours. Homogenized fusion mixtures were transferred into alumina crucibles and placed in a furnace at a previously set temperature. After the required fusion duration, the crucibles were removed and allowed to cool down to room temperature. Fusion products were then washed with water to remove eventual unreacted NaOH and some impurities. The mixtures were subsequently filtered. Solids were further leached using a 6M HCl solution. The filtrate was coprecipitated with 12 M NH_4OH to get Fe_2O_3. The solids, composed mainly of hydrous titanium and iron oxide and were subject to a second fusion process with NaOH at 550°C before being leached with 6 M H_2SO_4. The solid portion was dried and analysed with a simultaneous thermal analyser (STA), XRF, SEM, XRD, band gap analysis, a photocatalyst activity test and anti-microbial test.

A thermogravimetry (DTG) curve obtained using ilmenite (see Fig. 3.25) shows an intense mass loss of approximately 1.47% from room temperature up to 500°C. The rapid mass loss from room temperature to 79°C corresponds to moisture release. In Fig. 3.25, the broad curve shows an exothermic reaction of raw ilmenite with the maximum exothermic reaction occurring at approximately 700°C due to the weakening of the bonds inside ilmenite mineral. Table 3.14 shows specific heat capacity of the raw ilmenite at specific temperatures.

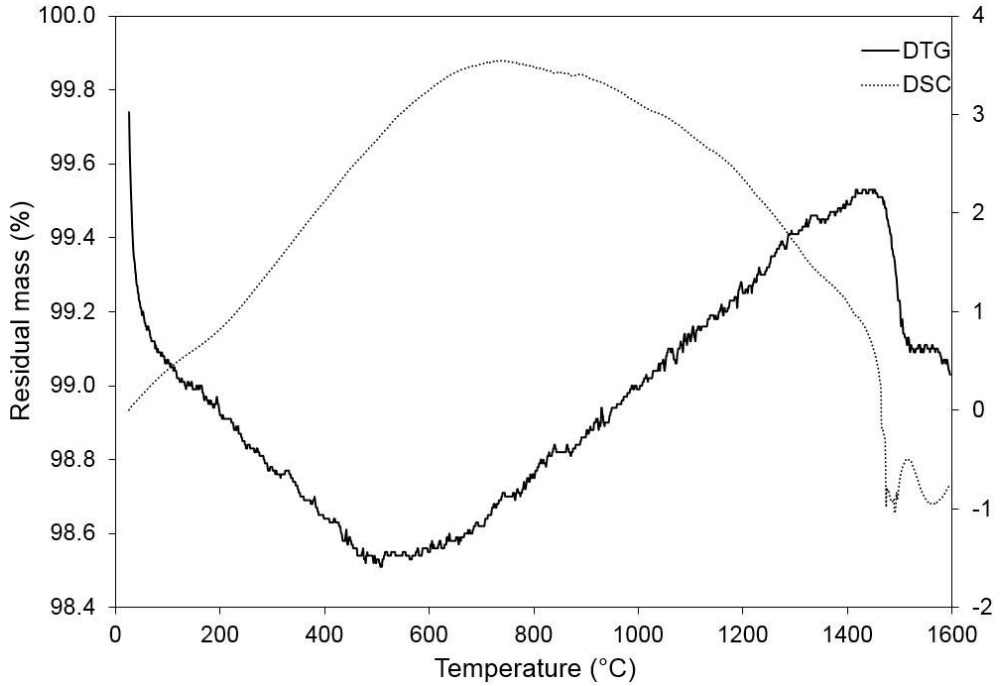

FIG. 3.25. DTG and DSC curves of ilmenite ore.

TABLE 3.14. SPECIFIC HEAT CAPACITY OF ILMENITE

Temperature range (°C)	CP (J $G^{-1}°C^{-1}$)
25–198	4.944
199–737	16.323
738–1331	12.509
1332–1430	3.601
1431–1472	3.629
1473–1475	3.586
1476–1490	4.244
1491–1515	3.025
1516–1559	2.694
1560–1600	1.258

The size of the raw ilmenite was mostly less than 280 μm as depicted in Fig. 3.26. In the next experimental procedure, the ilmenite was used without any pretreatment. A chemical analysis of the raw ilmenite material and its products after heating at different temperatures (550, 650, 750 and 850°C) is presented in Table 3.15. The highest purity of TiO_2 (94.32%) could be obtained at 650°C through fusion with NaOH and just 1.85% iron. No uranium was detected and only a few samples contained thorium, indicating that the product synthesis at this stage was less radioactive. Further separation techniques can be applied, to ensure that all radioactive elements can be extracted.

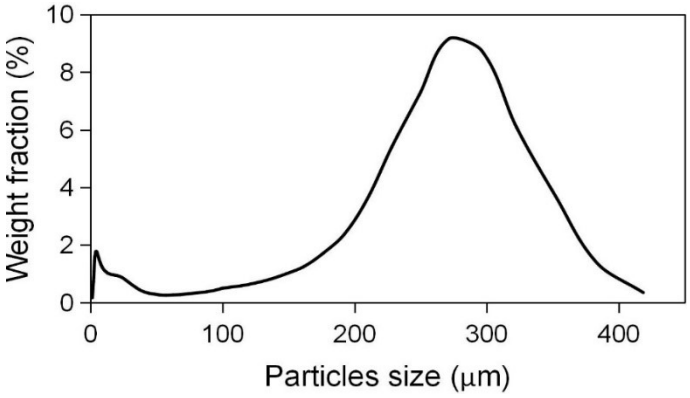

FIG. 3.26. Particle size distribution of raw ilmenite mineral.

TABLE 3.15. COMPOSITION OF ILMENITE RAW MATERIAL AFTER FUSION

Element	Raw ilmeniet	Element concentration (%) Fusion temperature (°C) 550	650	750	850
Ti	52.48	61.12	94.32	89.57	91.00
Fe	30.35	24.34	1.85	1.89	1.39
Si	5.28	2.85	0.25	4.13	3.08
Mn	2.48	2.59	0.01	-	-
Al	2.00	0.31	-	0.03	0.05
P	0.64	0.37	0.26	0.37	0.29
S	0.33	0.07	-	0.04	0.05
Ca	0.29	0.14	0.10	0.13	0.12
Y	0.78	0.03	Trace	-	Trace
Zr	0.80	0.30	0.14	0.71	0.76
Nb	0.58	0.82	0.50	0.92	0.95
Sn	2.70	3.14	-	0.70	0.32
Ce	0.17	-	-	-	-
Ta	0.14	0.22	0.06	0.22	0.26
W	0.27	0.04	-	-	0.08
Pb	0.10	0.02	-	0.01	0.01
Th	0.08	-	0.03	-	0.02
U	0.03	-	-	-	-
Cl	-	3.48	2.46	1.07	1.50

The XRD pattern of raw ilmenite and the product from the first stage is shown in Fig. 3.27. Even after fusing at 550°C, the samples were still in ilmenite form. After fusing at 650°C, all samples transformed into the rutile phase.

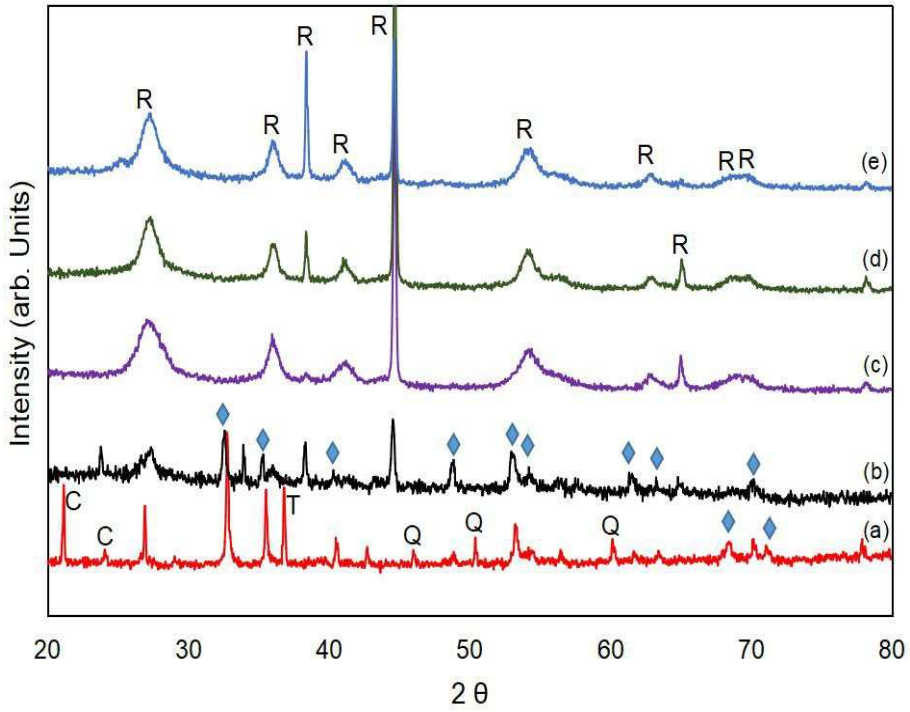

FIG. 3.27. XRD diffractograms of ilmenite raw materials after alkaline fusion, (a) ilmenite raw material, (b) 550°C, (c) 650°C, (d) 750°C and (e) 850°C. (R = rutile; C = iron cobalt titanate; T = terbium iron germanide gadolinium and the light blue diamond referring to ilmenite).

The morphology of the variation reaction occurring during the first stage was observed by SEM. Figure 3.28 shows ilmenite particles (see Fig. 3.28a) partially digested at 550°C (see Fig. 3.28b). It can be seen from the eroded part on the ilmenite surface. As the fusion temperature increases to 650°C, small flaky and round particles with approximately 2 μm diameter are obtained (see Fig. 3.28c). The size of the particles keeps decreasing as the temperature increases to 750°C (see Fig. 3.28d) and 850°C (see Fig. 3.28e).

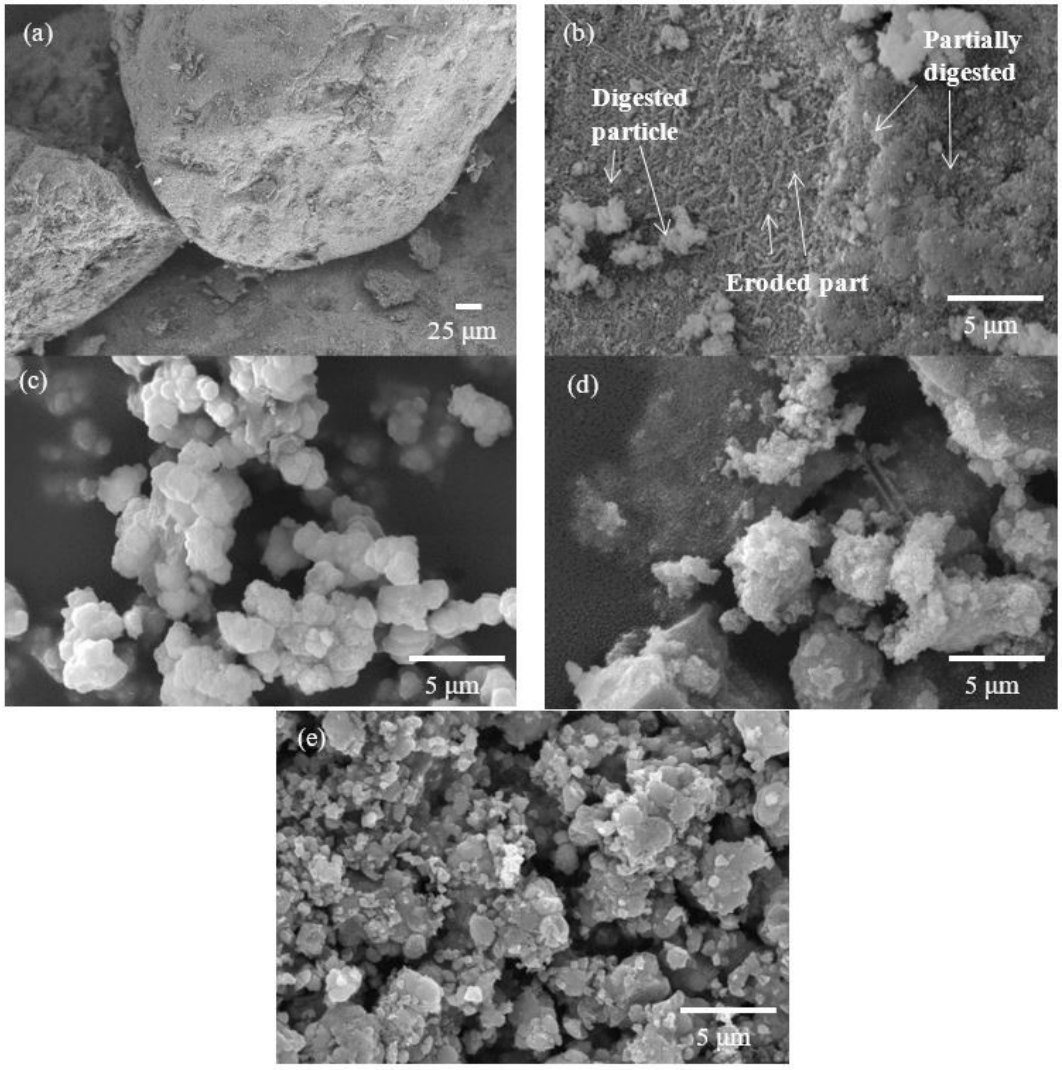

FIG. 3.28. Microstructure image of (a) raw ilmenite, sample after first stage fused at different temperature: (b) 550°C, (c) 650°C, (d) 750°C and (e) 850°C.

This is supported by a shrinking core model for particles during the digestion period [3.33]. The shrinking core model corresponds to the case that the reactant (NaOH and HCl) only acts at the edge of the particles before reacting deeper. As a result, an unreacted core remains in the particle centre and is reduced in size as the reaction progresses. This model has shown to represent a better understanding of the situation. However, as the particle size decreases, it tends to agglomerate with each other, and the agglomerated sizes are not uniform between each other.

As different elements behave differently with different reactants, specific locations of the elements need to be studied for a better strategy to eliminate most of the unwanted elements such as silicon and aluminium. Mapping of raw ilmenite was thus conducted, and results are depicted in Fig. 3.29.

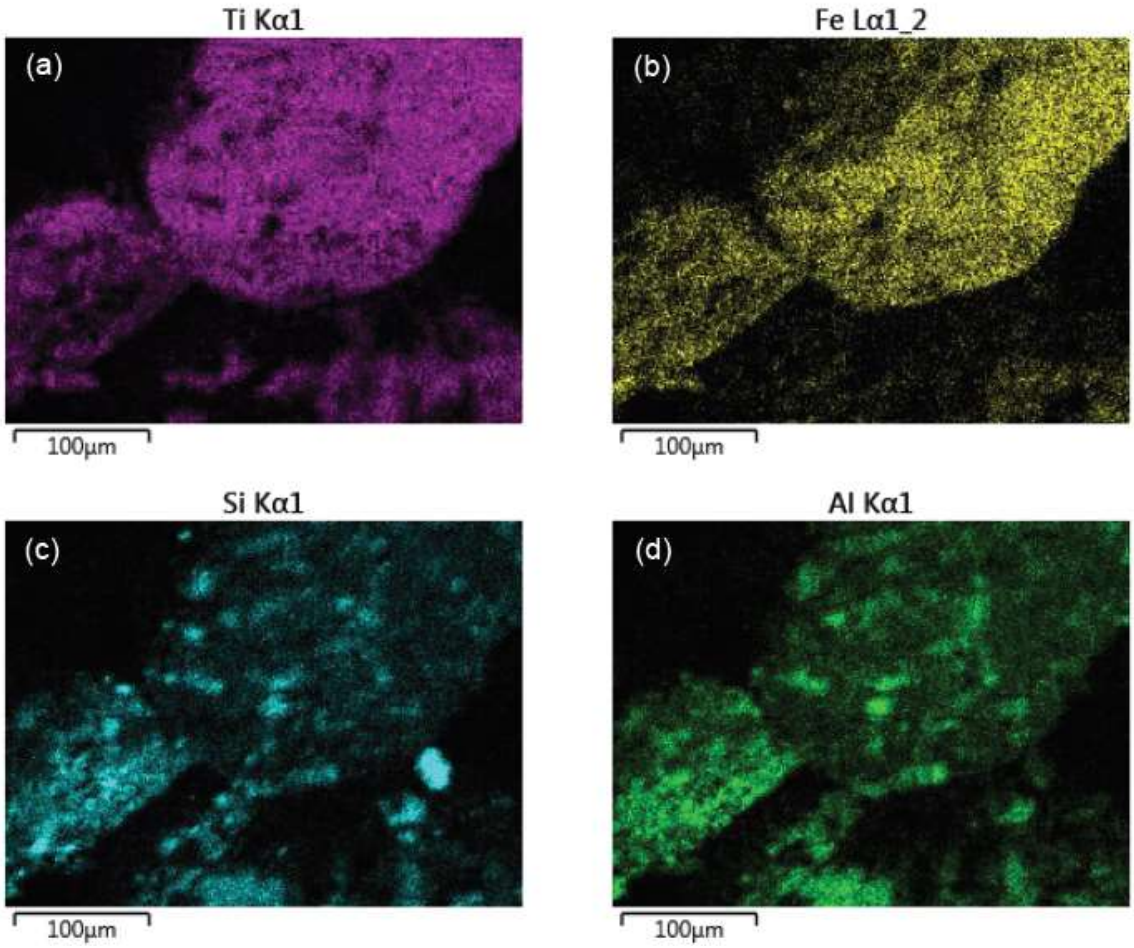

FIG. 3.29. Mapping of raw ilmenite particles.

It can be observed in Fig. 3.29 (a–b) that titanium and iron are distributed homogenously throughout the sample. Whereas silicon and aluminium only exist on the surface of the ilmenite particle. A pretreatment before alkaline fusion is therefore beneficial,.

The samples were further analysed by XRD to characterize the crystallographic structure, crystallite size (grain size) and preferred orientation in all powder solid samples. Unknown substances can be identified by comparing obtained data against a database maintained by the International Centre for Diffraction Data. The voltage and anode current used were 40 kV and 30 mA, respectively. The scanning range was from 10 to 80°.

The diffraction pattern obtained from the XRD analysis for each sample was compared with the diffraction pattern in the database as shown in Fig. 3.30. It was found that all the peaks for synthesized anatase TiO_2 and compared with commercially available anatase TiO_2 (P25) belong to the anatase phase, whereas all peaks for commercially available rutile belong to the rutile phase. The crystallite size obtained was 14.7, 2.1 and 8.1 nm for synthesized anatase TiO_2, P25 and commercial rutile, respectively.

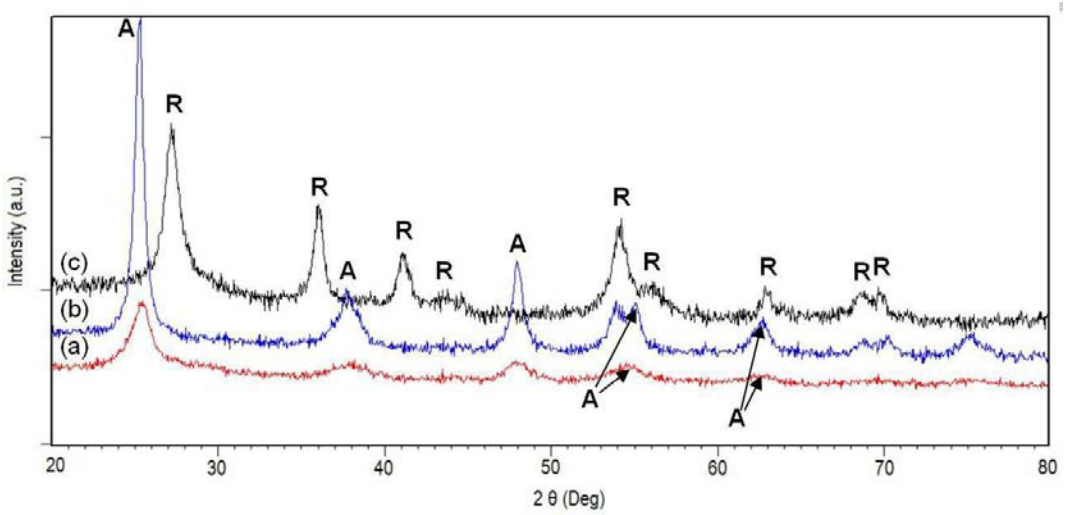

FIG. 3.30. XRD result for (a) laboratory anatase; (b) commercial anatase and (c) commercial rutile.

Samples from commercial anatase (P25) were compared with synthesized anatase TiO_2 produced in our laboratory. The similarities become particularly clear for peaks at 26° showing that the sample is 100% anatase. Lastly, for commercial rutile, there have been different peaks because it has a different crystal structure compared to anatase. Rutile has a primitive tetragonal unit cell, with unit cell parameter a = 4.584 Å and c = 2.953 Å.

Based on the results in Table 3.16, the degradation time of cigarette smoke between each sample were compared. The degradation time of the control sample was higher than that of other samples, followed by commercial rutile, commercial anatase and synthesized anatase TiO_2, respectively. Therefore, this study concluded that synthesized anatase TiO_2 from the laboratory is better for cigarette smoke degradation than other samples.

TABLE 3.16. DEGRADATION OF TiO_2 NANOPARTICLES BY CIGARETTE SMOKE

Type of sample	**Degradation time (Minutes)**
Control	13:36
Commercial rutile	13:02
Commercial anatase (P25)	12:02
Anatase TiO_2 from laboratory	10:59

The band gap of synthesized anatase TiO_2 was lower (2.95 eV) than that commercially available in the market (see Table 3.17). A lower band gap will increase the movement of electrons on the valence band to the conduction band.

TABLE 3.17. BAND GAP OF TiO_2

Sample	Band gap (eV)
Anatase commercial P 25	3.30
Anatase TiO_2 from laboratory	2.95

A photocatalyst reaction occurs when TiO_2 absorbs light to produce pairs of electrons and holes [3.34]. Then, an electron of the valence band becomes excited when illuminated by light. The excess energy of this excited electron promotes the electron to the conduction band. This process results in the creation of a negative electron (e-) and a positive hole (h+) pair. This stage is referred to as the semiconductor's photo excitation state.

The antibacterial activity of the synthesized anatase TiO_2 was studied on *E. coli* bacteria and results are shown in Fig. 3.31 and Fig. 3.32. In vitro results of the nutrient agar diffusion susceptibility test reveal that synthesized TiO_2 shows better antibacterial activity than the control sample. The presence of an inhibition zone by synthesized TiO_2 against bacteria strains clearly indicates the bactericidal potential of the synthesized TiO_2. Similar studies by Raza and colleagues [3.35] suggest that an increase in antibacterial activity with synthesized TiO_2 was due to synthesized TiO_2 accumulation in cytoplasm.

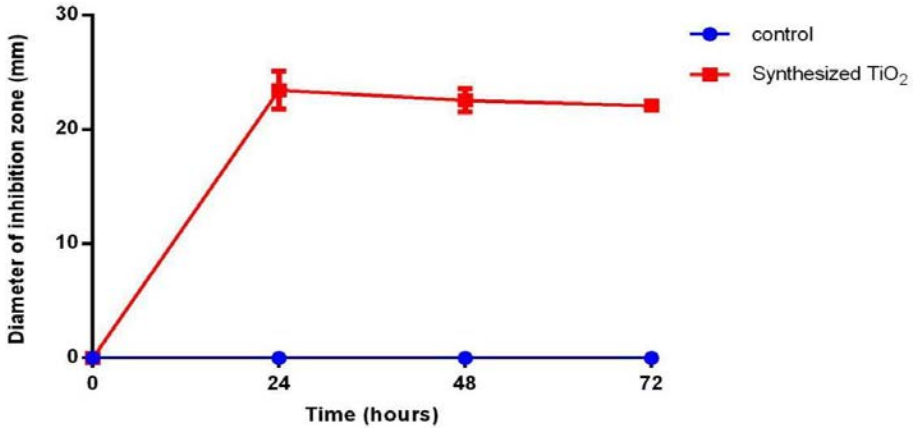

FIG. 3.31. Photocatalytic antibacterial activity on E. coli with positive control and synthesized TiO_2.

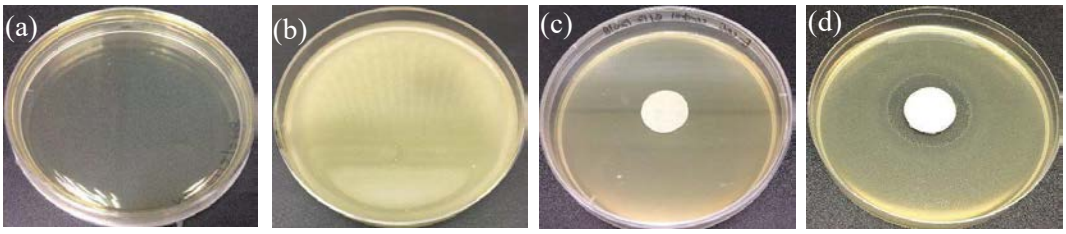

FIG. 3.32. Image for (a) nutrient agar without and (b) with E. coli and inhibition zone of E. coli bacteria on nutrient agar by (c) positive control and (d) synthesized TiO_2.

Specific techniques to obtain hematite from ilmenite, Fe_2O_3−$FeTiO_3$, exhibit interesting and useful properties that vary with changes in chemical and magnetic ordering. Most of this publication focuses on the recovery of titanium from ilmenite and that iron will be categorized

as waste [3.36]. For that reason, the recovery of iron oxide either as hematite or magnetite has been studied. This work was based on previous iron oxide synthesized research [3.37]. Judged from the low recovery of iron in the first stage, it may be suggested that most iron ions were dissolved in the filtrate. In the present situation, iron oxide particles were precipitated with the aid of the different volumes of concentrated NH_4OH solution. The highest per cent of recovery (62.7%) was reached by adding 150 mL concentrated NH_4OH to 100 mL of filtrate. To explore the performance of this recovered iron oxide, a further step to purify or alter the phase either by hematite or magnetite may be considered based on the final application of interest.

3.6 MALAYSIA: ALKALINE FUSION OF MALAYSIAN XENOTIME

Thorium (Th) is often present in xenotime in significant amounts. Depending on the amount of these radioactive element, it may be extracted along with REEs such as neodymium (Nd), gadolinium (Gd), ytterbium (Yb), holmium (Ho) and dysprosium (Dy) as a byproduct or the separation may be favoured to ensure much reduced waste accumulation.

The occurance of thorium in the earth's crust is more plentiful than uranium, by about a factor of three. Since 1994, the IAEA has developed programs and organized technical meetings on the thorium fuel cycle to develop a thorium based new fuel option for low carbon electricity generation. It is believed that thorium has the potential to provide more energy efficient nuclear energy generation. This motivation also includes larger availability of natural resources, thermal reactor sustainability, proliferation resistance and spent nuclear fuel radio toxicity [3.39].

Before chemical treatment, xenotime is typically concentrated through physical processing which comprises of floatation, magnetic separation, electrostatic separation, and gravity separation methods. Physical processing is followed by beneficiation and physical separation. Currently two major routes of xenotime decomposition that have been established are using sodium hydroxide (NaOH) or sulphuric acid to attack and break down the greatly stable xenotime structure [3.40]. Both techniques need energy intensive extraction conditions, for example elevated heat or pressure. NaOH was found to be more environmentally friendly compared to sulphuric acid roasting due to radioactive free thorium and uranium in the leach waste. Alkaline fusion with NaOH produces trisodium phosphate (TSP) as a byproduct that can be sold as compost to assist in alleviating the cost of NaOH.

Even though Malaysia has a lot of rare earth resources, most of the valuable minerals have to be imported, because of the lack of expertise to extract these minerals into purified single elements. Environmentally friendly methods are essential to assist in moving the country towards power source diversity and satisfy the demand for electricity sources. To recover thorium from xenotime, breaking up and cracking of this mineral is required [3.41]. A process consisting of alkaline fusion, followed by hydrochloric acid leaching, has been examined. Particle size (20–220 μm), time (2-6 hours), temperature (250–400°C) and caustic soda (NaOH) ratio to xenotime (0–1.0) were the different process parameters that were investigated in this work. NaOH has not been utilized commercially for REEs extraction from xenotime and only a few studies have systematically investigated the recovery from thorium using NaOH to date. The current effort intends to provide a foundation for the improvement of forthcoming business routes that exploit this unique technique for xenotime decomposition.

The xenotime ore used in this study was collected from Kinta Valley, Selangor, Malaysia. Some of the xenotime mineral was milled by Fritsch Pulverisette 6 classic line. The crushed xenotime mineral was then sieved until the desired particle size was obtained. Through this technique, the crushing sample is shaken through numerous meshing sieves, one above the other and set so that the sieve openings are successively smaller from top to bottom. The sample is consequently sorted into the different size portions (<20 μm, 20–45 μm, 45–90 μm, 90–180 μm and >180 μm).

Mineral cracking was done by mixing a xenotime mineral with NaOH beads in an alumina crucible before fusing it in a furnace. Sodium hydroxide was chosen as a fusion agent due to its relatively low fusion temperature requirement and it is also cheaper than most of the other chemicals available. Distilled water was added to the fused sample until the sample became soft. In some cases, the mixture of the fused sample and distilled water needs to be left

overnight, due to the strong adherent of the sample to the crucible surface. This mixture was then transferred to a beaker and was stirred, using an overhead stirrer. This process is called the washing process. After the washing and filtration process in vacuum, the sample undergoes an acid leaching process. The filter cake was dried and weighed. The cake and the filtrate known as trisodium phosphate (TSP) were both analysed.

The samples from the earlier stage, containing some of the salt of rare earth sodium was reacted in a glass beaker with hydrochloric acid (HCl). Leaching was done with highly concentrated HCl. The system revealed a mixture, containing a liquid phase (liquor) comprising of liquefied REEs and a solid phase, having insoluble impurities. After filtration, solid samples were labelled as residue while the filtrate was kept for further processing (separation). The xenotime samples were heated in nitrogen gas from 25°C to 1600°C at 2.5°C/min with the weight loss being constantly monitored.

Particle size analysis was performed using a Honeywell Microtrac X100 Particle Sizer. This machine scattered light from a laser beam and calculates the size distribution in the sample stream ranging from 0.02 μm to 700 μm using scattering theory for spherical particles.

XRD is a rapid analytical technique, primarily used for phase identification of a crystalline material and can provide information on unit cell dimensions. The analysed material is finely ground, homogenized and an average bulk composition is determined by an analysis of XRD patterns, collected using a PANalytical X'Pert PRO MPD PW 3040/60 (Cu Kα X ray source). XRD patterns from the as synthesized and annealed materials were collected in the 2θ range of 10−80° using a step size of 0.033°.

A scanning electron microscope (SEM) and field emission scanning electron microscope (FESEM) with energy dispersive spectrometer (SEM/EDX; FEI Quanta 400 and FESEM/EDX; Carl Zeiss GeminiSEM 500, Oxford Instrument X-Max 80 EDS Analyzer) were employed to evaluate the distribution of REEs in particles and the elemental composition of the samples.

TGA and DSC were performed using a Netzsch STA 449 F3 Jupiter instrument to determine phase transformation, decomposition, oxidation, and sample combustion. The xenotime samples were heated in nitrogen gas from 25°C to 1600°C at 2.5°C/min with the weight loss being constantly monitored.

The elemental percentage of raw xenotime is shown in Table 3.18.

TABLE 3.18. ELEMENTAL CONTENT OF RAW XENOTIME MINERAL

Element	Wt. %
P	28.71
Y	27.20
Fe	9.72
Yb	6.53
Si	6.36
Ti	4.22
Ba	4.19
Mn	2.56
Nd	1.64
Ho	1.58
Co	1.10
S	0.86
Zr	0.63
Th	0.53
Ca	0.46
U	0.39
Hf	0.37
K	0.21

The thorium content is 0.53% and the uranium content is 0.39%, making it sufficiently high to consider economic extraction. The byproducts that could be recovered from this process are neodymium (Nd), yttrium (Y) and ytterbium (Yb). Even though the combined REEs content in this ore is relatively small, these ore minerals can be mined and processed economically in Malaysia. This is largely due to the tremendous demands for REEs and the current import dependence that favor domestic REEs recovery.

Figure 3.32 shows a particle from the raw xenotime mineral via SEM (left) and an optical microscope (right). The range of particle sizes from raw xenotime minerals is 200 μm to 400 μm with an irregular shape. Mineral forming phenomena from different kinds of elements would affect the shape of the ore. More elements that exist in single particles would make the forming process more complicated [3.42]. The small white dot in the xenotime particle in Fig. 3.32 indicates the existence of REE inclusions. Upon extracting REEs via alkaline fusion, it is believed that advanced material properties can be enhanced.

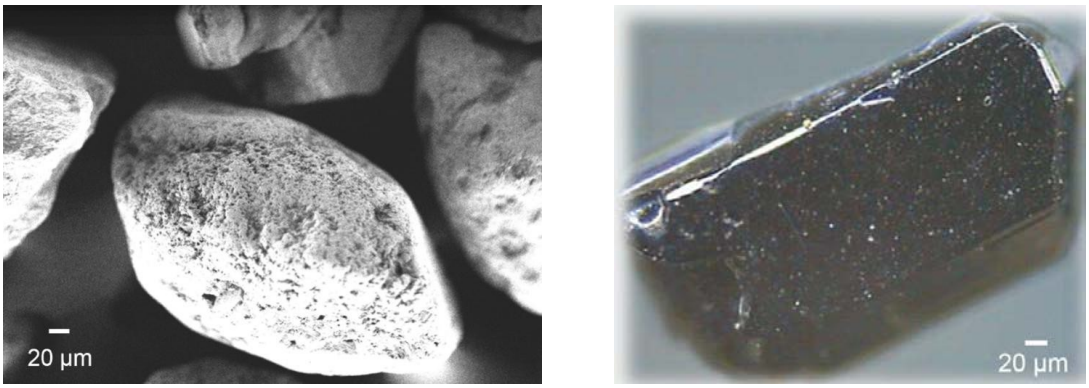

FIG. 3.33. FESEM image of raw xenotime mineral (left) and raw xenotime mineral observed by optical microscope (right).

A structural investigation of xenotime was carried out in this study using XRD and is shown in Fig. 3.34. The xenotime sample purchased for the demonstration plant experiment consists of 100% xenotime (ICDD No. 98-006-3171). However, the xenotime mineral purchased for a laboratory scale experiment, consists of a majority of xenotime with a minor cubic phase of sodium aluminosilicate (ICDD No. 98-001-5354), $Al_4Na_8O_{18}Si_4$ and cubic phase nickel palladium, Ni0.52Pd0.48 (ICDD No. 98-007-5129). Other minerals might be present in lower quantities and cannot be determined with the XRD analysis.

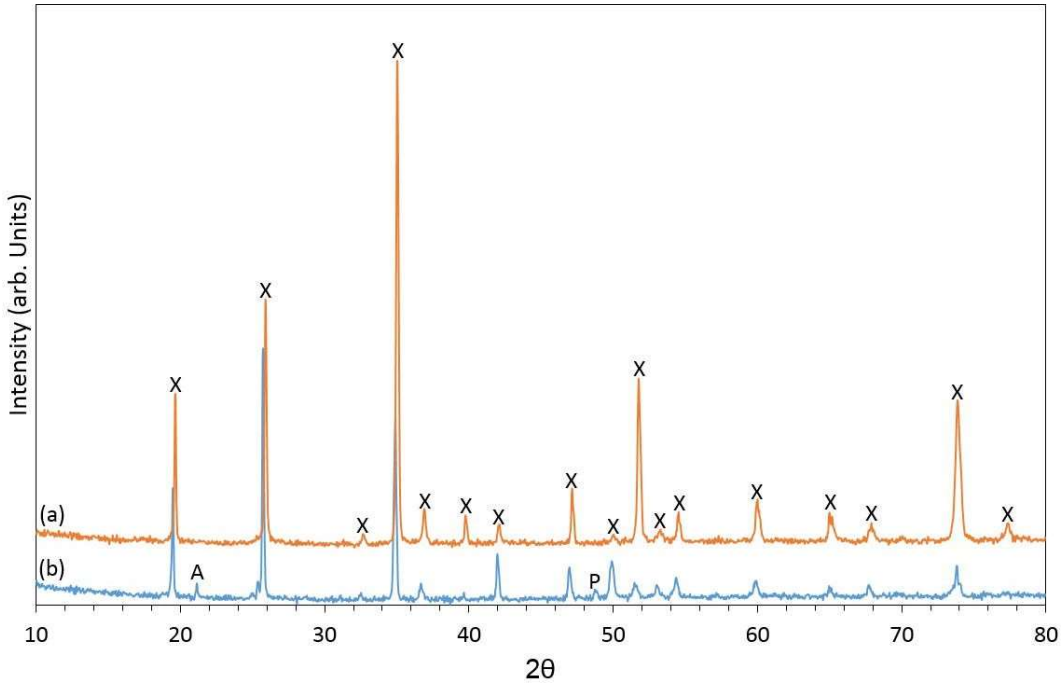

FIG. 3.34. XRD pattern of xenotime purchased for (a) demonstration plant and (b) laboratory scale. X, A and P represent xenotime, sodium aluminosilicate and nickel palladium respectively.

The xenotime mineral samples were studied by TG/DSC analyses to determine the amount of residual water in the powders and the thermal reaction that occur during the heating process. Using the heating program, powders were heated up to 1600°C with a constant heating speed of 10 K/min in air and the main mass losses caused by the removal of water from the initial powders were observed until 500°C and can be observed in the TG/DSC results in Fig. 3.35.

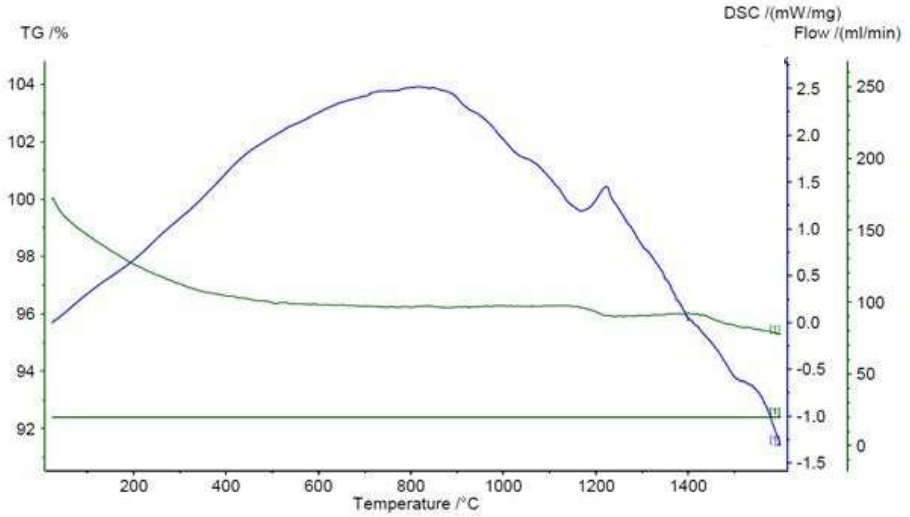

FIG. 3.35. TG/DSC data recorded for xenotime sample from ambient to 1600°C.

The occurring weight loss can be divided into three regions. In the first region below 500°C, a weight loss of about 3.5–4 wt% is assumed to be associated with the water adsorbed on the surface during the storage in air. It is likely that the amount of the adsorbed water depends on the surface area of the minerals. The second event between 1150°C and 1250°C with a corresponding maximum is assigned to the phase changes taking place in this region [3.43]. Table 3.19 shows a variation of the specific heat capacity in the function of the degradation of xenotime mineral.

TABLE 3.19. SPECIFIC HEAT CAPACITY OF XENOTIME

Temperature range (°C)	**CP (J $G^{-1}{}^{o}C^{-1}$)**
25–818	15.133
819–1171	7.936
1172–1225	1.547
1226–1598	16.442

The particle size reduction has been initially carried out using a Pulveristte 6 ball mill. The samples were milled and a few of the particle size fractions were used. This size fraction was subjected to alkaline fusion. The results of the milling duration were summarized in Fig. 3.36. These data show that the particle size of xenotime could be reduced upon 30 minutes milling (d50 = 19.51 μm) but there is no significant difference after as much as 60 minutes milling time (d50 = 7.76 μm).

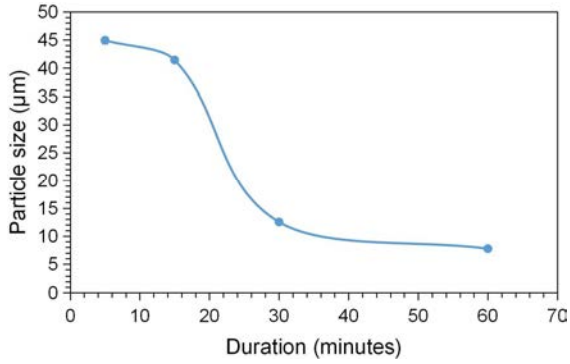

FIG. 3.36. Effect of milling duration to xenotime median diameter.

An additional experiment of milling with a different size of milling balls was also performed to see the difference on the resulting particle size. The results of these experiments are shown in Fig. 3.37. The most striking results are that very little difference in the size of the milling ball could give different results in particle size. As can be seen, a 15 mm diameter size of the milling balls could result in the smallest measured particle size of 5 µm compared to another milling ball size. This is a result of the different weight of the milling balls [3.44]. The impact strength is therefore the highest with the heaviest milling ball.

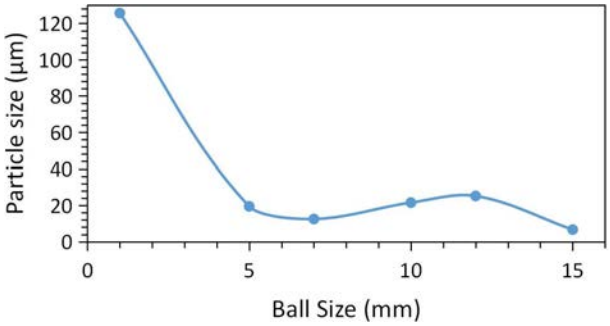

FIG. 3.37. Effect of milling ball size to xenotime median diameter.

Figure 3.38 shows a median diameter (d50) of the xenotime sample after milling at different speeds. This provides strong evidence that the optimum milling speed to reduce the xenotime particle size is at 300 rpm.

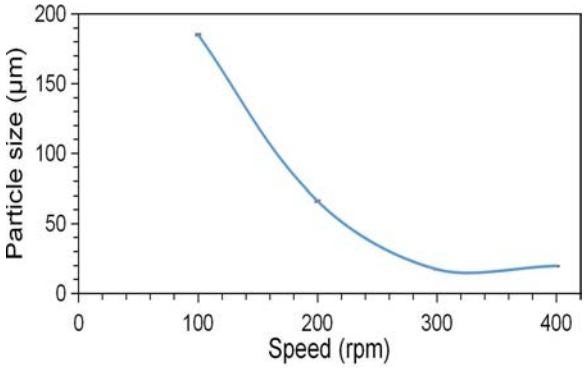

FIG. 3.38. Median diameter of xenotime sample after milling at different speed.

Figure 3.39 shows the data, comparing the particle size to thorium recovery. The thorium recovery from this reaction was performed with xenotime of different particle sizes: 20–45

μm >45–90 μm >90–180 μm. The smaller the particles size, the more thorium could be obtained. In a solid, only surface particles can interact with the other reactants. If the solid is divided into smaller pieces, then there is a greater surface area so that consequently, more particles are able to react, and the reaction rate increases. The raw mineral particle grains were relatively isolated from different types of elements that have a different behaviour. This can limit the occurring reaction. On the other hand, smaller particle sizes make the surface area larger. Therefore, higher thorium recovery is possible with a smaller particle size, due to the exposure of a larger surface area as a result of the finer grind used for alkaline fusion.

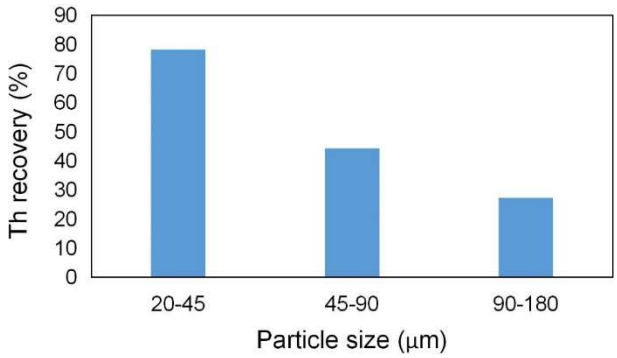

FIG. 3.39. Effect of the particle size on thorium recovery.

As a precaution, it is very important to take care of thorium-230, as it is an important precursor for radium-226 and has a long half-life (80 000 years). Leaching of thorium is an important part of the efficiency of the grinding process [3.45].

The effect of fused duration was optimized in this study. Figure 3.40 illustrates the experimental studies carried out on two different ratios of xenotime, fused with NaOH with various durations of the alkaline treatment. The influence of the fuse time was evaluated in the range of 1-6 hours. The results show that by increasing the fusion time from 1 hour to 4 hours, the percentage of recovery can be considerably increased. From this curve, the optimum parameter for a fusion duration for 1:3 and 1:2 xenotime to NaOH ratio was determined to be 3 hours. At this fusion time a thorium recovery of 60% could be realized. Even though the recovery rate of thorium is 3% higher after 4 hours of fusion such a long process is not economic because of the larger energy requirements.

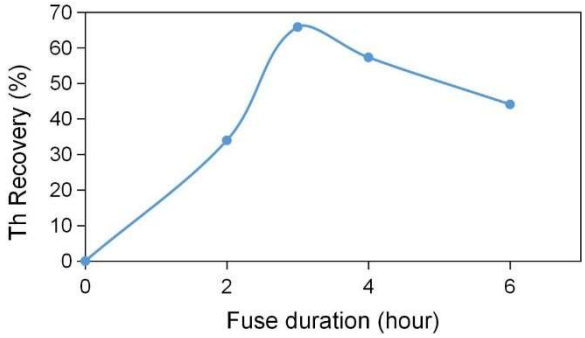

FIG. 3.40. Effect of fuse duration on thorium recovery.

The alkaline agent's ratio influences the results as shown in Fig. 3.41. The reaction tends to increase drastically from 50% to 67% NaOH. The percent recovery for thorim was higher for a sample fused with a ratio of 1:2. However, extra experiments can be conducted (for instance with a ratio of 1:3) to get the optimum parameters and to produce the highest thorium yield.

Furthermore, the percent recovery of uranium is nearly zero as the sample was precipitated at 0.2 pH. In order to get uranium to precipitate, it is essential to precipitate the sample at higher pH values ranging from 0.2 to 8.0. Based on the results shown in Fig. 3.41 below, the most crucial experimental part, is sample leaching. However, the successfulness of this leaching step is dependent on the fuse step. Uranium can be recovered by precipitating the sample at pH values up to 8.0.

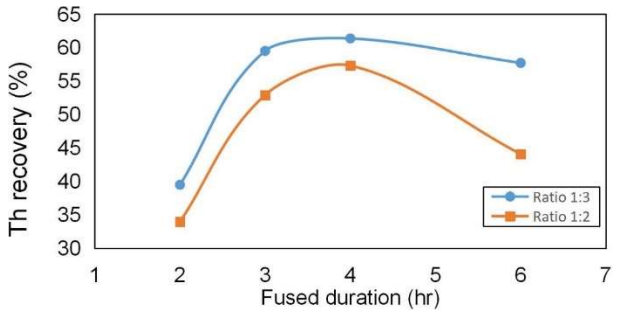

FIG. 3.41. Effect of fusion duration on Th recovery.

The FESEM images in Fig. 3.42 indicate that the optimum parameter to extract thorium is by cracking the sample with 67% NaOH. This way the needle like samples with the highest thorium concentation were obtained.

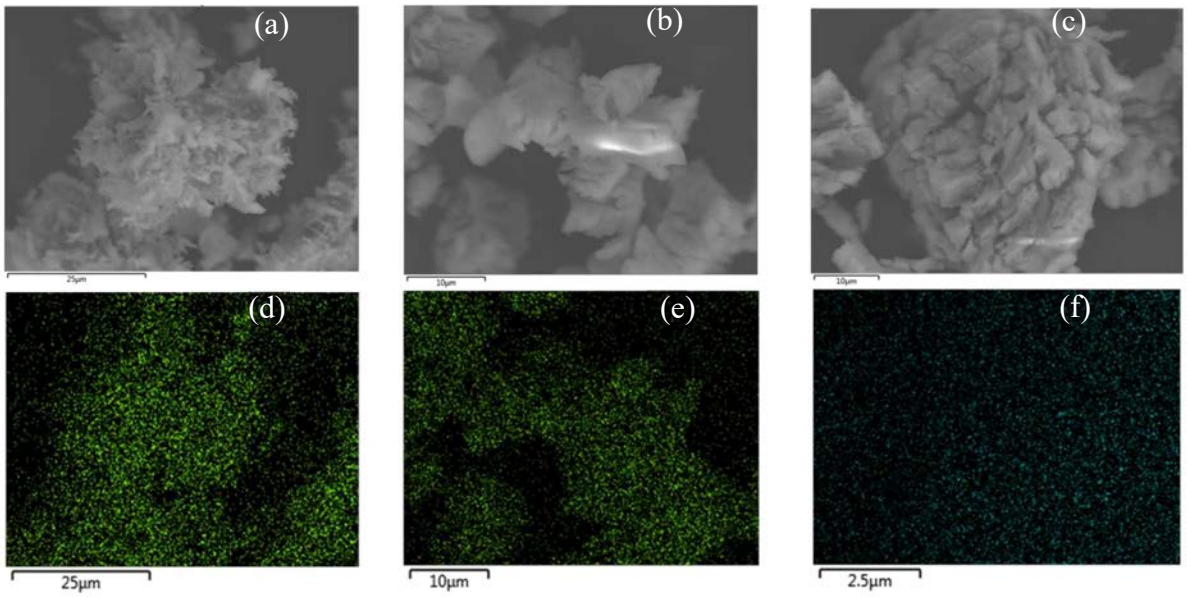

FIG. 3.42. Mapping of the precipitation product at pH 0.2 using 67% NaOH (a and d), 50% NaOH (b and e) and 33% NaOH (c and f).

Figure 3.43 shows the possibility of extracting REE with 67% NaOH. The prominent colouring of REE indicates the value of this element in the homogenous mixture. The elemental distribution mapping analysis of the sample indicates that it is rich in Y, Yb, Nd and Th. The brighter colouring of the particle further indicates a higher intensity of the elements analysed in the particle. The advantages of the alkaline fusion method are minimizing radioactive waste volume and the use of dilute acid for dissolution and recovery of phosphate as a byproduct. NaOH usage is favoured since it improved the separation of phosphate from the REEs [3.45].

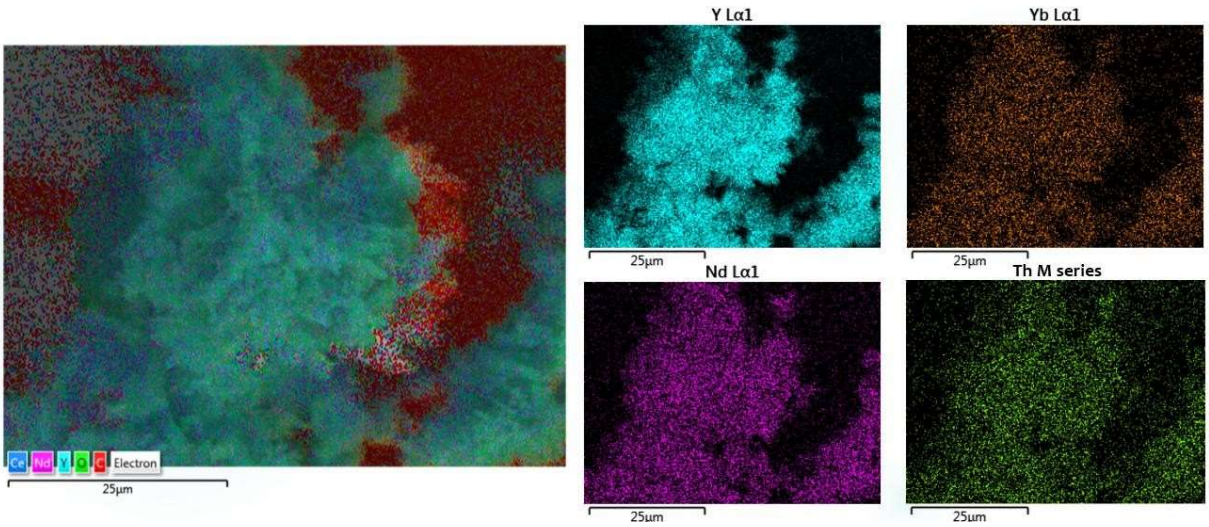

FIG. 3.43. EDX mapping for the element of interest.

TABLE 3.20. ELEMENTAL ANALYSIS OF PROCESSED XENOTIME

Element	**X – 1:2 (wt%)**	**X – 1:1 (wt%)**	**X – 2:1 (wt%)**
O	29.93	46.68	46.51
Y	33.31	30.31	32.79
La	1.92	1.05	1.29
Ce	4.79	2.66	1.45
Nd	2.6	3.79	1.51
Sm	1.56	0.73	0.77
Gd	3.02	2.30	2.16
Dy	7.12	3.71	4.93
Er	5.36	3.20	3.71
Yb	5.59	3.51	4.17
Th	2.14	0.80	0.72
U	ND	ND	ND
Pr	0.87	1.26	ND
Ho	1.65	ND	ND

The effect of fusion temperature variation in the recovery of thorium is illustrated in Fig. 3.44, for a temperature range from 250°C to 400°C and NaOH concentrations of 66.7 wt%. The reaction duration was 3 hours.

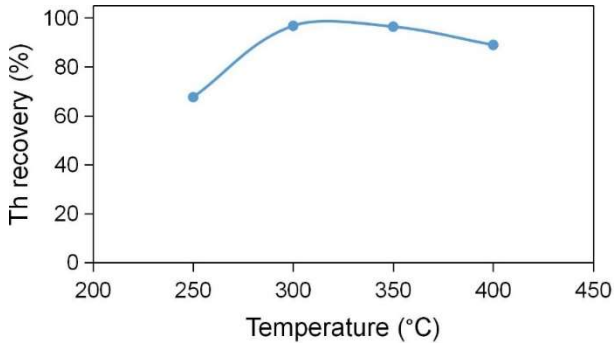

FIG. 3.44. Recovery of thorium at different fusion temperatures.

Figure 3.44 shows that the percentage of recovered thorium increases significantly at temperatures exceeding 250°C. Specifically, the extraction percentage increased from 68% to 97% when the temperature was increased from 250°C to 300°C. The process starts with fusing of NaOH at >250°C to crack the xenotime. Xenotime concentrate can be cracked at elevated temperatures to decompose to an orthophosphate lattice [3.45]. This disturbance of the crystal lattice permits diffusion of the xenotime out of the solid particles [3.44].

In the decomposition steps of monazite sands via alkaline fusion, the reaction below took place. Then, followed by preferential dissolution by HCl that is also provided below to produce mixed rare earth chloride. This mixed rare earth chloride can be further processed using selective precipitation and solvent extraction.

$$REEPO_4 + 3NaOH \rightarrow REE(OH)_3 + Na_3PO_4$$

$$Th_3(PO_4)_4 + 12NaOH \rightarrow 3Th(OH)_4 + 4Na_3PO_4$$

$$REE(OH)_3 + 3HCl \rightarrow REECl_3 + 3H_2O$$

$$Th(OH)_4 + 4HCl \rightarrow ThCl_4 + 4H_2O$$

The xenotime mineral was collected from the Kinta Valley in Perak that is characterized as a strategic place in Malaysia since the largest tin mine in Malaysia is located here. Kinta Valley, which covers areas like Kampar, Gopeng, Batu Gajah, Seri Iskandar (formly known as Tronoh), Ipoh, Tambun, Meru and Jelepang, used to be one of the most productive tin mining areas in the world. There are lots of mine tailings retreatment plants in Malaysia that are still actively suppling xenotime mineral today. The most popular are Kilang Amang Onn Sdn. Bhd., TOR minerals Sdn. Bhd. and BEH Minerals Sdn. Bhd. After the closure of several tin mines, the government alienated some areas to private developers for tourism related developments in an attempt to boost the local economy. Perak government aims to mine tin once again. The Perak government found that mining can be done without disturbing the environment. There has been a lot of studies which showed that tin or other elements inside the ore can be part of components for high tech equipment.

In conclusion, it can be noted that the cracking of raw xenotime mineral was successfully done, using a hydrothermal technique with various fusion durations. Through the experiments, the best parameters to recover most of the thorium from xenotime could be determined:

— Smaller particle size (45–90 μm);
— Feed material ratio was 1:2 (Xenotime to NaOH);
— Fusion temperature at 350°C;
— Fusion duration was 3 hours.

To get a smaller particle size (45–90 μm), the raw mineral of xenotime need to be milled with a 7 mm milling ball size at 300 rpm for 30 minutes. Modification and optimization of the concentration process in a xenotime cracking experiment, may be undertaken to produce a higher grade thorium. A further evaluation to select the extraction process of minerals concentrated into thorium, can be undertaken, based on their mineralogy, physical and chemical characteristics. To further boost the economy of xenotime processing in Malaysia inexpensive process heat from a greenhouse gas lean power source such as a HTGR or a CSP plant, could be employed as schematically shown in Fig. 3.45 for HTGRs.

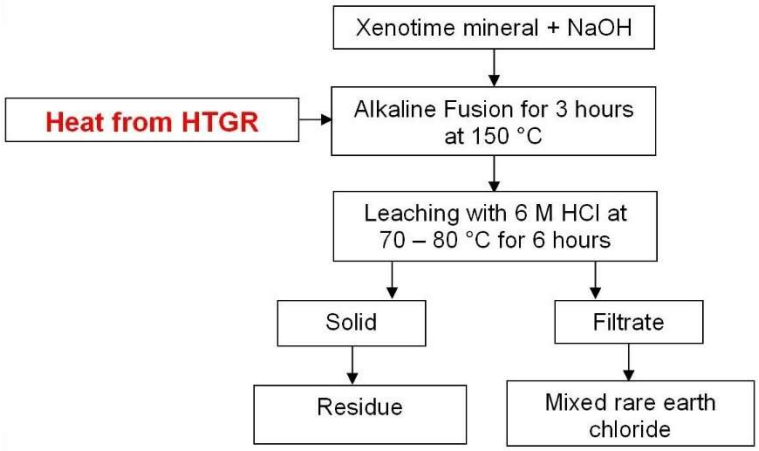

FIG. 3.45. Process flow of xenotime mineral via alkaline fusion with HTGR.

3.7 VENEZUELA, BOLIVARIAN REPUBLIC OF: HIGH TEMPERATURE REDUCTION OF CERRO IMPACTO MINERAL AND RED MUD

High temperature reduction tests of Cerro Impacto mineral and of Red Mud are reported. Samples of a mineral from Cerro Impacto, Bolivar state, Bolivian Republic of Venezuela and red mud refuse from the alumina production plant Bauxilum in Puerto Ordaz, Bolivian Republic of Venezuela, were mixed in stoichiometric and higher proportions with petroleum coke as reductant. Pellets of the mixtures were placed in a high temperature oven for varying amounts of time and the temperature as deduced from Ellingham diagrams with the purpose of reducing the contained iron without reducing other contained elements. Results of X ray diffraction, chemical assays and magnetic susceptibility tests carried out, to determine the extent of reduction achieved are reported.

The materials that were processed are:

— A mineral sample from the lateritic deposit of Cerro Impacto located in the Cedeño district of the Bolivar state in the Bolivian Republic of Venezuela, location: 5º 56' North, 65º 12.7' West;
— A red mud sample collected by the author at the refuse areas of the alumina production plant of Bauxilum. This is located in the city of Puerto Ordaz, Bolívar state, in the Bolivian Republic of Venezuela, 8º 19' North, 62º 47.7' West.

The material used for reduction is a sample of petroleum coke from the JOSE Refinery in the Anzoategui state in the Bolivian Republic of Venezuela, 10° 4' North, 64° 52' West provided by INTEVEP, a subsidiary of the Bolivian Republic of Venezuela national petroleum corporation PDVSA. Chemical analysis of the materials was performed with total reflection X ray fluorescence (TXRF) in the facilities of the Nuclear Physics Laboratory of the Universidad Simón Bolivar (USB). X ray diffraction was done in the microscopy laboratory of USB.

For both Cerro Impacto mineral and red mud, the materials were first treated in an oven to convert the contained goethite (FeO OH) into hematite (Fe_2O_3) at a temperature of 350°C. The thermodynamics was investigated, in order to see if the contained iron could be reduced while the other elements would remain as oxides. Using Ellingham diagrams it was concluded that it is possible to achieve the reduction of Fe in the ore above 720°C while the Nb begins to reduce to a temperature of 1480°C. The tool was also used with the previous elements and with several REEs. The Ellingham diagram indicate that the REE curves remain even lower, on the scale of free energy, than the curves for Nb. Hence it is also concluded that in the stated temperature range, the oxides of the REE will also remain unreduced.

The process expected to occur in mixtures of the carbon reductant and minerals has the following steps. The carbon, C, oxidizes with air to form CO gas; The CO reacts with Fe_2O_3 to Fe metal and CO_2 according to the following reactions [3.46]:

$$4C^{+4} + 4O^{-2} \rightarrow 4CO$$

$$Fe_2O_3 + CO + C \rightarrow 2Fe + 2CO_2$$

According to the stoichiometry established by both reactions, for every 159.7 grams of hematite 24 grams of carbon is best added. As the mineral contains 50% hematite, for the design of the reduction mixture hematite can be added at twice the mass of the mineral, that is: 319.4 g. Therefore, the stoichiometric mixture is 319.4 g ore and 24 g carbon (assuming that the carbon contains 100% C), for a total mixture of 343.4 g. This means that the pellets have to be 6.99wt% coal and 93.01wt% of the mineral.

Reactions below are an ideal case in which the coke is pure carbon and the oxide is completely reduced to metal. In practice, partial reduction takes place, producing intermediate magnetic iron compounds and the incorporation into the resulting material of elements, contained in small but significant amounts in the petroleum coke, significantly vanadium and nickel. The expected reactions are as following:

$$C + 4CO + 2Fe_2O_3 \rightarrow 4Fe + 5CO_2$$

$$O_2 + CO + 2Fe_2O_3 \rightarrow Fe_3O_4 + Fe + CO_2$$

$$CO + 2Fe_2O_3 \rightarrow 2FeO + CO_2$$

Partial reduction of the hematite produces iron compounds such as Magnetite (Fe_3O_4), wustite (FeO) and eventually metallic iron (Fe).

The minerals from Cerro Impacto and red mud were first treated at 350°C, as indicated above, to convert contained hydrated goethite into hematite. Appropriate amounts of the minerals were thoroughly mixed with petroleum coke in stoichiometric amounts in a ball mill and pressed into 12 mm diameter pellets. Also prepared were pellets with a higher coke concentration: twofold, threefold and fourfold of the stoichiometric amounts, in order to compensate for the possible direct formation of CO_2 from air. The Cerro Impacto pellets were first treated in a furnace at 750°C in an air atmosphere and the reduced material was analysed. On the basis of the partial reduction achieved, the red mud pellets were treated at a higher temperature of 830°C and the reduced material was analysed.

The reductant material used for both Cerro Impacto mineral and red mud was petroleum coke of which a chemical analysis is provided in Table 3.21.

TABLE 3.21. ANALYSIS RESULTS OF THE PETROLEUM COKE USE FOR THE REDUCTION TESTS

Element	Concentration (%)
S	1.819
Ca	0.013
Ti	0.003
V	0.238
Fe	0.036
Ni	0.059
Cu	0.054
Zn	0.029
Sr	0.001
C	97.7

Analysis of the Cerro Impacto material and the fractions after magnetic separation confirmed the fact that the mineral sample available is not representative of the deposit. This is due to

the absence of characteristic niobium and some REEs which are reported in the following chapters. Results of the analysis of the Cerro Impacto mineral sample are shown in Table 3.22. The material after reduction tests were analysed by XRD, showing changes of the crystal structure and evidence in the reduced material of the compounds: unreduced hematite, magnetite, wurstite and metallic iron.

TABLE 3.22. ELEMENT CONCENTRATION (%) OF THE MINERAL SAMPLE FROM CERRO IMPACTO OBTAINED BY TXRF

Element	**Concentration (%)**
Ti	0.445
V	0.100
Mn	3.269
Fe	17.127
Zn	0.195
Sr	0.032
Y	0.019
Zr	0.184
Ba	0.549
Ce	0.223
Pb	0.058
Th	0.276

Tests performed show that all the reduced Cerro Impacto material is highly magnetic and no effective separation in fractions with different susceptibilities was achieved. After the reduction process for red mud material for one hour, all the material acquired magnetic properties with absence of non magnetic fractions.

TABLE 3.23. DISTRIBUTION OF THE REDUCED RED MUD MATERIAL FOR TWO HOURS IN MAGNETIC FRACTIONS

Magnetic fractions	**Mass (%)**
Least	13.3
Middle	20.8
Most	65.9
	100.0

The data indicates that a higher proportion of the contained iron minerals were reduced into the more magnetic iron phases. The chemical analysis of the materials showed a changed distribution of thorium as shown in Table 3.24.

TABLE 3.24. RESULTS OF THE THORIUM CONCENTRATION IN THE MAGNETIC FRACTIONS OF RED MUD REDUCED FOR TWO HOURS

Fraction	Th concentration	Factor
Unreacted	0.076	1.0
Least magnetic	0.16	2.1
Middle magnetic	0.14	1.8
Most magnetic	0.219	2.9

However, chemical analysis of these fractions does not show an improvement in the thorium separation from the iron as can be seen in the results shown in Fig. 3.46 and Table 3.25. These results indicate that thorium accompanies the reduced iron without improvement of the element separation.

TABLE 3.25. THORIUM TO IRON RATIO IN THE MAGNETIC FRACTIONS

Magnetic fraction	Th to Fe ratio
Least	0.0026
Middle	0.0019
Most	0.0025

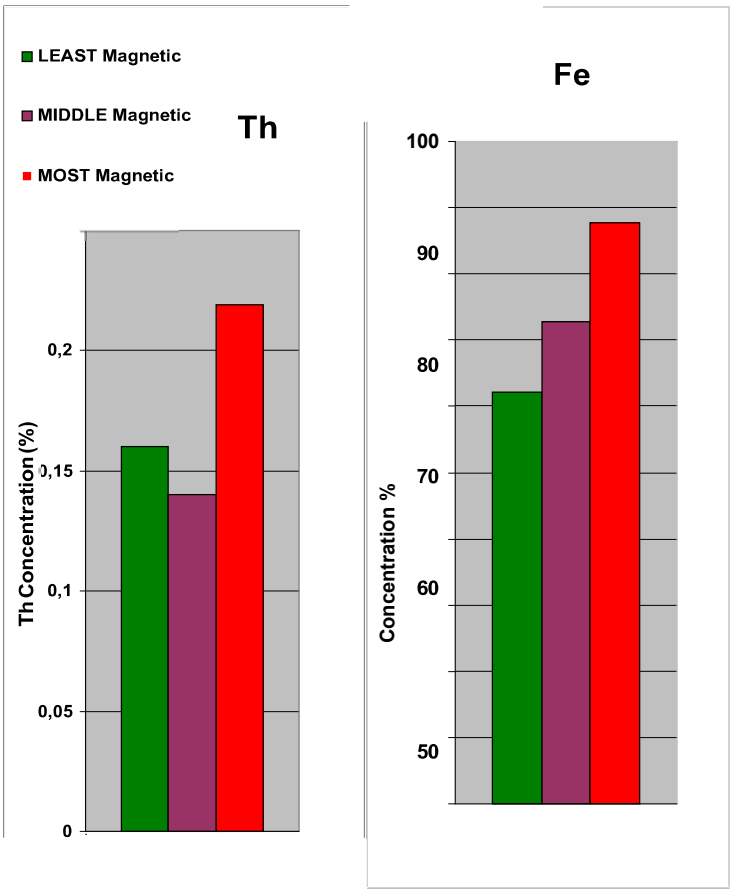

FIG. 3.46. Thorium and iron concentrations (%) obtained by XRF in the magnetic fractions of a red mud sample reduced for 2 hours at 830°C.

Although the chemistry and thermodynamics of the reduction process predict the possible reduction of the majority of the contained iron oxides into more magnetic compounds or into the metal under the conditions carried out in the tests, the results of the analysis indicate that thorium and the other elements remain intimately associated with the iron minerals which prevented the success of the magnetic separation. In the tests performed, the iron was only partially reduced to more magnetic compounds and only very little was transferred to the metallic state. The conclusion is that more aggressive reduction conditions at higher temperature and with reductive gases such as hydrogen or carbon monoxide are required to bring the iron into the metallic and molten state and allow for the separation to occur.

3.8 VENEZUELA, BOLIVARIAN REPUBLIC OF: HIGH TEMPERATURE PROCESSING OF COLTAN

A pyrometallurgical test for the processing of uranium bearing columbite tantalite minerals from the region of river Aguamena, Bolívar State, Bolivian Republic of Venezuela, are described. The process consists of a high temperature process for dissolving the mineral at ~830°C in molten alkali salt, KOH, followed by a low temperature process consisting of chemical separation of the contained elements. Tests carried out, prove the feasibility of using high temperature process heat for the treatment of this unconventional source of uranium.

An important source of tantalum for the electronics industry is the columbite tantalite mineral, known in the trade by the synonym of Coltan [3.47]. The mineral is found in certain limited zones of the world in Africa, South East Asia, and South America. The high dielectric constant of tantalum oxide layers allows the construction of high performance miniature capacitors required by all modern electronic devices. The expansion of the market for these devices has created a large demand for Coltan and fostered research into novel methods of chemical analysis and processing technologies for the mineral.

Furthermore, the high demand caused grave social problems in the Republic of Congo. The radioactive character of the columbite tantalite mineral is well known [3.48]. The presence of the radioactive element uranium has been reported in very closely associated uranium containing minerals. The possibility of recovering uranium from this unconventional source, implies the examination of the standard method of processing. The mineral is difficult to render into solution, being insoluble in HCl, HNO_3 and only slowly soluble in H_2SO_4 [3.49].

Dissolution for analytical purposes by standard methods such as AAS, ICP-OES, ICP-MS or TXRF requires a lengthy procedure. The processing methods developed by the industry involve the use of hydrofluoric acid solutions which imply grave environmental problems leading to costly abatement measures [3.50]. An alternative processing method has been considered here with a procedure which makes use of dissolution of the mineral in molten salts at high temperature and subsequent separation of the various elements. The use of three molten chloride systems ($ZnCl_2$-NaCl; LiCl-KCl, NaCl-$CaCl_2$) at temperatures of up to 600°C did not render the mineral in solution. The use of a fluoride eutectic composition of KF-LiF-NaF (FLiNaK) showed incipient dissolution at a temperature of 650°C. However, the recommended higher temperatures were not possible with the instrumentation at hand. Here first work on the implementation of a pyrometallurgical process at higher temperatures, in order to explore the potential of recovering the contained uranium from columbite tantalite is reported.

The process tested, consisted of the dissolution of a sample of pure Venezuelan columbite tantalite mineral in a molten alkali KOH salt at a temperature of ~820°C [3.51]. The process tested, was carried out in air with the material added to a crucible containing an excess alkali in the order of 10:1. Heat was supplied by a natural gas fire burner directly to the crucible. It was found that the mineral dissolves completely in the molten alkali and is left as a solid inside the crucible after cooling. The solid melt containing the mineral elements was dissolved at low temperature (60°C) in an aqueous media containing KOH, leaving all contained elements in the solution. The solution was then treated to precipitate manganese, leaving a clear solution containing tantalum and niobium. This was treated with a solution of NaCl and an adjustment of the pH, producing a precipitate containing hydrated sodium tantalate and niobiate. The solids recovered by filtration were analysed to determine the presence of Ta and Nb.

The mineral samples analysed consisted of specimens originating in the region of the river Aguamena, in the North East of the State of Bolivar, Bolivian Republic of Venezuela. The approximate coordinates: 6° 15.8' North 67° 7.6' West, were supplied by a miner collaborator. The mineral specimen used in the tests was analysed for structural purity by X ray diffraction (XRD) and for chemical content by total reflection X ray fluorescence (TXRF), using a variety of sample preparation techniques. The XRD analysis revealed that the sample is a pure specimen of columbite tantalite. To analyse the mineral with TXRF, the usual and recommended procedure is to dissolve the sample to avoid measurement problems, derived from the minute amount used as analysis specimen in this technique. However, due to the notorious difficulty of dissolving this mineral, a special technique was employed which avoids the dissolution step. It consists of preparing a suspension of carefully weighed very finely ground material with an internal standard element added. With thorough agitation, the suspension is sampled and an aliquot of 10 mL is deposited on a quartz reflector, dried and used for the analysis. Results of the analysis are shown in Table 3.26, indicating that EA6 is a high Ta specimen.

TABLE 3.26. RESULTS OF THE TXRF ANALYSIS OF THE EA6 MINERAL SAMPLE USED IN THIS WORK

Element	**Concentration %**
Ta	59 637
Mn	14 877
Nb	9484
Fe	7787
W	4655
Dy	2002
Ti	0.642
Sc	0.376
Ca	0.258
Pb	0.256
U	0.027
Sum	**100 000**

A finely ground sample of the EA6 columbite tantalite mineral was processed at high temperature as described above. The mineral dissolved completely at the estimated temperature of 820°C. The molten salt with the dissolved mineral elements was cooled and the solid material redissolved and was subjected to a short chemical procedure, to prove the feasibility of the technique to affect a separation of the elements.

The work reported, provides strong evidence of the potential of the high temperature process described for the treatment of the mineral columbite tantalite and its ability to separate tantalum from the other contained elements and the possibility of recovering the contained uranium from this unconventional source.

3.9 VENEZUELA, BOLIVARIAN REPUBLIC OF: SEPARATION OF TANTALUM AND NIOBIUM FROM COLTAN

The experimental work described here was implemented at the laboratory at the USB after the pyrometallurgical procedure described in [3.51] for the separation of tantalum and niobium from Columbita Tantalita (Coltan) of nominal composition (Fe,Mn) $(Ta,Nb)_2$ O_6 and the possible recuperation of the contained uranium in this mineral.

15 g of potassium hydroxide was weighed, placed inside a nickel crucible, and melted by heating with a Bunsen burner. When the boiling stopped, the heating stopped, and the melt cooled. Then 1.5 g of finely ground pure Coltan was added, and the heating was resumed to bring the crucible to high temperature (approximately 800°C) for a period of 30 minutes, during which a strong boiling could be observed. Heating was stopped and the molten mass was allowed to solidify, which resulted in a blueish colouration. The crucible was subsequently introduced into a 400 mL glass beaker, containing 200 mL of hot aqueous potassium hydroxide solution (50 g/L KOH). The temperature of the alkaline solution was maintained at 60°C by heating it until the solid dissolved completely. The resulting solution had a dark colour and contained a large amount of a suspension of solid precipitate. After cooling to room temperature, it was filtered. The brown solid residue was washed thoroughly with deionised water and allowed to dry for further analysis, (solid filtering 1). The solution was intentionally left to stand overnight, exposed to air. A very small dark precipitate was subsequently removed by filtration, washed with water and allowed to dry (solid filtering 2).

The filtered liquid was transferred to a 600 mL beaker and the temperature of the solution was raised to 60°C, then 12 mL of a saturated aqueous solution of sodium chloride (25.4% by weight of NaCl) was added. The pH of the resulting solution was gradually increased by the cautious drop wise addition (approximately 270 drops) of concentrated sulphuric acid (98% by weight of H_2SO_4) until the pH was in a range of about 6–7. This produced a white precipitate, which was recovered by filtration, using filter paper and subsequently rinsed with diluted hydrochloric acid, (liquid filtering 1).

The filter paper with the hydrolyzed sodium tantalate and niobate was transferred to a 250 mL vial, containing 100 mL hydrochloric acid (20% by weight HCl) and left for a period of 30 minutes. (The filter paper was digested during this treatment, forming a pulp). The resulting solution was passed through a strainer to remove the filter paper pulp and subsequently the white solid formed was filtered and washed thoroughly with a hot and diluted solution of hydrochloric acid followed by washing with deionised water. The solid was allowed to dry in the environment and analysed (solid filtering 3 and liquid filtering).

The samples of the solid filtrates 1 and 3 and of the liquid filtrates 1 and 2, were analysed semi quantitatively, by means of TXRF. The solid 2 was very small and could not be separated from the filter paper. For liquids, an aliquot of the solution of approximately 5 to 50 µL was taken and placed in the centre of a glass reflector, and dried, obtaining a thin film. For the case of solid filtrates, they were previously treated with the suspension technique of the Tween solution, a technique previously validated and applied in the Nuclear Physics Laboratory at USB . The results are depicted in Table 3.27, Table 3.28 and Table 3.29.

TABLE 3.27. SEMI QUANTITATIVE CONCENTRATIONS OF ELEMENTS PRESENT IN SOLID FILTRATE 1 (DL = DETECTION LIMIT)

Element	**Concentration %**
K	22 909
Sc	0.356
Ti	0.419
Mn	13 463
Fe	6598
Ni	0.738
Zr	0.352
Nb	13 189
Ta	41 941
Pb	0.035
U	DL 0.003

TABLE 3.28. SEMI QUANTITATIVE CONCENTRATIONS OF ELEMENTS PRESENT IN SOLID FILTRATE 3

Filtrate 3	
Element	**Concentration %**
Cl	0.910
Ca	0.188
Ti	0.499
V	0.047
Mn	0.058
Fe	1.349
Nb	11.280
Ta	76.686
W	8.738
Pb	0.013
Th	0.038
U	0.193

TABLE 3.29. SEMI QUANTITATIVE CONCENTRATIONS OF ELEMENTS PRESENT IN LIQUIDS 1 AND 2 (DL = DETECTION LIMIT)

Liquid 1		Liquid 2	
Element	**Concentration %**	**Element**	**Concentration %**
S	32.610	S	24.931
Cl	24.340	Cl	40.778
K	42.938	K	29.668
Br	0.005	Ti	0.140
Rb	0.012	V	DL 0.008
Nb	DL 0.108	Cr	0.606
Ta	DL 0.001	Mn	0.113
W	0.096	Fe	3.157
		Ni	0.380
		Cu	0.012
		Zn	0.042
		Rb	0.007
		Nb	DL 0.210
		Ta	0.054
		W	0.108
		Pb	0.004

According to reference [3.51], the solid residues resulting from the experimental part 1 of the fusion and dissolution of Coltan in KOH are: iron, titanium, zirconium, rare earths, uranium and thorium, as well as the oxides and hydroxides of these compounds. The significant presence of manganese, niobium and tantalum, which have been soluble and remain in the liquid solution after filtration, according to the reactions in Table 3.30, could also be observed. It also shows the presence of nickel, which is due to the crucible used, and traces of lead that are assumed as contamination.

TABLE 3.30. CHEMICAL REACTIONS OF PART 1 AND SOLUBILITY OF THE PRODUCTS ACCORDING TO REFERENCE [3.52]

Products	**Reactions**
Soluble	$3Ta_2O_5 + 8KOH \rightarrow K_8Ta_6O_{19} + 4H_2O$
Soluble	$3Ta_2O_5 + 6KOH \rightarrow 2K_3Ta_3O_9 + 3H_2O$
Soluble	$3Nb_2O_5 + 8KOH \rightarrow K_8Nb_6O_{19} + 4H_2O$
Soluble	$3Nb_2O_5 + 6KOH \rightarrow 2K_3Nb_3O_9 + 3H_2O$
Soluble	$2MnO_2 + 6KOH + 0.5O_2 \rightarrow 2K_3MnO_4 + 3H_2O$
Soluble	$MnO_2 + 2KOH + 0.5O2 \rightarrow K_2MnO_4 + H_2O$
Soluble	$SnO_2 + 2KOH \rightarrow K_2SnO_3 + H_2O$
Soluble	$SiO_2 + 2KOH \rightarrow K_2SiO_3 + H_2O$
Soluble	$WO_3 + 2KOH \rightarrow K_2WO_4 + H_2O$
Soluble	$Al_2O_3 + 2KOH \rightarrow 2KAlO_2 + H_2O$
Insoluble	$Sc_2O_3 + 2KOH \rightarrow 2KScO_2 + H_2O$
Insoluble	$Fe_2O_3 + 2KOH \rightarrow K_2Fe_2O_4 + H_2O$
Insoluble	$TiO_2 + 2KOH \rightarrow K_2TiO_3 + H_2O$
Insoluble	$2TiO_2 + 2KOH \rightarrow K_2Ti_2O_5 + H_2O$
Insoluble	$ZrO_2 + 2KOH \rightarrow K_2ZrO_3 + H_2O$
Insoluble	$UO_2 + 2KOH \rightarrow K_2UO_4 + H_2O$

These results may be due to the fact that the fusion process was not carried out correctly, since the expected temperature of 800°C was not reached. This is due to the crucible which had very thick walls, contrary to the one indicated by Cardarelli et al. [3.51] of 25 mL that would reach the desired temperature in the indicated 30 minutes. So, one of the improvements to the experimental process proposed by this first analysis is to increase the temperature of the fusion using a more powerful burner, or a high temperature oven and increase the reaction time at high temperature.

On the other hand, according to the article of Wang et al. [3.53] the reactions of niobium and tantalum oxides present in Coltan (Nb_2O_5 y Ta_2O_5) with potassium hydroxide can be either:

$$Ta_2O_5 + KOH \rightarrow K_3TaO_4 + H_2O$$

$$Nb_2O_5 + KOH \rightarrow K_3NbO_4 + 3H_2O$$

or

$$Ta_2O_5 + KOH \rightarrow KTaO_3 + H_2O$$

$$Nb_2O_5 + KOH \rightarrow KNbO_3 + 3H_2O$$

The products of the reaction are hydrolyzed to $K_8Nb_6O_{19}$ y $K_8Ta_6O_{19}$ which are soluble in water. Therefore, one of the possible reasons why Ta and Nb report in the solid precipitate is because the reaction of the insoluble products was favoured by the conditions of the experiment. To confirm this hypothesis, it would be ideal to carry out an XRD analysis to observe which compounds constitute the Ta and Nb present. In this article, however, it was found that the reaction temperature, the molar ratio of KOH and Nb_2O_5/Ta_2O_5 and the reaction time are the main parameters that affect the dissolution of niobium and tantalum in water.

Regarding the molar ratio K_2O to Nb_2O_5/Ta_2O_5, according to Wang et al. [3.53] when it is less than 1:1, the reaction product is mostly $KNbO_3/KTaO_3$ and when it is greater than 4:3, the product is largely K_3NbO_4/K_3TaO_4. Regarding the reaction temperature, it is evident that it is the parameter with the greatest influence on the experimental process and the results show that the rate of dissolution of the oxides increases significantly with the increase of the reaction temperature. The temperatures studied by Wang et al. [3.53] range from 350°C to 450°C. In all the experiments carried out, the reaction time was 1 hour.

For our experiment, the molar relation in the fusion is 1:10, which was reported to work successfully before [58]. For this reason, increasing the temperature and time of the reaction for the process of aqueous dissolution of KOH, following the fusion at high temperature is proposed.

On the other hand, when studying the Gibbs free energy of formation of the compounds of interest, it can be estimated to which condition their formation reaction is spontaneous, according to an article by Bhat and Borgstedt [3.54]. There is evidence that the presence of oxygen influences the formation of K_3NbO_4/K_3TaO_4, and there is a concentration of 1600 ppm and above, for O_2 to occur. The reaction time validated by this experimental procedure to favour the reaction of the soluble ternary oxide was 24 hours. This supports the previous proposal on the importance of reaction time as a parameter to be studied, since solids naturally take longer to react.

The possible hypothesis that the presence of oxygen can be a cause of the precipitation of Ta and Nb, by the formation of oxides, is also discarded. In fact, the soluble oxide of interest is more oxidized than the insoluble one, which is why a greater presence of oxygen is favoured. However, since oxygen concentration is a very difficult parameter to control, it was decided not to consider it as a parameter to be studied or to vary in the experimental process.

The complete dissolution of the tantalite columbite (Coltan) mineral sample was accomplished with the high temperature pyrometallurgical procedure described in this work, following [3.54]. The subsequent low temperature procedure carried out, shows that a partial separation of the Ta and Nb elements was achieved, while complete separation of W, Th and uranium was accomplished.

REFERENCES TO CHAPTER 3

[3.1] NEA/IAEA Uranium 2016: Resources, Production and Demand, OECD 2016 NEA No. 7301 (2016).

[3.2] WNA Nuclear Power in India (2020).

[3.3] Future Directions Meeting India's Energy Requirements in 2030, http://www.futuredirections.org.au/publication/meeting-india-s-energy-requirements-in-2030-1/

[3.4] Australia, M.C. of Energy Fact Sheet India, https://minerals.org.au/file_upload/files/resources/MCA_energy_fact_sheet_India_April_2016.pdf

[3.5] SEVER, J.C., "CALIX calciner: A green application in the production", Drying, Roasting, Calcining of Miner. (2016) 121–126.

[3.6] DINSDALE, J., TIRZINS, P., SCEATS, M., Flash Calcining Technology for Cementitious Binders and Additives, (Proc. Future Cement Conference, London, UK, 8 February 2011) (2011) 17.

[3.7] SURI, A.K., Innovative Process Flowsheet for theRecovery of Uranium from Tummalapalle Ore, BARC Newsletter Issue No. 317 (2010) 6–12.

[3.8] MCGARVEY, F.X., UNGAR, J., The influence of resin functional group on the ion-exchange recovery of uranium, J. South Afr. Inst. Min. Metall. **81** (1981) 93–100.

[3.9] RAO, K.A., SCREENIVAS, T., VINJAMUR, M., SURI, A.K., Kinetics of alkaline leaching of UO_2 and FeS_2 in co-existing system, Trans. Indian Inst. Met. **69** (2016) 23–31.

[3.10] AMD Department of Atomic Energy, Atomic Minerals Directorate for Exploration and Research Government of India (2020).

[3.11] Uranium Corporation of India Limited, Recovery of Uranium from Rohil-Ghateswar (Rajasthan) Uranium Ore: A Report on Bench Scale Studies (2017).

[3.12] SURI, A.K., SREENIVAS, T., "Developments in processing of conventional uranium ore resources of India", Proc. XXVI Int. Mineral Processing Congress (IMPC 2012), 24–28 September 2012, New Delhi, India (2012).

[3.13] ANAND RAO, K., NATARAJAN, R., PADMANABHAN, N.P.H., Studies on recovery of copper, nickel, cobalt and molybdenum values from a bulk sulphide concentrate of an Indian uranium ore, Hydrometallurgy **62** (2001) 115–124.

[3.14] SUSILANINGTY, A.S. Penentuan kondisi digesti monasit dengan asam sulfat, Eksplorium **105** (1996) 2–4 (In Indonesian).

[3.15] SUBRAMANIAN, C., SURI, A.K., Recovery of niobium and tantalum from low grade tin slag — A hydrometallurgical approach, Environ. Waste Manag. (1998) 100–107.

[3.16] ANGGRAINI, M., WAFA'NAWAWI, F., WIDANA, K., Sulfat dan solvent extraction trioctylamine (TOA) determination of optimal conditions for extracting uranium and thorium from tin slag II with a sulfuric acid leaching and trioctylamine (TOA) solvent

extraction method, Eksplorium **40** (2019) 11–18.

[3.17] SUHARYANTO, A., FIRDIYONO, F., SULISTIYONO, D.A., Penentuan jenis pelarut pada pemisahan uranium dan thorium dari slag iiimah, Maj. Met. Hal. **2014**, 197–204 (In Indonesian).

[3.18] SUHARYANTO, A., SULISTIYONO, E., FIRDIYONO, F., Pelarutan terak timah bangka menggunakan larutan NaOH, Maj. Met. **29** (2014) 191–196 (In Indonesian).

[3.19] WALUYO, S., ANGGRAINI, M., RUSYDI, D., Penentuan jenis pelarut pada pemisahan uranium dan thorium dari slag II, Tekhnol. Nukl. (2012) 141–147 (In Indonesian).

[3.20] SALIMY, D.H., HAFID, A., SRIYONO, M., Utilization of HTGR for phosphate fertilizer production and uranium recovery, IOP Conf. Series: Journal of Physics: Conf. Series 1198 (2019) 022069.

[3.21] WAI, A.M., Selective precipitation of neodymium oxide (Nd2O3) from monazite, Int. J. Sci. Eng. Technol. Res. **7** (2018) 1–5.

[3.22] GANGWAR, P., PANDEY, M., SIVAKUMAR, S., PALA, R.G.S., PARTHASARATHY, G., Increased loading of Eu^{3+} ions in monazite LaVO4 nanocrystals via pressure-driven phase transitions, Cryst. Growth Des. **13** (2013) 2344–2349.

[3.23] RAHMAN, M.A., POWNCEBY, M.I., HAQUE, N., BRUCKARD, W.J., ZAMAN, M.N., Valuable heavy minerals from the Brahmaputra River sands of Northern Bangladesh, Appl. Earth Sci. **125** (2016) 174–188.

[3.24] MEOR YUSOFF, M.S., KAIRONIE, M.T., NURSAIDATUL, K., AHMAD KHAIRULIKRAM, Z., NUR AQILAH, S., An alternative alkaline fusion process for the production of heavy rare earth, thorium, uranium and phosphate from Malaysian xenotime, Recent Adv. Environ, Ecosyst. Dev. **1799** (2015) 163–167.

[3.25] TEIXEIRA, L.A.V., SILVA, R.G., AVELAR, A., MAJUSTE, D., CIMINELLI, V.S.T., Selective extraction of rare earth elements from monazite ores with high iron content, Min. Metall. Explor. **36** (2019) 235–244.

[3.26] FARIS, N., RAM, R., TARDIO, J., BHARGAVA, S., MCMASTER, S., POWNCEBY, M.I., Application of ferrous pyrometallurgy to the beneficiation of rare earth bearing iron ores — A review, Miner. Eng. **110** (2017) 20–30.

[3.27] LAPIDUS, G.T., DOYLE, F.M., Selective thorium and uranium extraction from monazite: I. single-stage oxalate leaching, Hydrometallurgy **154** (2015) 102–110.

[3.28] CARP, O., HUISMAN, C.L., RELLER, A., Photoinduced reactivity of titanium dioxide, Prog. Solid State Chem. **32** (2004) 33–177.

[3.29] TSENG, Y., KUO, C.-S., HUANG, C.-H., LI, Y.-Y., CHOU, P.-W., CHENG, C.-L., WONG, M.-S., Visible-light-responsive nano-TiO_2 with mixed crystal lattice and its photocatalytic activity, Nanotechnology **17** (2006) 2490.

[3.30] IWASAKI, I., PRASAD, M.S., Processing Techniques for difficult-to-treat ores by combining chemical metallurgy and mineral processing, Miner. Process. Extr. Metall. Rev. **4** (1989) 241–276.

[3.31] THAMAPHAT, K., LIMSUWAN, P., NGOTAWORNCHAI, B., Phase characterization of TiO_2 powder by XRD and TEM, Nat. Sci. **42** (2008) 357–361.

[3.32] GUILLARD, C., DEBAYLE, D., GAGNAIRE, A., JAFFREZIC, H., Physical properties and photocatalytic efficiencies of TiO_2 films prepared by PECVD and sol-gel methods, Mater. Res. Bull. **39** (2004) 1445–1458.

[3.33] CANAGUIER, V.Y., Synthesis of Ilmenite, NTNU at Dept of Materials Science and Engineering, Master Thesis, Norwegian University of Science and Technology (2014).

[3.34] PALANIVELU, K., IM, J.-S., LEE, Y.-S., Carbon doping of TiO 2 for visible light photo catalysis — A review, Carbon Lett. **8** (2007) 214–224.

[3.35] RAZA, W., FAISAL, S.M., OWAIS, M., BAHNEMANN, D., MUNEER, M., Facile fabrication of highly efficient modified ZnO photocatalyst with enhanced photocatalytic, antibacterial and anticancer activity, RSC Adv. (2016) 78335–78350.

[3.36] TAI, M.F., LAI, C.W., ABDUL HAMID, S.B., Facile synthesis polyethylene glycol coated magnetite nanoparticles for high colloidal stability, J. Nanomater. **2016** (2016).

[3.37] SANCHEZ-SEGADO, S., LAHIRI, A., JHA, A., Alkali roasting of bomar ilmenite: Rare earths recovery and physico-chemical changes, Open Chem. **13** (2015) 270–278.

[3.38] SONGIP, A.R., SULAIMAN, M., YUSOF, M., The Digestion of Thorium Cake in Nitric Acid (Proc. 5th Symposium of Malaysian Chemical Engineers) (1989) 470–478.

[3.39] NEA Introduction of Thorium in the Nuclear Fuel Cycle, OECD 2015 NEA No. 7224 (2015).

[3.40] GALVIN, J., SAFARZADEH, M.S., Decomposition of monazite concentrate in potassium hydroxide solution, J. Environ. Chem. Eng. **6** (2018) 1353–1363.

[3.41] SULAIMAN, MEOR M.Y., Recovery of Yttrium, Uranium and Phosphate from Mineral Xenotime (1992).

[3.42] BARBOSA, J.P., RIBEIRO, R.A., CUNHA, O.G.C., Alkaline Leaching of a Xenoitme Concentrate (VI SHMMT/XVIII ENTMME, Rio de Janeiro, Brasil) (2001) 451–456.

[3.43] FISHER, D.M. Jr., Phase Developments between Xenotime (YPO_4) Refractory and an Alkali Aluminosilicate Glass Melt, Master of Science, Alfred University (2015).

[3.44] RYON, A.D., HURST, F.J., SEELEY, F.G., Nitric Acid Leaching of Radium and other Significant Radionuclides from Uranium Ores and Tailings, ORNL/TM-5944 (1977).

[3.45] XIE, F., ZHANG, T.A., DREISINGER, D.B., DOYLE, F.M., A critical review on solvent extraction of rare earths from aqueous solutions, Miner. Eng. **56** (2014) 10–28.

[3.46] CHRYSANTHOU, A., MACFARLANE, D., CHINYAMAKOBVU, O.S., Carbothermic reduction of a columbite concentrate to produce cemented carbides and metal-matrix composites, J. Alloys Compd. **206** (1994) 77–81.

[3.47] KLEIN, S., WEITZEL, H., Magnetische struktur von $Mn(Nb_{0,5}Ta_{0,5})2O_6$, manganotantalit, Acta Crystallogr. Sect. A **32** (1976) 587.

[3.48] DAMPARE, S.B., NYARKO, B.J.B., OSAE, S., AKAHO, E.H.K., ASIEDU, D.K., SERFOR-ARMAH, Y., NUDE, P., Simultaneous determination of tantalum, niobium, thorium and uranium in placer columbite-tantalite deposits from the Akim Oda District

of Ghana by epithermal instrumental neutron activation analysis, J. Radioanal. Nucl. Chem. **265** (2005) 53–59.

[3.49] JONES, M.P., FLEMING, M.G., Identification of mineral grains, Soil Sci. Soc. Am. J. **29** 1965.

[3.50] ALBRECHT, W.W., Production, properties and application of tantalum, niobium and their compounds, Lanthanides, Tantalum and Niobium (1989) 345–358.

[3.51] CARDARELLI, F., Process for Upgrading Tantalum and Niobium Ores and Concentrates with the Recovery of Manganese and Rare Earths Oxides, Patent W02013040694A1 (2013).

[3.52] ÖZAYTEKIN, H.H., UYANÖZ, R., Trace and rare earth element (REE) status of Çarsamba fan soils in the Ancient Konya lake region, Turkey, Afr. J. Agric. Res. **7** (2012) 1110–1117.

[3.53] WANG, X., SHI-LI, Z., HONG-BIN, X.U., YI, Z., Dissolution behaviors of Ta2O5, Nb2O5 and their mixture in KOH and H2O system, Trans. Nonferrous Met. Soc. China **20** (2010) 2006–2011.

[3.54] BHAT, N.P., BORGSTEDT, H., Standard Gibbs energy of formation of K3NbO4 and K3TaO4 and threshold oxygen levels for their formation in potassium, niobium and tantalum, Liq. Met. Syst. (1995) 243–249.

CONCLUSIONS

This report presents a first overview of the potentials of energy neutral mineral processing through a collection of case studies from experts in Member States. Although it is unlikely that energy neutral mineral processing will be realized in full, the report provides relevant information about unconventional uranium recovery from primary ores and nuclear process heat application to support the extractive industries that have realistic chances to be realized in the near future.

Resource identification

The contributions from the CRP clearly showed that ores should not be categorized according to the concentration of a single material. A more holistic approach of the ore body that considers the potential of comprehensive extract and more importantly the composition of potential tailing materials as well as their longterm management if these tailings are not processed is desirable.

Uranium recovery

The project showed that presently considered unconventional resources can play an important role in Member States uranium supply. Unconventional uranium from phosphate ore mining alone could supply some 10% of the world's uranium requirements. Besides, not recovering the uranium during primary ore processing means that the radiotoxic element will either be found in the final product (as is for instance the case with phosphate fertilizers) or the mine tailings. These are mitigatable risks that could lead to potentially higher external costs.

Thermal processes

The CRP discussed the use of HTRs and CSP as alternative energy sources to fossil fuels in thermal processing of minerals. Considering both greenhouse gas lean energy forms open up new avenues to deep decarbonization that have thus far often been overlooked. Both technologies are at a technical maturaty that they can in some cases compete economically with fossil fuels. The results of the project show that they should be considered not just for environmental but also for economic reasons.

The case of phosphorus

Evermore critical societies rightfully request cleaner mineral processing that positions itself in support of circular economy principles. Energy neutral mineral processing will not be able to completely solve this challenge but can be a meaningful approach in some cases. The CRP showed that particularly phosphate ore processing could profit from a more holistic approach that deviates from current practices. Phosphate ore that is the raw material used to produce mineral fertilizers and is the fifth most mined material on earth can contain considerable concentrations of naturally occurring uranium. These heavy metals transfer under current processing techniques to the final fertilizer products, and subsequently, the environment. The potential risks to the environment and human health of necessary fertilizer use, could be dramatically reduced if uranium is recovered during fertilizer production. This can be realized by simply adding a recovery step to the current wet chemical processing of fertilizers as demonstrated in the case studies from Egypt and Morocco. Another interesting approach towards cleaner production could be the replacement of fossil fuel sources in energy intensive

mineral processes discussed in this document with greenhouse gas lean nuclear and solar energy.

In the case of phosphate processing, it was found in this CRP that energy neutral mineral processing may best be realized if HTRs, or other greenhouse gas lean energy sources such as CSP, are used to calcine phosphate ore before the WPA process. Extracting uranium from the phosphoric acid, an intermediate product in the WPA process, is well known and has been successfully employed on an industrial scale at several locations worldwide. In addition, upcoming promising uranium extraction techniques such as the two examples discussed in this document can further reduce recovery costs, and successfully target WPA with lower uranium concentrations. It is well known that calcination before phosphate ore digestion produces phosphoric acid with fewer impurities (sometimes referred to as light green phosphoric acid). Experts participating in the CRP went as far as believing that costs for extracting uranium from this phosphoric acid might be reduced by as much as 50% in case of proven solvent extraction techniques compared to extracting uranium from a phosphoric acid produced without calcination before the digestion process. Not considering potentially higher costs for calcination, uranium byproduct extraction from phosphoric acid would thus be monetarily profitable to some fertilizer companies despite relatively low uranium world market prices.

Due to the large energy requirements, calcination is presently performed at only a few locations (approximately 10% of phosphate ore beneficiated worldwide is calcined) where cheaper flotation techniques are not sufficient to concentrate the ore, cheap natural gas is available, and a higher grade phosphoric acid is needed.

Using HTRs will be challenging and technical competence for HTR process heat applications as well as comprehensive licensing frameworks will have to be developed. China is currently the only country with an existing licensing framework for HTGRs. China is the largest phosphate ore processing country in the world though and lacks domestic uranium resources so that energy neutral mineral processing may be a real option here. This is particularly true if higher uranium content phosphate ore resources would be imported and are processed. China's phosphate rock resources show (on average) a relatively low uranium content of 26-31 ppm while phosphate ore from Florida, Morocco or Brazil for instance show concentrations beyond 130 ppm. Importing phosphate ore is not uncommon as the examples of Europe as well as India. Both regions lack domestic phosphate ore resources and import nearly all their required phosphorous in the form of phosphate rock, pre-concentrated phosphate ore, that is subsequently processed domestically. Estimates conducted as part of this CRP indicate that some 10% of uranium requirements of China could be covered by uranium extracted during phosphate ore processing.

Using HTRs in Northern Africa where high uranium content phosphate ore is present may be another option in the far future. It is questionable though if phosphate ore producing countries like Morocco, Algeria, Tunisia, Egypt, Israel, Syria, Jordan, Iraq and Saudi Arabia where phosphate ore with relatively high uranium content can be found need to employ HTRs and the associated (costly and complicated) nuclear infrastructure needed for their use. Employing HTRs on floating platforms and providing services that include nuclear fuel supply and disposal as currently investigated by some suppliers may be a real option for these Member States.

Though all phosphate ore rich countries have looked or are actively looking into the deployment of nuclear power plants, using CSP may be an attractive alternative given the good to excellent solar radiation present in Northern Africa and the Middle East. After calcination and phosphoric acid production, uranium could again be extracted and simply sold the same way commercial uranium mines sell their product. The resulting higher quality fertilizer could potentially be sold at higher market value and the recovered uranium cold be purchased by nuclear utilities, and in this way be used to contribute to climate change mitigation elsewhere.

In the end, energy neutral phosphate rock processing may thus just be realized in parts, i.e. calcination using HTRs without uranium extraction in China and uranium extraction from high-quality phosphoric acid or other primary resources calcined with CSP plants in Northern Africa and the Middle East.

Recommendations for future work

(1) The economics of unconventional uranium recovery from primary ores need to be improved to make these processes economically competitive. Besides more economic recovery processes, business models that allow for secure investment in uranium recovery infrastructure should be further explored.

(2) HTRs and CSP could play a relevant role in deep decarbonization of our society. Specifically, these technologies can help reduce the carbon emissions of mineral calcination. Future work should focus on the development of larger scale pilot and demonstration plants that can explore the technical and economic feasibility of indirect calcination using HTRs and CSP.

APPENDIX

PUBLICATIONS RESULTING FROM THE CRP

ABBES, N., BILAL, E., HERMANN, L., STEINER, G., HANEKLAUS, N., Thermal beneficiation of Sra Ouertane (Tunisia) Low-Grade Phosphate Rock, Minerals 10 (2020) 937.

AL-KHALEDI, N., TAHA, M., HUSSEIN, A., EL-YAHYAOUI, A., HANEKLAUS, N., Direct leaching of rare earth elements and uranium from phosphate rocks, IOP Conf. Series: Materials Science and Engineering, 479 (2019) 012065.

HANEKLAUS, N., BAYOK, A., FEDCHENKO, V., Phosphate rocks and nuclear proliferation, Sci. Glob. Secur. 25 (2017) 143–158.

HANEKLAUS, N., REITSMA, F., TULSIDAS, H., High temperature reactors for a new IAEA coordinated research project on energy neutral mineral development processes, Nucl. Eng. Des. (2015) 1–5.

HANEKLAUS, N., REITSMA, F., TULSIDAS, H., SCHNUG, E., LOTTERMOSER, B.G., ALLELEIN, H.-J., Energy neutral mineral development processes — An overview. In Proc. Aachen Int. Mining Symposia (AIMS 2016), Aachen (2016) 35.

HANEKLAUS, N., REITSMA, F., TULSIDAS, H., TYOBEKA, B., SCHNUG, E., ALLELEIN, H.-J., BIRKY, B., PETERSON, P.F., DYCK, G., KOSHY, T., Using high temperature reactors for energy neutral mineral development processes a proposed IAEA Coordinated Research Project, Conference: International Symposium on Uranium Raw Material for the Nuclear Fuel Cycle: Exploration, Mining, Production, Supply and Demand, Economics and Environmental Issues, (URAM2014), Vienna, Austria (2014).

HANEKLAUS, N., REYES, R., LIM, W.G., TABORA, E.U., PALATTAO, B.L., PETRACHE, C., VARGAS, E.P., KUNITOMI, K., OHASHI, H., SAKABA, N., et al., Energy neutral phosphate fertilizer production using high temperature reactors: A Philippine case study, Philipp. J. Sci. 144 (2015) 69–79.

HANEKLAUS, N., SCHNUG, E., Energy neutral phosphate fertilizer production using high temperature reactors, Phosphorus in Agriculture: 100 % Zero (2016) 309–316.

HANEKLAUS, N., SCHNUG, E., TULSIDAS, H., TYOBEKA, B., Using high temperature gas-cooled reactors for greenhouse gas reduction and energy neutral production of phosphate fertilizers, Ann. Nucl. Energy 75 (2015) 275–282.

HANEKLAUS, N., SCHRÖDERS, S., ZHENG, Y., ALLELEIN, H.-J., Economic evaluation of flameless phosphate rock calcination with concentrated solar power and high temperature reactors, Energy 140 (2017), 1148-1157.

HANEKLAUS, N., SUN, Y., BOL, R., LOTTERMOSER, B.G., SCHNUG, E., To Extract, or not to extract uranium from phosphate rock, that is the question, Environ. Sci. Technol. 51(2) (2017).

HANEKLAUS, N., TULSIDAS, H., REITSMA, F., SCHNUG, E., Using high temperature reactors for energy neutral phosphate fertilizer and phosphogypsum processing, In: Merkel B., Arab A. (eds) Uranium — Past and Future Challenges, Proc. 7th Int. Conf. Uranium Mining and Hydrogeology 2014 (UMH VII), September 2014, Freiberg, Germany (2014) 785–792.

HANEKLAUS, N., ZHENG, Y., ALLELEIN, H.-J., Stop smoking—Tube-in-tube helical system for flameless calcination of minerals, Processes 5 (2017) 67.

LÓPEZ, L., CASTRO, L.N., SCASSO, R.A., GRANCEA, L., TULSIDAS, H., HANEKLAUS, N., Uranium supply potential from phosphate rocks for Argentina's nuclear power fleet, Resour. Policy 62 (2019) 397–404.

REITSMA, F., WOODS, P., FAIRCLOUGH, M., KIM, Y., TULSIDAS, H., LÓPEZ, L., ZHENG, Y., HUSSEIN, A.E.M., BRINKMANN, G., HANEKLAUS, N., KACHAM, A.R., SREENIVAS, T., SUMARYANTO, A., TRINOPIAWAN, K., AL KHALEDI, N., ZAHARI, A., EL YAHYAOUI, A., AHMAD, J., REYES, R., KIEGIEL, K., ABBES, N., MWALONGO, D., GREAVES, E.D., On the sustainability and progress of energy neutral mineral processing, Sustainability 10 (2018) 235.

SCHEUERMANN, W., HANEKLAUS, N., FÜTTERER, M., editor(s), KUGELER K, NABIELEK H and BUCKTHORPE D. The High Temperature Gas-cooled Reactor: Safety considerations of the (V)HTR-Modul, EUR 28712 EN, Publications Office of the European Union, Luxembourg, (2017), ISBN 978-92-79-71311-8, doi:10.2760/270321, JRC107642.

SCHNUG, E., HANEKLAUS, N., "Uranium in phosphate fertilizers - review and outlook", In: Merkel B., Arab A. (eds) Uranium — Past and Future Challenges, Proc. 7th Int. Conf. Uranium Mining and Hydrogeology 2014 (UMH VII), September 2014, Freiberg, Germany (2014) 123–130.

SHANG, D., GEISSLER, G., MEW, M., SATALKINA, L., ZENK, L., TULSIDAS, H., BARKER, L., EL-YAHYAOUI, A., HUSSEIN, A., TAHA, M., ZHENG, Y., WANG, M., YAO, Y., LIU, X., DENG, H., ZHONG, J., LI, Z., STEINER, G., BERTAU, M., HANEKLAUS, N., Unconventional uranium in China's phosphate rock: Review and outlook. Renewable and Sustainable Energy Reviews, 140 (2021) 110740.

STEINER, G., GEISSLER, B., HANEKLAUS, N., Making uranium recovery from phosphates great again? Environ. Sci. Technol. 54 (2020) 1287–1289.

TULSIDAS, H., GABRIEL, S., KIEGIEL, K., HANEKLAUS, N., Uranium resources in EU phosphate rock imports, Resour. Policy 61 (2019) 151–156.

YE, Y., AL KHALEDI, N., BARKER, L., DARWISH, M.S., EL NAGGAR, A.M.A., EL YAHYAOUI, A., HUSSEIN, A.E.M., HUSSEIN, E.-S., SHANG, D., TAHA, M., et al., Uranium resources in China's phosphate rocks — identifying low-hanging fruits, Earth Environ. Sci. 227 (2019) 052033.

LIST OF ABBREVIATIONS

AC	Activated carbon
ANS	Argan nutshell
BATAN	National Nuclear Energy Agency of Indonesia
BWI	Bond work index
CHTR	Compact high temperature reactor
CNEA	National Atomic Energy Commission of Argentina
CSP	Concentrated solar power
CRP	Coordinated research project
D-R	Dubinin-Radushkevich
DSC	Differential scanning calorimetry
DTA	Differential thermal analysis
eU	Uranium equivalent
FCT	Flash calcination technology
FTIR	Fourier-transform infrared spectroscopy
GDP	Gross domestic product
HTGR	High temperature gas-cooled reactor
HTR	High temperature reactor
ICP-MS	Inductively coupled plasma-mass spectrometry
ICP-OES	Inductively coupled plasma-optical emission spectrometry
IX	Ion exchange
LWR	Light water reactor
min	minute(s)
MSC	Malaysia Smelting Corporation
MSR	Molten salt reactor
PHWR	Pressurized heavy water reactor

ppm	parts per million
REEs	Rare earth elements
SEM	Scanning electron microscope
STA	Simultaneous thermal analyzer
SX	Solvent extraction
TBP	Tributyl phosphate
TDS	Total dissolved solids
TENORM	Technologically enhanced naturally occurring radioactive material
TG-DTA	Thermogravimetry and differential thermal analysis
TGA	Thermogravimetric analysis
TSP	Trisodium phosphate
TXRF	Total reflection X-ray fluorescence
UOC	Uranium ore concentrate
USB	Universidad Simón Bolivar
WPA	Wet phosphoric acid
XRD	X-ray powder diffraction
XRF	X-ray fluoresence

CONTRIBUTORS TO DRAFTING AND REVIEW

Abbes, N.	Groupe Chimique Tunisien, Tunisia
Ahmad, J.	Pakistan Atomic Energy Commission, Pakistan
Al Khaledi, N.	Radiation Protection Department, Kuwait
Al Yahyaoui, A.	Centre National de l'Energie, des Sciences et des Techniques Nucléaires, Morocco
Alonso, G.	National Institute of Nuclear Research, Mexico
Brinkmann, G.	BriVa Tech Consulting, Germany
Fairclough, M.	International Atomic Energy Agency
Greaves, E.C.	Universidad Simon Bolivar, Bolivian Republic of Venezuela
Haneklaus, N.	RWTH Aachen University, Germany
Hussein, A.	Nuclear Materials Authority, Egypt
Kacham, A.R.	Bhabba Atomic Research Centre, India
Kiegiel, K.	Institute of Nuclear Chemistry and Technology, Poland
Kim, Y.	International Atomic Energy Agency
Lopez, L.	National Atomic Energy Commission, Argentina
Mwalongo, D.	Tanzania Atomic Energy

	Commission, United Republic of Tanzania
Reitsma, F.	International Atomic Energy Agency
Reyes, R.	Philippine Nuclear Research Institute, Philippines
Sinha, R.	Bhabba Atomic Research Centre, India
Sreenivas, T.	Bhabba Atomic Research Centre, India
Sumaryanto, A.	National Nuclear Energy Agency, Indonesia
Trinopiawan, K.	National Nuclear Energy Agency, Indonesia
Tulsidas, H.	International Atomic Energy Agency
Woods, P.	International Atomic Energy Agency
Zahari, A.	Malaysian Nuclear Agency, Malaysia
Zheng, Y.	Tsinghua University, China

Research Coordination Meetings

Vienna, Austria: 2-5 November 2015, 3–6 July 2017, 2–6 July 2018

IAEA
International Atomic Energy Agency

No. 26

ORDERING LOCALLY

IAEA priced publications may be purchased from the sources listed below or from major local booksellers.

Orders for unpriced publications should be made directly to the IAEA. The contact details are given at the end of this list.

NORTH AMERICA

Bernan / Rowman & Littlefield

15250 NBN Way, Blue Ridge Summit, PA 17214, USA
Telephone: +1 800 462 6420 • Fax: +1 800 338 4550

Email: orders@rowman.com • Web site: www.rowman.com/bernan

REST OF WORLD

Please contact your preferred local supplier, or our lead distributor:

Eurospan Group

Gray's Inn House
127 Clerkenwell Road
London EC1R 5DB
United Kingdom

Trade orders and enquiries:

Telephone: +44 (0)176 760 4972 • Fax: +44 (0)176 760 1640
Email: eurospan@turpin-distribution.com

Individual orders:

www.eurospanbookstore.com/iaea

For further information:

Telephone: +44 (0)207 240 0856 • Fax: +44 (0)207 379 0609
Email: info@eurospangroup.com • Web site: www.eurospangroup.com

Orders for both priced and unpriced publications may be addressed directly to:

Marketing and Sales Unit
International Atomic Energy Agency
Vienna International Centre, PO Box 100, 1400 Vienna, Austria
Telephone: +43 1 2600 22529 or 22530 • Fax: +43 1 26007 22529
Email: sales.publications@iaea.org • Web site: www.iaea.org/publications

International Atomic Energy Agency
Vienna